

Detection of high energy neutralinos with neutrino telescopes

Marthe Marie Meltzer

Master's thesis

Supervisor: Michael Kachelrieß

Trondheim, June 2007

Department of Physics

Faculty of Natural Sciences and Technology

The Norwegian University of Science and Technology

NTNU

Abstract

In this thesis, we investigate the prospect of observing a well-motivated candidate for dark matter — the neutralino — in the future IceCube neutrino telescope. The neutralino is the lightest supersymmetric particle of the minimal supersymmetric extension of the Standard Model. It has been suggested that high energy neutralinos and neutrinos are produced in the decay of superheavy dark matter particles. High energy neutralinos could interact with matter in a neutrino telescope and produce observable muons. A challenge is then to differentiate between muons originating from neutralinos and from neutrino-produced muons.

To model neutralino interactions with matter, we consider the neutralino cross section in the squark-resonance approximation. The results depend heavily on the mass of the squark. We consider two cases for the mass of the squark, $m_{\tilde{q}} = 1 \text{ TeV}$ and $m_{\tilde{q}} = 250 \text{ GeV}$. For a given flux, we calculate the corresponding event rates. Our results show that it is unlikely to detect a neutralino signal for either of the cases in IceCube. On the positive side, it is possible to differ between neutrinos and neutralinos in the case of $m_{\tilde{q}} = 1 \text{ TeV}$. In order to detect an unmistakable neutralino signal, the volume of the detector has to be extended, or new observation techniques have to be developed.

Acknowledgments

I wish to thank my supervisor, professor Michael Kachelrieß, for helpful guidance and careful reading of this thesis. Besides giving advise on the physics of this thesis, he has introduced me to Fortran, gnuplot, emacs and have given me some useful L^AT_EX tips. I am grateful for his suggestion to attend the International School on AstroParticle Physics European Doctorate School: “Dark matter and dark energy” in Sorrento, Italy, and making it possible by letting me travel on his expense account.

I would also like to thank all my fellow students and friends for fun discussions at lunch time, mutual exchange of L^AT_EX tips and their support during ups and downs during my studies at NTNU.

Lastly, I am thankful for my family for all their never-ending support.

Marthe Marie Meltzer

Contents

Abstract	iii
Acknowledgments	v
1 Introduction	1
2 The nature of dark matter	3
2.1 Dark matter and cosmology	3
2.1.1 The Standard Model of cosmology	3
2.1.2 Problems of standard cosmology	5
2.1.3 The inflationary Universe	6
2.1.4 The Concordance Model of cosmology	8
2.2 Evidence for dark matter	8
2.3 Candidates for dark matter	12
2.3.1 Thermal dark matter	12
2.3.2 Non-thermal dark matter	16
3 The Minimal Supersymmetric Standard Model	23
3.1 Motivational reasons for Supersymmetry	24
3.2 R -parity	25
3.3 Supersymmetry algebra	26
3.4 The particle content of the MSSM	27
3.4.1 Neutralinos	31
4 Indirect detection	35
4.1 Decay of superheavy dark matter	35
4.1.1 Neutralino and neutrino fluxes	36
4.2 Neutrino telescopes	40
4.2.1 IceCube	41
4.3 Deep inelastic scattering in the parton model	43
4.3.1 The naive parton model	43
4.3.2 Deep inelastic scattering	44
4.3.3 The QCD improved parton model	46
4.4 Neutrino interactions with matter	48
4.4.1 Quark distribution functions	49

4.5	Neutralino interactions with matter	52
4.5.1	Kinematics and cross section	52
4.6	Influence of the Earth	60
4.6.1	The Preliminary Earth Model	60
4.6.2	Interaction length	61
4.6.3	Shadow factor	62
4.6.4	Average range of muons	66
4.6.5	Probability for creating muons	70
4.6.6	Event rates	72
5	Discussions	73
5.1	Theoretical and experimental uncertainty	73
5.2	Numerical limitations	75
6	Closing remarks	77
	Appendices	79
A	Pauli and Dirac matrices	81
B	Selected Feynman rules in the MSSM	83
	References	85

“The most beautiful thing we can experience is the mysterious. It is the source of all true art and all science. He to whom this emotion is a stranger, who can no longer pause to wonder and stand rapt in awe, is as good as dead: his eyes are closed.”

Albert Einstein

1

Introduction

There is almost a general consensus among astronomers that most of the matter in the Universe is dark. We call the matter dark because it does not emit or reflect enough electromagnetic radiation to be detected. So far, we have only inferred the presence of dark matter from its gravitational effects on luminous matter, but it may have electromagnetic, weak or strong interactions as well. The fact that we know so little about it, makes the nature of dark matter one of the most intriguing problems in physics.

The numerous observational cosmology experiments that has been carried out in recent years have given us a better understanding of the Universe. There seems to be a close connection between cosmology and fundamental physics. The problem of dark matter is deeply rooted in elementary particle physics. In order to solve the dark matter problem, joint efforts between cosmologists and particle physicists are necessary.

The possibility of observing a hypothetical non-baryonic, supersymmetric dark matter candidate — neutralino — is the topic of this thesis. In order to observe such a particle one has to understand the nature and properties of the particle in mind. The neutralino can constitute the missing dark matter by itself, or it can be a stable particle resulting from the decay of another dark matter particle — a supermassive particle X . It is assumed that such a decay would produce a particle cascade, with high energy neutrinos and neutralinos among the end products. To observe these weakly interacting particles, we have to look for upward-going muons, produced in charged-current interactions with the matter below a detector.

The background for this signal consists of showers generated by ultra-high energy cosmic neutrinos. To establish a clear neutralino signal, it is necessary to differentiate the neutralinos from neutrinos. The neutralino-nucleon cross section depends on the choice of parameters of the neutralino. If this cross

section is significantly smaller than the neutrino-nucleon cross section, they will have very different absorption properties in the Earth. Thus, it should be possible to filter out the background neutrinos by using the Earth as a filter. Given a sufficient cosmic flux, these neutralinos may be detected in future experiments.

The outline of this thesis is as follows. We will start in chapter 2 with the role of dark matter in cosmology. Then we will continue with presenting some of the evidence for dark matter before we give an overview of some of the proposed dark matter candidates and how they can be produced. After a brief outline of the supersymmetric theory in chapter 3, the properties and possibilities for neutralino dark matter are shown in section 3.4.1. Chapter 4 concerns the indirect detection of neutrinos and neutralinos via deep inelastic scattering on nucleons. The likelihood of such processes is linked to the cross sections. The cross sections of neutrinos and neutralinos are discussed and numerical evaluation of these will be presented in section 4.4 and 4.5, respectively.

We then explain the effect the Earth has on the particle fluxes, and calculate the mean ranges of muons and the shadowing factors on the fluxes. In the end, we calculate the event rates for detecting high energy neutralinos in the high energy neutrino telescope IceCube. The results are discussed in chapter 5 before the closing remarks are given in chapter 6. For completeness, we present some selected Feynman rules, the Pauli and Dirac matrices and some trace rules in the appendices.

“It is not clear how these startling results must ultimately be interpreted.”

Fritz Zwicky

2

The nature of dark matter

2.1 Dark matter and cosmology

2.1.1 The Standard Model of cosmology

The standard model of cosmology is the hot Big Bang model, in which the Universe expanded via an explosion — the Big Bang — of an initial singularity of infinitely high density. After the Big Bang, the Universe has expanded and cooled to reach its present state. Today, we perceive that the observable Universe is a homogeneous, isotropic and expanding Universe. A homogeneous, isotropic spacetime is one for which the geometry is spherically symmetric about any one point in space (isotropic) and the same point in space as any other (homogeneous)¹. Although the Universe seems inhomogeneous considering its lumpy distribution of galaxies and their galaxy clusters — the large-scale structure of the Universe — it is approximately homogeneous on distance scales above several hundred megaparsecs².

The Universe can be described by the Friedman-Robertson-Walker family of cosmological models. The metric for a homogeneous, isotropic cosmological model expressed in comoving coordinates (t, r, θ, ϕ) and natural units ($c = \hbar = k_B = 1$) is

$$ds^2 = dt^2 - a^2(t) \left[\frac{dr^2}{1 - kr^2} + r^2(d\theta^2 + \sin^2\theta d\phi^2) \right], \quad (2.1)$$

where $a(t)$ is the scale factor, which represents the relative expansion of the Universe, and the curvature $k = 1, 0, -1$ for closed (spherical geometry), flat

¹The assumption of a homogeneous and isotropic Universe, known as the *cosmological principle*, means that no observer occupies a special position in the Universe.

²1pc = 3.086×10^{16} m = 3.262 ly.

(Euclidean geometry) or open (hyperbolic geometry) universes, respectively.

The comoving coordinates of any point in space remain constant in time as long as the expansion of the Universe is perfectly homogeneous and isotropic. The physical distance d between two points comoving with respect to the cosmological expansion increase linearly with the scale factor

$$d \propto a(t). \quad (2.2)$$

The expansion rate is determined by the Hubble parameter

$$H(t) \equiv \frac{\dot{a}(t)}{a(t)}. \quad (2.3)$$

The Hubble parameter is not constant, but is time-dependent. The Hubble time (or Hubble radius) H^{-1} sets the scale of the expansion.

A spatially flat Universe is only reached for a certain density, which we call the critical density. This is given as [1]

$$\rho_c \equiv \frac{3H_0^2}{8\pi G} \approx 1.88 \times 10^{-29} h^2 \text{g/cm}^3, \quad (2.4)$$

where G is the Newtonian gravitational constant, and

$$H_0 \equiv H(t_0) \equiv \frac{\dot{a}(t_0)}{a(t_0)} \quad (2.5)$$

is the Hubble constant which determine the present expansion rate of the Universe. We will in this chapter denote the present values of all quantities with a zero. The present day normalized Hubble expansion rate is [1]

$$h \equiv \frac{H_0}{100(\text{km/s/Mpc})} = 0.73_{-0.03}^{+0.04}. \quad (2.6)$$

It is convenient to normalize to this density, so that the cosmological density parameter of a species i is quoted using

$$\Omega_i = \frac{\rho_i}{\rho_c}, \quad (2.7)$$

where ρ_i is the density of the species averaged over the Universe, and ρ_c is the critical density. To get the total density parameter Ω_{tot} , we sum up all the contributions from the different species. If we could measure the present total density relative to the critical density,

$$\Omega_{\text{tot}} \equiv \frac{\rho_0}{\rho_c}, \quad (2.8)$$

we could determine the curvature of the Universe. If $\Omega_{\text{tot}} = 1$ the Universe is Euclidean, i.e. flat. An $\Omega_{\text{tot}} > 1$ implies a closed Universe, while an $\Omega_{\text{tot}} < 1$ implies an open Universe.

2.1.2 Problems of standard cosmology

The Universe as we observe it today seems flat, and thus the preferred cosmological model is a spatially flat Universe. However, for the Universe to look like today, very fine tuned initial conditions near the Big Bang are needed, which seems highly unlikely. Several problems arise from this fact. Among these problems are the *horizon problem* and the *flatness problem*.

The horizon problem

Determining why the Universe is homogeneous and isotropic is known as the horizon problem. The particle horizon demarcates the boundary between the observable Universe and the part of the Universe from which light signals have not reached us. Assuming that the Universe is flat, the maximum distance light has traveled since the beginning of the Universe, $t = 0$, is

$$d_{\text{H}}(t) = a(t) \int_0^t \frac{dt'}{a(t')} = \frac{t}{1-n} \quad \text{for } a \propto t^n. \quad (2.9)$$

The scale goes like $a \sim t^{2/3}$ for a matter dominated Universe, and $a \sim t^{1/3}$ for a radiation dominated one. In standard cosmology, the horizon distance and the Hubble radius is essentially equal:

$$d_{\text{H}} \propto H^{-1}. \quad (2.10)$$

In the present Universe, points in regions separated by vast distances are not in causal contact with each other, that is, these regions have not yet had the time to communicate with each other via light signals. There are at least $\sim 10^5$ separate regions in the Universe that are causally disconnected [2]. Since no physical interaction can travel faster than the speed of light, we would expect that the physical properties of the regions should be different, yet they are the same. For instance, the cosmic microwave background has almost the same temperature everywhere in the sky, measured to be (2.725 ± 0.001) K [1].

The flatness problem

The energy density in the Universe today is very close to the critical density, $\Omega_0 = 1.003_{-0.017}^{+0.013}$ [1]. Both the average density of the Universe and the critical density change with time. If the current value of Ω is extrapolated backwards in time, the energy density becomes even closer to unity. At the closest theoretically time we can get to the Big Bang, at one Planck time $t_{\text{Pl}} = \sqrt{G} \approx 5.39121 \times 10^{-44}$ sec, the value of Ω is such that $\Omega \leq 1 \pm 10^{-60}$.

If Ω was only slightly larger or smaller than unity in the instant following the Big Bang, the Universe would either quickly recollapse or quickly reach a state of maximal entropy with a temperature of the Universe close to absolute zero. This remarkable closeness of Ω to unity in the early Universe is known as the flatness problem.

2.1.3 The inflationary Universe

A solution to both of these problems is the hypothesis [3, 4, 5] of an inflationary Universe, in which the Universe experienced a phase of exponential expansion, with a scale factor growing like

$$a(t) \propto e^{Ht}, \quad H = \text{const.} \quad (2.11)$$

within a time interval $t \in [t_i, t_R]$, where t_i is the initial time at which inflation begins and t_R is the reheating time at which inflation ends.

Inflation solves the horizon problem by proposing that prior to the inflationary period, the entire observable Universe was causally connected. During inflation, the causal regions are stretched on scales much larger than the Hubble radius. Because the spacetime background expands exponentially with the scale factor, whereas the Hubble radius remains approximately constant, particles that initially were in causal contact with another can no longer communicate. Large scale homogeneity is assured since the physical properties were established before inflation took place, and any small inhomogeneity would diminish as the Universe rapidly stretches. The already homogeneous region is then stretched by inflation to become large enough to encompass the entire observable Universe, as shown in figure 2.1.

After inflation ends, and the Universe enters the radiation/matter dominant era, the particle horizon begins to grow faster than the spacetime. When we look at the sky today, we are still seeing the regions of uniformity that were stretched outside the particle horizon during inflation [2].

The flatness problem is solved naturally in inflationary models, since the radius of curvature of the Universe today should be much greater than the present Hubble radius. Thus inflation predicts a flat Universe.

Even though inflation guarantees homogeneity (on large scales), we do not want the Universe to be completely homogeneous at the end of inflation, or else there would be no structure formation. It turns out that inflation can also provide density perturbations. During the expansion, it is possible that tiny quantum fluctuations in the inflaton field — the scalar field which is thought to be responsible for inflation — lead to the necessary density perturbations.

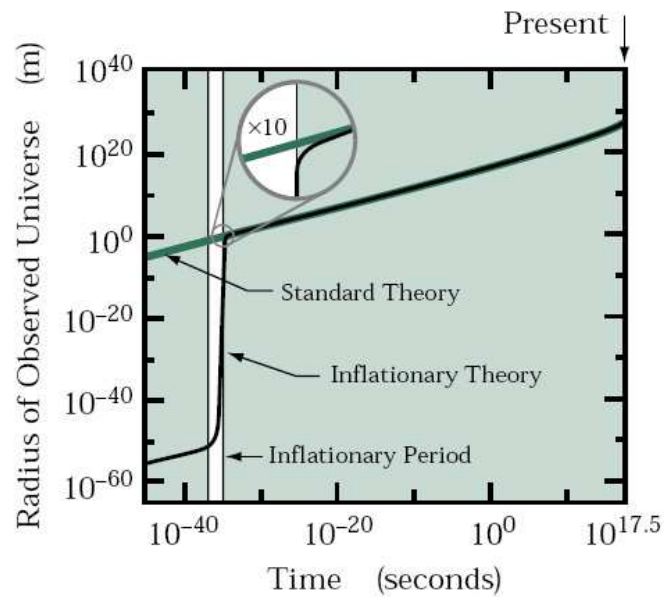


Figure 2.1: The solution to the horizon problem. The line marked as “Standard Theory” shows the radius of the region that evolves to become the presently observed Universe, as described by the traditional Big Bang theory. Because of the tremendous growth during inflation, the inflationary curve shows a much smaller Universe than in the standard period before inflation. The uniformity of the Universe is established at this early time. The region is then stretched by inflation to become large enough to encompass the observed Universe [6].

In most models, inflation occurs at an energy scale $M \sim 10^{14}$ GeV when the Hubble time is only about $H^{-1} \sim 10^{-34}$ sec [7]. It is driven by a negative-pressure vacuum energy density that is the dominant energy density of the Universe once the temperature fall below the critical temperature $T_c \simeq M$. The initial entropy contained within the inflating patch was far less than in our present Universe. During the expansion, the Hubble volume cools like $T \propto \exp(-Ht)$ with the entropy fixed.

At the end of inflation, the vacuum energy of the inflaton field is transferred to ordinary particles. As the particles thermalize, the Universe is reheated (typically at $T_{\text{RH}} \simeq M$), causing a massive entropy production. After inflation ended, the entropy remained constant as long as the expansion was adiabatic.

2.1.4 The Concordance Model of cosmology

Observations of the cosmic microwave background, supernova Ia data and the large-scale structure of the Universe have established a Concordance Model of cosmology, in which the Universe consists of 76 % dark energy, 20 % dark matter and 4 % baryonic matter [1]. This model is called Λ CDM, which is an abbreviation for Lambda-Cold Dark Matter.

The Λ stands for the cosmological constant which is a dark energy term that allows for the current accelerating expansion of the Universe. Cold dark matter (CDM) is the prevailing model of dark matter, in which dark matter is explained as being non-relativistic at freeze-out, i.e. cold. It is a bottom-up model, where structures grow hierarchically, with small objects merging to form more and more massive objects. This is in agreement with observations of large-scale structure. But the theory does not explain the fundamental physical origin of dark matter. That is yet to be decided.

2.2 Evidence for dark matter

The existence of dark matter was first proposed in 1933 by the astronomer Fritz Zwicky [8]. He applied the virial theorem of classical mechanics to the Coma galaxy cluster to determine its total mass, and noticed that the cluster had to contain more mass than could be accounted for by luminous matter. The virial theorem states that the time average of the total gravitational binding energy in a bound system should be twice the time average of the total kinetic energy,

$$2\langle E_{\text{kin}} \rangle + \langle E_{\text{pot}} \rangle = 0. \quad (2.12)$$

2.2. EVIDENCE FOR DARK MATTER

The angle brackets denote time averaged quantities. The gravitational potential energy of a system with N galaxies, each of which can be approximated as a point mass, with a mass m_i ($i = 1, 2, \dots, N$), a position \vec{x}_i and a velocity \vec{v}_i , is

$$E_{\text{pot}} = -\frac{G}{2} \sum_{\substack{i,j \\ j \neq i}} \frac{m_i m_j}{|\vec{x}_j - \vec{x}_i|}. \quad (2.13)$$

The kinetic energy is

$$E_{\text{kin}} = \frac{1}{2} \sum_i m_i |\vec{v}_i|^2 = \frac{1}{2} M_{\text{cluster}} \bar{v}^2, \quad (2.14)$$

where the mean square velocity of all the galaxies in the cluster is

$$\bar{v}^2 \equiv \frac{1}{M_{\text{cluster}}} \sum_i m_i |\vec{v}_i|^2. \quad (2.15)$$

The total mass of the cluster is then given in terms of the average square of the velocities of the individual galaxies which constitute the cluster. From this application based on the motions of galaxies near the edge of the cluster, Zwicky derived [9] a lower limit of $M_{\text{Coma}} > 4.5 \times 10^{13} M_{\odot}$. The Coma cluster contains about one thousand galaxies, so the average mass of one of these galaxies is $\bar{M}_{\text{gal}} > 4.5 \times 10^{10} M_{\odot}$. This result was quite unexpected since the luminosity of an average galaxy is about $8.5 \times 10^7 M_{\odot}$. Hence, the Coma galaxy cluster seemed to contain about 400 times more mass than expected. This discrepancy between the mass and the observed luminosity is quantified by the mass-to-luminosity, M/L , ratio, which is often expressed in terms of solar mass and luminosity.

It was not until the late 1960s — nearly 40 years after Zwicky’s initial observations — that the suggestion of dark matter was taken seriously. At that time, the astronomers Vera Rubin and Kent Ford observed further evidence for the existence of dark matter — the observation of flat rotation curves in spiral galaxies [10]. Spiral galaxies are structures containing billions of stars rotating around a central “bulge”. A rotation curve is the velocity of the luminous matter as a function of the radial distance from the center. Assuming that the stars have a circular orbit around the galactic center, the rotation velocities of single stars can be calculated from the equality of the gravitational and centrifugal forces, according to

$$\frac{GmM(r)}{r^2} = \frac{mv^2}{r}, \quad (2.16)$$

where $M(r)$ is the mass within the orbit of radius r . From this we would expect stars in spiral galaxies to move more slowly further away from the galactic center according to

$$v(r) = \sqrt{\frac{GM(r)}{r}}. \quad (2.17)$$

If we assume that the bulge is spherically symmetric with constant density ρ , then

$$M = \rho V = \rho \frac{4}{3} \pi r^3. \quad (2.18)$$

Inside the bulge we would then have a rotation curve of

$$v(r) \propto r. \quad (2.19)$$

From a point outside of the galaxy, M corresponds to the total mass of the galaxy, and we would expect that

$$v(r) \propto r^{-1/2} \quad (2.20)$$

beyond the optical disc. But when the rotation curves are measured using the Doppler shift of spectral lines, it turns out that most stars orbit at roughly the same speed. This results in a characteristic flat behavior at large distances, even far beyond the visible discs [10, 11]. The fact that $v(r)$ is approximately constant implies the existence of a dark matter halo with $M(r) \propto r$. As an example, the flat rotation curve of the spiral galaxy NGC 6503 compared with a best fit model is shown in figure 2.2.

After numerous observations in recent years, it is now clear that all galaxies and galaxy clusters possess a dark matter component. Spiral galaxies have a mass-to-luminosity ratio of typically $M/L \sim (5-10)M_{\odot}/L_{\odot}$, while clusters of galaxies usually have $M/L \sim 300M_{\odot}/L_{\odot}$.

In 2006, direct evidence for the existence of dark matter was claimed [13], based on X-ray and weak gravitational lensing³ observations of a merging cluster system named the Bullet cluster. Only 10 % of the visible baryons in a galaxy cluster are in the cluster galaxies. The remaining 90 % are hot plasma clouds, which fill the cluster volume. The hot plasma will slow down during a collision of two galaxy clusters, emitting X-rays. But the galaxies — and presumably the dark matter — will sail straight through, physically separating dark matter from most of the visible matter. The map of matter surface density obtained by the analysis of the weak lensing data, shows that

³The bending of light due to the gravitational potential of a massive object between the source and the observer.

2.2. EVIDENCE FOR DARK MATTER

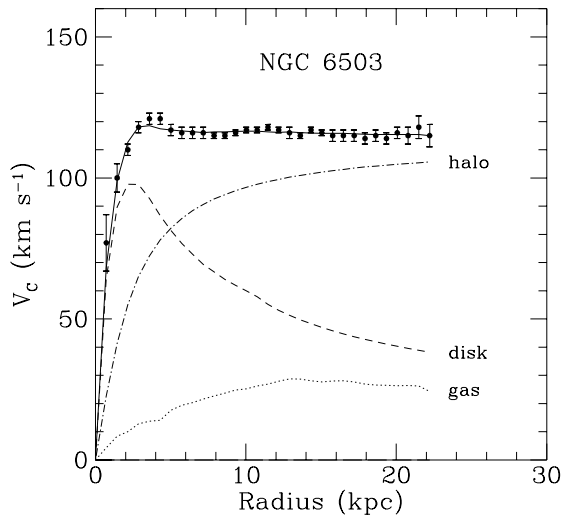


Figure 2.2: The rotation curve for the spiral galaxy NGC 6503 (points) compared with a best fit model (continuous line) as sum of the halo contribution (dashed-dotted line), the stellar disk (short dashed line) and the gas contribution (dotted line) [12].

the gravitational potentials are not centered around the plasma, implying that most of the matter is unseen. Radio and X-ray images together with the map of surface matter density of the Bullet cluster are shown in figure 2.3.

Although all clues point toward the existence of dark matter, other explanations not involving (much) dark matter has been proposed. Theories like Modified Newtonian dynamics (MOND) [15, 16] introduced in 1983, which adjust Newton's 2nd law for small accelerations, and the more recent relativistic Tensor-Vector-Scalar (TeVeS) gravity [17] that is equivalent to MOND in the non-relativistic limit, has been introduced to explain the flat rotation curves. In contrast to MOND, TeVeS can also explain structure formation (without CDM) and the Bullet cluster if ~ 2 eV massive neutrinos are invoked [18, 19]. But the TeVeS theory meets other challenges, like explaining the cosmic microwave background anisotropies and structure formation at the same time [20]. We will dismiss it for now and focus our attention on dark matter as the real thing.

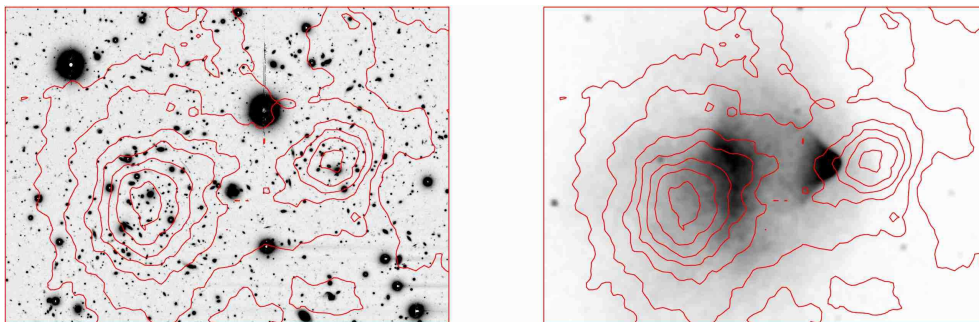


Figure 2.3: Images of the Bullet cluster seen in radio (left) and in X-ray (right). The contours superimposed on the images is the matter density map retrieved from weak gravitational lensing [14].

2.3 Candidates for dark matter

Several candidates have been suggested to constitute the dark matter. To make life somewhat easier, we can divide them in two main classes; thermal and non-thermal dark matter.

2.3.1 Thermal dark matter

Baryonic dark matter

Some of the dark matter must be composed of ordinary atoms and molecules which are too dim to be observed. Such contributions are termed baryonic dark matter (BDM). The main baryonic candidates are massive compact halo objects (MACHOS). This category includes brown dwarfs, jupiter-like objects, black holes, white dwarfs and neutron stars [21]. These are bodies that either never managed to begin nuclear fusion of hydrogen to become stars ($M < 0.8M_{\odot}$, such as planets or brown dwarfs), or are the remnants of a star, such as white dwarfs or black holes. Another contribution to baryonic dark matter could be low surface brightness galaxies or cold hydrogen clouds which escape observation [22].

If we combine the non-luminous matter together with the luminous we get the total baryonic matter density $\Omega_b \equiv \Omega_{\text{lum}} + \Omega_{\text{bdm}}$. The amount of baryons in the Universe is predicted from our understanding of the big-bang theory and the formation of light elements (Big Bang nucleosynthesis) as shown in figure 2.4. To agree with the measured abundances of helium, deuterium and lithium, the baryonic content in the Universe must be $\Omega_b h^2 = 0.0223^{+0.007}_{-0.009}$ or equivalently $\Omega_b = 0.042^{+0.003}_{-0.005}$ [1]. This leaves a dark matter density component of the Universe of $\Omega_{\text{dm}} = 0.20^{+0.02}_{-0.04}$, which has not yet

been accounted for.

Non-baryonic dark matter

In addition to the dark matter in the form of baryons, there is non-baryonic dark matter. Most of the non-baryonic candidates proposed are hypothetical exotic particles. A new stable particle, called X , could have a significant cosmological abundance today. To explain how we have to go back to the early Universe, when the temperature of the Universe exceeded the mass m_X of the particle. Such a particle would exist in thermal equilibrium with the radiation, maintained by annihilations of the particle with its anti-particle \bar{X} into lighter particles and vice versa [21]. As the Universe cools and the temperature drops below the particle's mass, the particle experience freeze-out. Freeze-out occurs when the annihilations cannot keep the particle in equilibrium with the rest of the cosmic plasma. The evolution of the abundance of a species is described by the Boltzmann equation

$$\frac{dn_X}{dt} = -3Hn_X - \langle\sigma_a|v|\rangle[n_X^2 - (n_X^{\text{eq}})^2], \quad (2.21)$$

where n_X is the particle's actual number density, n_X^{eq} is the number density of X 's in equilibrium and v is the relative velocity of the annihilating particles and $\langle\sigma_a|v|\rangle$ is the thermal average of the total annihilation cross section.

We can further classify dark matter into two categories; hot and cold, according to the velocity of the particles at decoupling. Hot dark matter (HDM) are low mass particles moving at relativistic speeds at freeze-out. We already know one component of this category, the light neutrinos. But neutrinos alone as the dark matter cannot explain today's large scale structure. Because of the high velocities of hot dark matter, structures on small scales are wiped out. Perturbations in a nearly collisionless component (e.g. neutrinos etc.) are subject to free streaming. Such a species can travel in free fall in the expanding Universe after decoupling from the plasma. Collisionless particles can smooth out inhomogeneities by streaming out of overdense regions into underdense regions.

In a radiation dominated era (like in the early Universe), the free streaming scale is

$$\lambda_{\text{fs}} = \frac{t_{\text{nr}}}{a_{\text{nr}}} \left(2 + \ln \frac{t_{\text{eq}}}{t_{\text{nr}}} \right), \quad (2.22)$$

where a_{nr} is the scale factor and t_{nr} is the time the particle becomes non-relativistic and $t = t_{\text{eq}} \simeq 4.4 \times 10^{10} (\Omega_0 h^2)^{-2} \text{sec}$ [7] is the time of matter-radiation equality. A particle X becomes non-relativistic when $T_X \simeq m_X/3$. Considering this and the fact that for a weakly interacting particle, T_X is

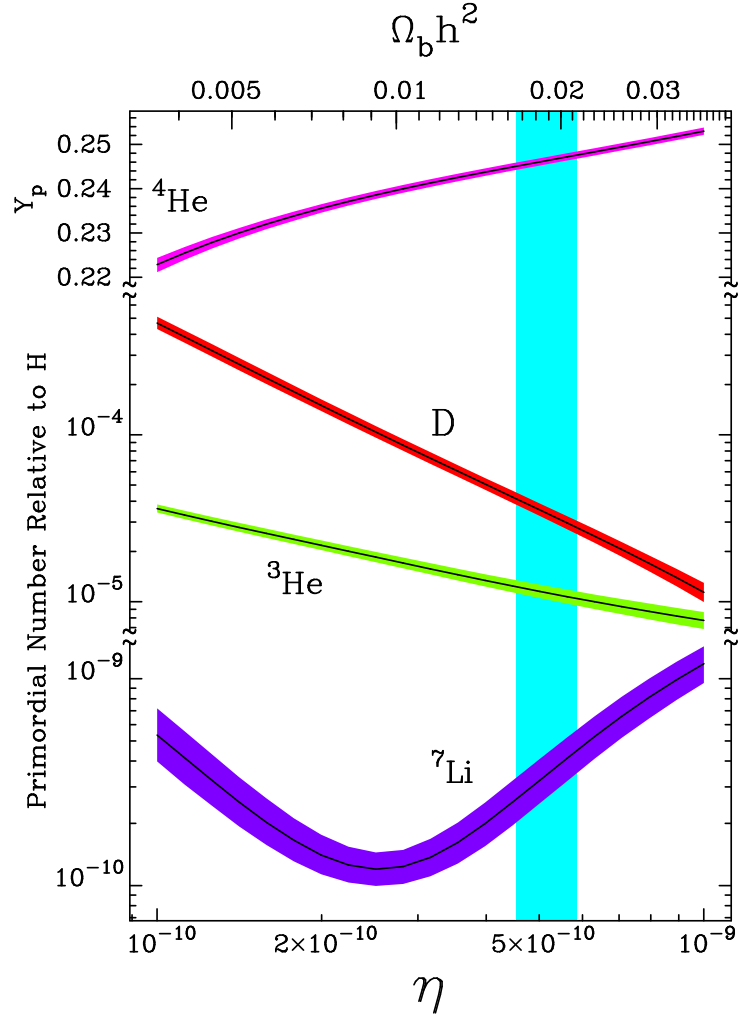


Figure 2.4: Predicted abundance ratios of the light elements relative to hydrogen from standard Big Bang nucleosynthesis as a function of the baryon-to-photon ratio, η , and the baryon density, $\Omega_b h^2$, of the Universe. The widths of the curves represents 95 % confidence level. The vertical band specifies 95 % confidence level in η , based on the combined result of observations of abundances of D, ${}^4\text{He}$ and ${}^7\text{Li}$ [23, 24].

2.3. CANDIDATES FOR DARK MATTER

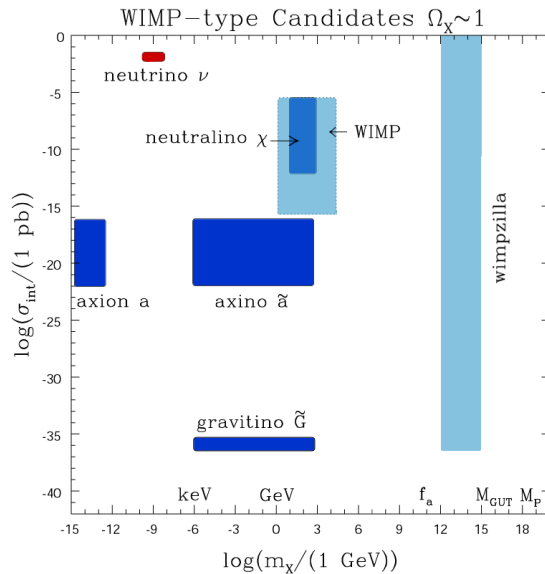


Figure 2.5: Overview of some well motivated WIMP dark matter candidates for which one can have $\Omega \sim 1$. The interacting cross section σ_{int} represents a typical order of magnitude of interaction strength with ordinary matter. The box marked “WIMP” stands for several possible candidates [25].

likely to be less than the photon temperature, it is possible to calculate t_{nr} and a_{nr} [7]. For a neutrino the free streaming scale is about [7]

$$\lambda_{\text{fs}} \simeq 20 \text{Mpc} \left(\frac{m_\nu}{30 \text{eV}} \right)^{-1}. \quad (2.23)$$

Neutrino clustering is strongly suppressed below this scale. On scales much larger than the free-streaming scale, however, the neutrinos will cluster as cold dark matter.

The effect of free-streaming constrains the amount of hot dark matter in the Universe. For the hot dark matter to be the main component of the dark matter, the galaxies must have been formed by fragmentation of larger structures (superclusters), and the number of galaxies must have been a lot less than the number of galaxies observed.

The exotic particles that could constitute the cold dark matter may be Weakly Interacting Massive Particles (WIMPs), with interaction strength comparable to those of neutrinos. Such WIMPs would be long lived relics or stable particles left over from the Big Bang [26]. An overview of some of the WIMP candidates, both thermal and non-thermal, is shown in figure 2.5. The most promising WIMP candidate is the neutralino, a postulated supersymmetric particle, which we will review in section 3.4.1.

The relic density of a non-baryonic cold dark matter species is inversely proportional to the annihilation cross section and the mass of the particle,

$$n_X \propto \frac{1}{m \langle \sigma_a |v| \rangle}. \quad (2.24)$$

From this we can see that the smaller the annihilation cross section, the greater the relic abundance, i.e. the more weakly interacting particles will decouple earlier. The abundance of a particle that stays in thermal equilibrium indefinitely will be suppressed by the Boltzmann factor $e^{-m/T}$. There would be no such particles in the observable Universe [7, 27].

If a dark matter particle is a thermal relic of the early Universe, the maximum possible annihilation cross section $\sigma_a v$ compatible with unitarity together with the constraint of the relic density, set an upper limit for the mass of [11]

$$m_{\text{dm}} \lesssim 34 \text{ TeV}. \quad (2.25)$$

The evolution of a typical WIMP number density in the early Universe is shown in figure 2.6.

2.3.2 Non-thermal dark matter

Axions

Axions are hypothetical pseudo-scalar particles arising from a possible solution of the strong CP problem of quantum chromodynamics (QCD) [29, 30]. CP violation has been observed in the weak, but not in the strong interactions. Because of the existence of non-trivial, vacuum gauge configurations, non-Abelian gauge theories — like QCD — have a complex vacuum structure. QCD has an infinite number of vacuum states $|n\rangle$, classified by a topological winding number n , which characterizes the different vacuum gauge configurations that cannot be continuously rotated into each other. The vacuum state of the theory is a superposition of all the degenerate states $|n\rangle$, called the Θ -vacuum,

$$|\Theta\rangle = \sum_n \exp(-in\Theta) |n\rangle, \quad (2.26)$$

where Θ is an arbitrary parameter, and n the topological winding number. The effects of the Θ -vacuum can be described via an additional non-perturbative term in the Lagrange density of QCD,

$$\mathcal{L}_{\text{QCD}} = \mathcal{L}_{\text{pert}} + \bar{\Theta} \frac{g^2}{32\pi^2} G^{a\mu\nu} \tilde{G}_{a\mu\nu}, \quad (2.27)$$

$$\bar{\Theta} = \Theta + \text{Arg det } \mathcal{M}, \quad (2.28)$$

2.3. CANDIDATES FOR DARK MATTER

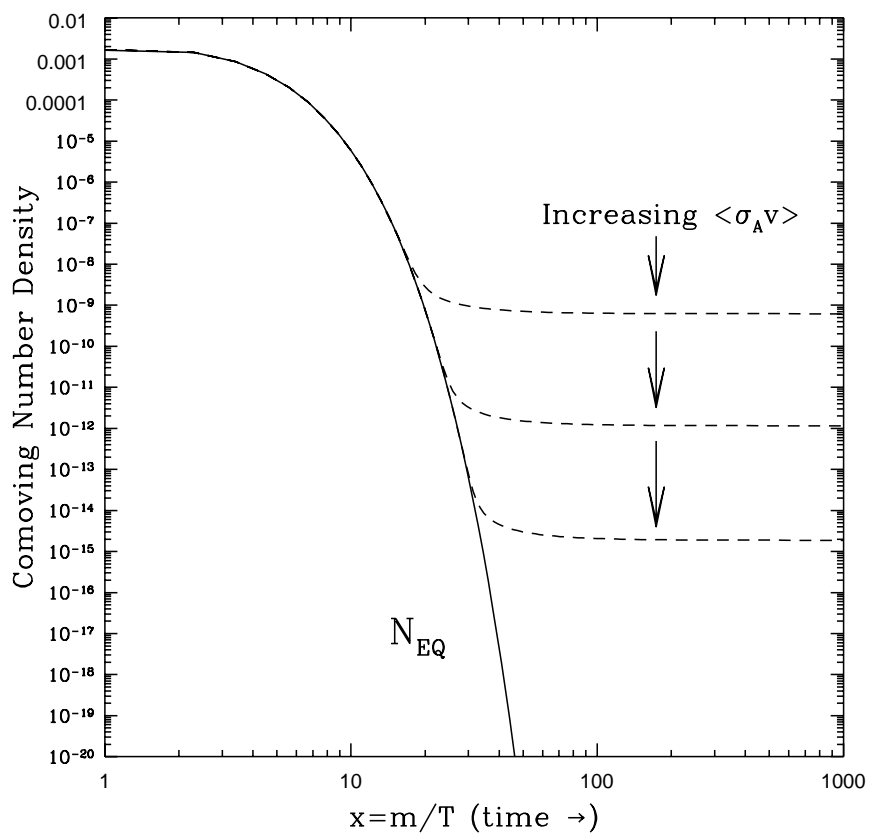


Figure 2.6: Evolution of a typical WIMP comoving number density in the early Universe. The dashed line is the actual abundance, and the solid line is the equilibrium abundance [28].

where G is the gluon field strength tensor, \tilde{G} is the corresponding dual tensor and \mathcal{M} is the quark mass matrix. The second term in equation (2.27) violates CP, T and P. This leads to a contribution to the electric dipole moment of the neutron of

$$d_n \simeq 5 \times 10^{-16} \bar{\Theta} e \text{ cm} \quad (2.29)$$

in contrast to experimental results, which gives an upper limit of

$$d_n < 1.2 \times 10^{-25} e \text{ cm}. \quad (2.30)$$

This implies a $\bar{\Theta} \leq 10^{-10}$, which could even be exactly zero. Why the $\bar{\Theta}$ -parameter in QCD is so small is known as the strong CP problem.

The most favored solution to this problem is the one proposed by Peccei and Quinn in 1977 [31]. By introducing a new global (chiral) symmetry (known as PQ symmetry), the $\bar{\Theta}$ -parameter can be made a dynamical variable, whose minimum energy value lies at zero. PQ symmetry is spontaneously broken at an energy scale f_a , which gives rise to a new particle, a Nambu-Goldstone boson called the axion (a), as pointed out by Weinberg [29] and Wilczek [30] in 1978. The introduction of an additional field, the axion field a , leads to a further term in the Lagrange density:

$$\mathcal{L} = \dots + C_a \frac{a}{f_a} \frac{g^2}{32\pi^2} G_a^{\mu\nu} \tilde{G}_{\mu\nu}^a, \quad (2.31)$$

where C_a is a model dependent constant. Since equations (2.27) and (2.31) both contribute to the axion field, it can be minimized or set to zero by

$$\langle a \rangle = -\frac{\bar{\Theta} f_a}{C_a}, \quad (2.32)$$

compensating the troublesome term in equation (2.27).

Axions are pseudoscalar particles, similar to neutral pions. They can mix with the neutral pions through axion-gluon interactions that allows for transitions to $q\bar{q}$ states. As a result of this mixing, the axion picks up a small mass of [32]

$$m_a = \frac{f_\pi m_\pi}{f_a} \left(\frac{z}{(1+z+w)(1+z)} \right)^{1/2} = 0.60 \text{ eV} \frac{10^7 \text{ GeV}}{f_a}, \quad (2.33)$$

where $m_\pi = 135 \text{ MeV}$ is the neutral pion mass and $f_\pi = 93 \text{ MeV}$ is the pion decay constant. The quark mass ratios are

$$z \equiv m_u/m_d = 0.568 \pm 0.042, \quad (2.34)$$

2.3. CANDIDATES FOR DARK MATTER

$$w \equiv m_u/m_s = 0.0290 \pm 0.0043. \quad (2.35)$$

The axion has only one free parameter, the mass m_a . The mass and all interactions scale with the inverse of the energy scale of PQ breaking, f_a^{-1} . This allows the axions to be arbitrarily light and arbitrarily weakly interacting (“invisible” axions) [32].

At high temperatures, $T > \Lambda_{\text{QCD}}$, where $\Lambda_{\text{QCD}} = (100 - 250)$ MeV characterizes the chiral QCD phase transition, the axions can not obtain mass by pion mixture because pions do not exist. But below $T \simeq f_a$ the PQ-symmetry is broken and a massless axion is produced because of QCD instanton effects [32]. The temperature dependence of the axion mass is given by [7]

$$m_a(T) \simeq 0.1m_a(T=0)(\Lambda_{\text{QCD}}/T)^{3.7}, \quad (2.36)$$

valid for $\pi T/\Lambda_{\text{QCD}} \gg 1$.

Axions can be produced by both non-thermal and thermal mechanisms. A non-thermal axion is the most important dark matter candidate. If thermal axions existed in numbers sufficient to make up the dark matter, they would have lifetimes too short to still be around in sufficient quantity. There are two production processes for non-thermal axions; through coherent production due to an initial misalignment of the axion field at early times [33, 34, 35], and through the decay of axionic strings [36, 37]. If the Universe underwent inflation, non-thermal axions are produced in the misalignment process. But if the Universe did not inflate, axionic string decay is the production mechanism.

In the misalignment production the initial value of $\bar{\Theta}$ is different from zero, since no special value of $\bar{\Theta}$ is dynamically preferred. Because the axion is massless before the quark-hadron phase transition, all values of $\bar{\Theta}$ are equally acceptable. At early times, the axion field is misaligned with the minimum of its potential, $\bar{\Theta} = 0$. When the axion acquires a mass around a temperature of $T \sim \Lambda_{\text{QCD}}$, (and becomes comparable to the expansion rate of the Universe), the axion field will start to roll toward $\bar{\Theta}$, and end up oscillating around the minimum. These cosmic oscillations produce a zero-momentum condensate of axions, which could constitute the cold dark matter. The axion contribution to the density due to this process is estimated to be [7]

$$\Omega h^2 = 0.85 \times 10^{\pm 0.4} \left(\frac{\Lambda_{\text{QCD}}}{200 \text{ MeV}} \right)^{-0.7} \left(\frac{m_a}{10^{-5} \text{ eV}} \right)^{-1.18}. \quad (2.37)$$

The production of axions through the decay of axionic strings is more complex. One-dimensional defects — strings — arise when a $U(1)$ gauge

symmetry is spontaneously broken. They also arise when a global $U(1)$ symmetry is broken, $U(1)_{PQ}$ in this case. The axionic strings dissipates its energy by radiation of axions. The contribution to the density from this process is [7]

$$\Omega h^2 \simeq \left(\frac{m_a}{10^{-3} \text{ eV}} \right)^{-1.18}. \quad (2.38)$$

These two non-thermal processes leads to a lower mass limit of about 10^{-3} or 10^{-5} eV in order to reach a significant density in the Universe. A light axion is a possible CDM candidate if $m_a \lesssim 2$ eV [32].

Superheavy dark matter

Other candidates in the dark matter particle zoo are supermassive X particles. Such particles go under the name of superheavy dark matter (SHDM). If such a particle is weakly interacting it can be called *wimpzilla*, or *simpzilla* if it interacts strongly. The stability of X particles can be ensured by discrete gauge symmetries, which must be somehow weakly broken if we want long-lived particles with lifetime $\tau_X \gtrsim t_0$, where t_0 is the age of the Universe.

A superheavy particle must be a non-thermal relic in order to fulfill $\Omega_0 \sim 1$. The abundance of a thermal relic depends on the inverse of its annihilation cross section, which again is inversely proportional to the mass squared. Superheavy thermal relics will then decouple early in the Universe, and their present abundance will be far too large, cf. figure 2.6.

Being non-thermal relics, X particles have never been in chemical equilibrium with radiation. It is likely that they were produced at the end of inflation, when it is enough to transfer only a small fraction from the energy of radiation to SHDM particles. In order to have the observed density of dark matter, $\Omega_{dm} = 0.20$, a fraction of energy less than 10^{-18} is needed [38]. This tiny fraction of energy can be transferred to X particles in many ways, such as production by topological defects, thermal production at reheating, preheating and by gravitational production [38, 39].

The most elegant production mechanism for SHDM is its gravitational production [40, 41]. In this mechanism, superheavy particles are produced gravitationally at the end of inflation in the early Universe, naturally achieving the desired abundance of SHDM. What makes this mechanism so elegant is that it is quite model independent. It can generate particles with mass of the order of the inflaton mass even when the SHDM only interacts extremely weakly with other particles, including the inflaton. This mechanism is similar to the generation of gravitational perturbations during inflation, which causes the formation of large scale structures. The X particles are created as a result of time-variable gravitational fields acting on vacuum fluctuations

2.3. CANDIDATES FOR DARK MATTER

during the transition from the inflationary phase to a matter or radiation dominated phase. Assuming that the Universe is flat, a scalar field (particle) X of mass m_X in the expanding Universe can be expanded in spatial Fourier modes as [39]

$$X(\vec{x}, \eta) = \int \frac{d\mathbf{k}}{(2\pi)^{3/2}a(\eta)} [a_k \phi_k(\eta) e^{i\vec{k}\cdot\vec{x}} + a_k^\dagger \phi_k^*(\eta) e^{-i\vec{k}\cdot\vec{x}}], \quad (2.39)$$

where η is the conformal time⁴ and $a(\eta)$ the time dependence of the expansion scale factor. Here a_k and a_k^\dagger are creation and annihilation operators, and $\phi_k(\eta)$ are mode functions. The Klein-Gordon equation for the field modes ϕ_k of a scalar field in a Friedman-Robertson-Walker Universe can be written as

$$\ddot{\phi}_k(\eta) + m_{\text{eff}}^2(\eta) \phi_k(\eta) = 0, \quad (2.40)$$

where the effective mass is

$$m_{\text{eff}}^2(\eta) = k^2 + M_X^2 a^2 + (6\xi - 1) \frac{\ddot{a}}{a}. \quad (2.41)$$

The parameter ξ is $\xi = 0$ for a minimally-coupled field and $\xi = \frac{1}{6}$ for a conformally-coupled field. Since m_{eff} is time dependent, vacuum fluctuations will be transformed into real particles. Thus, the expansion of the Universe leads to particle production [40].

The predicted density of X particles in inflationary cosmology is

$$\Omega_X h^2 = \left(\frac{M_X}{10^{11} \text{ GeV}} \right)^2 \frac{T_{RH}}{10^9 \text{ GeV}}, \quad (2.42)$$

where M_X is the mass of the X particle and T_{RH} is the temperature at reheating. This result is independent on details of particle physics, and is valid for any $M_X \lesssim H_I$, where $H_I \sim m_\phi \sim 10^{13}$ GeV is the Hubble constant at the end of inflation and m_ϕ is the mass of the inflaton.

The existence of superheavy dark matter was first suggested [42, 43] to explain the puzzle of ultrahigh energy cosmic rays. High energy cosmic rays are particles, most likely protons, from extragalactic sources. Very energetic protons should gradually lose energy from colliding with photons and creating pions, when propagating in the cosmic microwave background. This process has an effective threshold energy of 5×10^{19} eV, called the Greisen-Zatsepin-Kuzmin (GZK) cutoff [44, 45]. Above this cutoff, the proton energy loss

⁴In general, the conformal distance η is the distance away that is not causally connected to the observer. The conformal distance η in a FRW Universe at a cosmic time t is given by $\eta = \int^t \frac{dt'}{a(t')}$, which can also be thought of as a time variable [27].

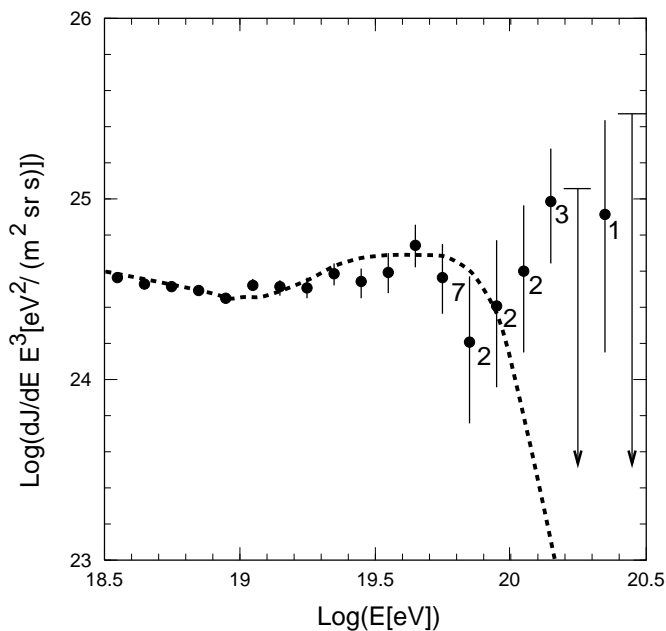


Figure 2.7: Energy spectrum of cosmic rays observed with AGASA. The dashed curve displays the theoretical GZK cutoff. (The numbers attached to the data points show the number of events observed in each energy bin.) [47]

length is near 10 Mpc. Thus, particles with energies above this cutoff should be produced within our local neighborhood. Observations made by the Fly's Eye Cosmic Ray Detector [46] and later by the Akeno Giant Air Shower Array (AGASA) [47] have determined that the spectrum of the highest energy cosmic rays extends beyond 10^{20} eV, as shown in figure 2.7. The trouble with these observations is that no astrophysical sources has been found in the direction of the observed events. Thus the origin of these ultrahigh energy cosmic rays remains a puzzle. A possible explanation is the decay or annihilations of supermassive particles, creating the highest energy cosmic rays.

If the gravitational production is the sole mechanism for producing X particles that has a density of today of the order of the critical density, then $0.04 \lesssim M_X/H_I \lesssim 2$ [39]. This agrees with the mass of X particles, $M_X \gtrsim 10^{13}$ GeV, in order to produce cosmic rays of energies $E \gtrsim 10^{11}$ GeV [42]. If the X particles are to play the role of cold dark matter and be the source of UHE cosmic rays, the lifetime must be of the order $\tau_X \sim 10^{22}$ years [41].

“For every complex natural phenomenon there is a simple, elegant, compelling, but wrong explanation.”

Thomas Gold

3

The Minimal Supersymmetric Standard Model

The Standard Model of particle physics is the $SU(3)_C \otimes SU(2)_L \otimes U(1)_Y$ gauge theory of the strong, weak and electromagnetic interactions. The $SU(3)_C$ part describes the strong (color) interaction and is known as quantum chromodynamics (QCD), while the $SU(2)_L \otimes U(1)_Y$ describes electroweak interaction. Here C refers to color, L to left and Y to weak hypercharge.

As already mentioned, all dark matter candidates, apart from the neutrinos, cannot be explained by the Standard Model of particle physics (SM). This is one of the reasons why many physicists now turn to the possibilities for physics beyond the Standard Model, where our Standard Model is the low-energy limit of a more fundamental theory [11]. One extension of the Standard Model is the idea of supersymmetry. Supersymmetry is an extra symmetry between fermions and bosons: every spin- $\frac{1}{2}$ fermion has a supersymmetric spin-0 partner while every spin-1 boson has a spin- $\frac{1}{2}$ partner. The supersymmetric partner of the graviton (spin-2) is the gravitino (spin- $\frac{3}{2}$). This theory was not intended to solve the dark matter problem, but it turns out that it can provide excellent particle candidates nevertheless, depending on which supersymmetric theory one has in mind.

One of these theories is the Minimal Supersymmetric Standard Model (MSSM), which is the simplest possible supersymmetric extension of the Standard Model. It was first introduced in 1981 by Howard Georgi and Savas Dimopoulos to solve the *hierarchy problem*. By introducing supersymmetry in the Standard Model, we get a doubling of all the known particles. The nomenclature for new particles is quite simple. The names for the scalar superpartners of the fermions is obtained by adding a prefix “s”, e.g. the spin-0 partners of the quarks and leptons are called squarks and sleptons.

The supersymmetric partners of the vector bosons receive the ending “-ino” to the name of the Standard Model particle. To distinguish the supersymmetric particles from the Standard Model particles, we add a tilde to the symbol.

3.1 Motivational reasons for Supersymmetry

There are several motivations for introducing supersymmetry. One is the coupling constant unification. The coupling constants of the strong, weak and electromagnetic interactions change as the momentum transfer of the interaction increases. They meet only approximately in the Standard Model, but they meet almost together in one point around 10^{16} GeV in the MSSM, allowing a “Grand Unification” of the strong, weak and electromagnetic interactions, as shown in figure 3.1 [48].

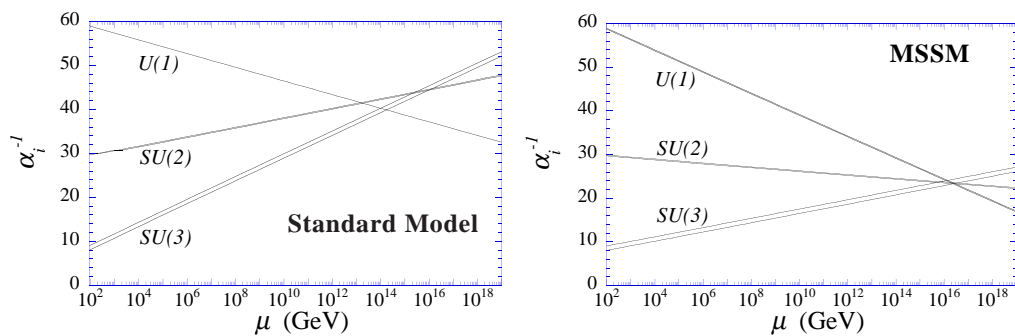


Figure 3.1: The running of the gauge coupling constants in the Standard Model and in the MSSM [48].

Another reason for introducing supersymmetry is its role in understanding the *hierarchy problem*, which is linked to the enormous difference between the electroweak and Planck energy scales. This problem arises in the radiative corrections to the mass of the Higgs boson [11]. All the Standard Model particles, except for the Higgs boson, acquire their masses via spontaneous symmetry breaking of the electroweak gauge symmetry. The mass of the Higgs boson is a free parameter. Estimates from data gathered so far favor the mass to be around 100 GeV, with an upper limit of 200 GeV. Theoretically though, the mass should be closer to the Planck scale. Due to quantum effects, the Higgs boson will receive enormous corrections to its mass from the virtual effects of every particle that couples to the Higgs field. This huge discrepancy in the mass is known as the *hierarchy problem*. Supersymmetry provide an elegant remedy for this problem. The small Higgs mass is guaranteed by cancellations of the radiative corrections; for every loop of particles

providing a correction to the Higgs mass, there is a loop of virtual superparticles that cancels it. This ensures that the hierarchy of energy scales is maintained.

3.2 *R*-parity

Baryon and lepton numbers are approximately conserved quantities in the Standard Model¹, but they are no longer conserved by all of the renormalizable couplings in the supersymmetric extension. This has for instance a most undesirable effect on the limit of the decay time of the proton, which is known experimentally to be in excess of 10^{32} years. Without baryon and lepton number being conserved, a decay process like $p^+ \rightarrow e^+ \pi^0$, mediated by a strange squark, would be possible. With the couplings to the squark present and unsuppressed, the proton would decay in a fraction of a second.

In order to prevent such a rapid proton decay, we impose a new, discrete symmetry in the MSSM, which sets all of the renormalizable baryon and lepton number violating couplings to zero. This symmetry is known as *R*-parity [49]. The *R*-parity is an additional multiplicative quantum number defined for each particle as

$$R_p = (-1)^{3B+L+2s}, \quad (3.1)$$

where B is the baryon number, L is the lepton number and s is the spin. The Standard Model particles and Higgs bosons have even *R*-parity ($R_p = +1$), while all their superpartners have odd *R*-parity ($R_p = -1$). Conservation of *R*-parity implies that

1. supersymmetric particles can only be created or annihilated in even numbers. This means that a single supersymmetric particle cannot disappear by decaying into ordinary particles only,
2. heavy supersymmetric particles decay into lighter supersymmetric particles,
3. the lightest particle with odd *R*-parity, i.e. the lightest supersymmetric particle (LSP) must be absolutely stable since it has no allowed state to decay into without violating *R*-parity. The LSP turns out to be an excellent candidate for cold dark matter.

¹Non-perturbative effects, like chiral anomalies, violate conservations of baryon and lepton numbers.

R -parity leads to important consequences for collider phenomenology and cosmology. Pairwise superparticles produced in collider experiments decay eventually into the LSP, which escapes detection. Typical signature of supersymmetry at collider experiments is the missing energy or momentum [48].

3.3 Supersymmetry algebra

The mathematical formalism describing the relation between bosons and fermions is in the supersymmetry algebra. A supersymmetry transformation turns a bosonic state into a fermionic state, and vice versa [50]. Symmetry in physics refer to a group of transformations that leaves the Lagrangian invariant. A global supersymmetry extends the normal Poincaré algebra for the description of spacetime with an extra generator. The generator Q of such transformations must be an anticommuting spinor, with

$$Q|\text{Boson}\rangle = |\text{Fermion}\rangle, \quad Q|\text{Fermion}\rangle = |\text{Boson}\rangle. \quad (3.2)$$

The generator Q^α is fermionic, i.e. it has spin $\frac{1}{2}$. It changes spin by $\frac{1}{2}$.

The simplest case of supersymmetry involves only one fermionic (2-component Weyl spinor) generator Q_α and its conjugate $\bar{Q}_{\dot{\beta}}$. Theories that have more than one distinct copies of $Q_\alpha, \bar{Q}_{\dot{\beta}}$ are called extended supersymmetries. Such models have no phenomenological prospect in four-dimensional field theories, since they cannot allow for chiral fermions or parity violation as observed in the Standard Model [50]. The phenomenological viable theory is the non-extended type of supersymmetric model. This model is called $N = 1$ supersymmetry, with N referring to the number of supersymmetries (the number of distinct copies of Q_α and its conjugate $\bar{Q}_{\dot{\beta}}$).

The generators Q_α and $\bar{Q}_{\dot{\beta}}$ must satisfy an algebra of commutation and anticommutation relations with the form

$$[P_\mu, Q_\alpha] = [P_\mu, \bar{Q}_{\dot{\beta}}] = 0, \quad (3.3)$$

$$\{Q_\alpha, Q_\beta\} = \{\bar{Q}_{\dot{\alpha}}, \bar{Q}_{\dot{\beta}}\} = 0, \quad (3.4)$$

$$\{Q_\alpha, \bar{Q}_{\dot{\beta}}\} = 2(\sigma^\mu)_{\alpha\dot{\beta}}P_\mu, \quad (3.5)$$

where P^μ is the four-momentum generator (operator) of spacetime translations, and $\sigma^\mu = (1, \sigma_i)$ with σ_i being the Pauli matrices. The indices α, β of Q and $\dot{\alpha}, \dot{\beta}$ of \bar{Q} take values 1 or 2. Spinors with undotted indices (the first two components of a Dirac spinor) transform according to $(\frac{1}{2}, 0)$ -representation of the Lorentz group, while spinors with dotted indices (the last two components of a Dirac spinor) transform according to $(0, \frac{1}{2})$ -representation.

3.4 The particle content of the MSSM

All particles in supersymmetric theories fall into irreducible representations of the supersymmetry algebra, called supermultiplets. These supermultiplets have both bosonic and fermionic components (states), which are known as superpartners of each other.

For each fermionic state there is a bosonic state with the same mass. This can be seen if we consider a fermionic state $|f\rangle$ with mass m . The bosonic state is $|b\rangle = Q_\alpha|f\rangle$. Then

$$P^2|f\rangle = m^2|f\rangle \quad (3.6)$$

$$\Rightarrow P^2|b\rangle = P^2Q_\alpha|f\rangle = Q_\alpha P^2|f\rangle = Q_\alpha m^2|f\rangle = m^2|b\rangle. \quad (3.7)$$

The squared mass operator P^2 commutes with the operators Q_α , $\bar{Q}_{\dot{\beta}}$, and with all spacetime rotation and translation operators, which means that particles inhabiting the same irreducible supermultiplet must have equal eigenvalues of P^2 , and therefore equal masses.

Particles in the same supermultiplet must also be in the same representation of the gauge group since the generators Q_α , $\bar{Q}_{\dot{\beta}}$ also commute with the generators of gauge transformations. The particles must then have the same electrical charges, weak isospin and color degrees of freedom [50].

Another property of supermultiplets is that they contain equal number of fermion and boson degrees of freedom,

$$n_B = n_F. \quad (3.8)$$

There are two types of supermultiplets which appear in renormalizable field theories; chiral and vector supermultiplets. The simplest possibility for a supermultiplet consistent with equation (3.8) has a single Weyl fermion and two real scalars. The Weyl fermion has two spin helicity states, so that $n_F = 2$, while the two real scalars have $n_B = 1$ each. The two real scalar degrees of freedom is usually assembled into a complex scalar field. The combination of a two-component Weyl fermion and a complex scalar field is called a *chiral* or *matter* or *scalar* supermultiplet. The chiral multiplets in the MSSM are shown in table 3.1.

Only chiral supermultiplets can contain fermions whose left-handed components transform differently under $SU(2) \times U(1)_Y$ than their right-handed components [50]. The Standard Model fermions are chiral, so they must be members of chiral supermultiplets. For each fermion there are two sfermions, corresponding to the superpartners of the right-handed and left-handed components of the fermion. The sfermions get either a subscript R or L , which

3. THE MINIMAL SUPERSYMMETRIC STANDARD MODEL

Particles	spin 0	spin $\frac{1}{2}$	$SU(3)_C \times SU(2)_L \times U(1)_Y$
squarks, quarks ($\times 3$ families)	$(\tilde{u}_L, \tilde{d}_L)$	(u_L, d_L)	$(3, 2, \frac{1}{6})$
	\tilde{u}_R^*	u_R^\dagger	$(\bar{3}, 1, -\frac{2}{3})$
	\tilde{d}_R^*	d_R^\dagger	$(\bar{3}, 1, \frac{1}{3})$
sleptons, leptons ($\times 3$ families)	$(\tilde{\nu}, \tilde{e}_L)$	(ν, e_L)	$(1, 2, -\frac{1}{2})$
	\tilde{e}_R^*	e_R^\dagger	$(1, 1, 1)$
Higgs, higgsinos	$(H_u^+ H_u^0)$	$(\tilde{H}_u^+ \tilde{H}_u^0)$	$(1, 2, +\frac{1}{2})$
	$(H_d^0 H_d^-)$	$(\tilde{H}_d^0 \tilde{H}_d^-)$	$(1, 2, -\frac{1}{2})$

Table 3.1: Chiral supermultiplets in the Minimal Supersymmetric Standard Model.

Particles	spin $\frac{1}{2}$	spin 1	$SU(3)_C \times SU(2)_L \times U(1)_Y$
gluino, gluon	\tilde{g}	g	$(8, 1, 0)$
winos, W bosons	$\tilde{W}^\pm \tilde{W}^0$	$W^\pm W^0$	$(1, 3, 0)$
bino, B boson	\tilde{B}^0	B^0	$(1, 1, 0)$

Table 3.2: Gauge supermultiplets in the Minimal Supersymmetric Standard Model.

refers to the right or left handedness, respectively, of the Standard Model fermions. The neutrinos are always left-handed if we neglect their small masses, so this nomenclature does not apply to sneutrinos. The gauge interactions of squark and slepton fields are the same as for the corresponding Standard Model fermions [50].

A slightly more complicated possibility for a supermultiplet contains a spin-1 vector boson. This must be a massless gauge boson if the theory is to be renormalizable. Such a gauge boson has two helicity states, i.e. $n_B = 2$. Its corresponding superpartner is therefore a massless spin- $\frac{1}{2}$ Weyl fermion with two helicity states, i.e. $n_F = 2$. A massless spin- $\frac{3}{2}$ superpartner is not possible, since the theory would not be renormalizable.

The fermionic partners of the gauge bosons are called gauginos. Like their Standard Model partners, they transform as the adjoint representation of the gauge group. The right- and left-handed components follow the same gauge transformation properties, since the adjoint representation of a gauge group is always its conjugate [50]. A combination of spin- $\frac{1}{2}$ gauginos and spin-1 gauge bosons is called a *gauge* or *vector* supermultiplet. The gauge multiplet in the MSSM is shown in table 3.2.

3.4. THE PARTICLE CONTENT OF THE MSSM

The most important technical difference from the Standard Model is in the Higgs sector. As opposed to the one doublet required in the Standard Model, the Higgs sector is required to contain two complex Higgs doublets, leaving eight degrees of freedom before the symmetry breaking. Three of these states disappear as the longitudinal components of the weak gauge bosons (W^+ , W^- and Z) after the usual Higgs mechanism. The five physical states left are the two neutral scalar (CP -even) Higgs particles H^0 and h^0 (where h^0 is the lighter state by convention), one neutral pseudoscalar (CP -odd) state A^0 , and two charged scalars H^\pm .

The superpartners of the charged W bosons (W^+ , W^-) and charged Higgs bosons, the charged winos and the charged higgsino, carry the same $SU(3)_C \times U(1)_{EM}$ quantum numbers. They will in general mix after electroweak-symmetry breaking, the breaking of $SU(2) \times U(1)_Y$. This results in two mass eigenstates that are linear combinations called charginos.

The spin- $\frac{1}{2}$ superpartners of the spin-1 gauge bosons W^0 and B^0 are the wino \tilde{W}^0 and the bino \tilde{B}^0 . After electroweak symmetry breaking, the W^0 , B^0 gauge eigenstates mix to give mass eigenstates Z^0 and γ . The corresponding gaugino mixtures of \tilde{W}^0 and \tilde{B}^0 are called zino (\tilde{Z}^0) and photino ($\tilde{\gamma}$). Together with neutral Higgs bosons, these states mix into four Majorana fermionic mass eigenstates called neutralinos. The neutralinos are labeled $\tilde{\chi}_1^0, \tilde{\chi}_2^0, \tilde{\chi}_3^0, \tilde{\chi}_4^0$, ordered with increasing mass. An overview of the Standard Model particles and fields and their supersymmetric partners is presented in figure 3.3.

Supersymmetry is obviously a broken symmetry. An exact supersymmetry requires particles and sparticles to have the same mass. No supersymmetric particles with masses like that of their Standard Model partner has been seen. The scale of supersymmetry breaking is expected to be of order the weak scale. This assumption is necessary to stabilize the weak scale. The mass difference between particles and their superpartners should be less than about 10^3 GeV:

$$|m_{\text{particle}}^2 - m_{\text{superpartner}}^2| < (10^3 \text{ GeV})^2. \quad (3.9)$$

There is no firm experimental evidence for supersymmetric particles. This means that their rest energies, if they exist, lie beyond the range currently probed by accelerators, or that they are very weakly coupled.

Normal particles/fields			Supersymmetric partners					
Symbol	Name	Spin	Interaction eigenstates		Mass eigenstates			
			Symbol	Name	Symbol	Name	Spin	
$q = d, c, b, u, s, t$	quark	$\frac{1}{2}$	\tilde{q}_L, \tilde{q}_R	squark	\tilde{q}_1, \tilde{q}_2	squark	0	
$l = e, \mu, \tau$	lepton	$\frac{1}{2}$	\tilde{l}_L, \tilde{l}_R	slepton	\tilde{l}_1, \tilde{l}_2	slepton	0	
$\nu = \nu_e, \nu_\mu, \nu_\tau$	neutrino	$\frac{1}{2}$	$\tilde{\nu}$	sneutrino	$\tilde{\nu}$	sneutrino	0	
g	gluon	1	\tilde{g}	gluino	\tilde{g}	gluino	$\frac{1}{2}$	
W^\pm	W -boson	1	\tilde{W}^\pm	wino	}	$\tilde{\chi}_{1,2}^\pm$	chargino	$\frac{1}{2}$
H^-	Higgs boson	0	\tilde{H}_1^-	higgsino				
H^+	Higgs boson	0	\tilde{H}_2^+	higgsino				
B	B -field	1	\tilde{B}	bino	}	$\tilde{\chi}_{1,2,3,4}^0$	neutralino	$\frac{1}{2}$
W^0	W^0 -field	1	\tilde{W}^0	wino				
h^0	Higgs boson	0	\tilde{h}^0	higgsino				
H^0	Higgs boson	0	\tilde{H}^0	higgsino				
A^0	Higgs boson	0						
G	graviton	2	\tilde{G}	gravitino	\tilde{G}	gravitino	$\frac{3}{2}$	

Table 3.3: Particles and their superpartners in the MSSM. Adapted from [51].

3.4.1 Neutralinos

The mixtures of the neutral gaugino states form four distinct Majorana fermions, called neutralinos. In contrast to the usual Dirac fermion, a Majorana fermion is a particle which is its own antiparticle. Thus, neutralinos can annihilate with themselves.

The neutralinos are eigenstates of a symmetric mass matrix. The neutralino mass matrix in the gauge-eigenstate basis $\psi^0 = (\tilde{B}, \tilde{W}^0, \tilde{h}^0, \tilde{H}^0)$ is given by [52]

$$\mathcal{M}_N = \begin{pmatrix} M_1 & 0 & -m_Z c_\beta s_W & m_Z s_\beta s_W \\ 0 & M_2 & m_Z c_\beta c_W & -m_Z s_\beta c_W \\ -m_Z c_\beta s_W & m_Z c_\beta c_W & 0 & -\mu \\ m_Z s_\beta s_W & -m_Z s_\beta c_W & -\mu & 0 \end{pmatrix}, \quad (3.10)$$

where M_1, M_2 and μ are the bino, wino and higgsino mass parameters, respectively, m_Z is the mass of the Z -boson, θ_W is the Weinberg angle and $\tan\beta$ is the ratio of the vacuum expectation values of the Higgs bosons. Here $c_\beta = \cos\beta$, $s_\beta = \sin\beta$, $c_W = \cos\theta_W$ and $s_W = \sin\theta_W$. The mass matrix is symmetric because of the Majorana nature of the neutralinos, for which we have the following identity for anticommuting four-component Majorana spinors [52]:

$$\bar{\tilde{\chi}}_j^0(1 \pm \gamma_5)\tilde{\chi}_k^0 = \bar{\tilde{\chi}}_k^0(1 \pm \gamma_5)\tilde{\chi}_j^0. \quad (3.11)$$

In order to obtain mass eigenstates the symmetric matrix \mathcal{M}_N can be diagonalized by a unitary mixing matrix, N_{ij} where the indices i and j are mass and gauge eigenstate labels respectively. Only one diagonalizing matrix is required since \mathcal{M}_N is symmetric. The four-component mass-eigenstates are defined as

$$\tilde{\chi}_i^0 = N_{ij}\psi_j^0, \quad i, j = 1, \dots, 4, \quad (3.12)$$

or

$$\begin{pmatrix} \tilde{\chi}_1^0 \\ \tilde{\chi}_2^0 \\ \tilde{\chi}_3^0 \\ \tilde{\chi}_4^0 \end{pmatrix} = N \begin{pmatrix} \tilde{B} \\ \tilde{W}^0 \\ \tilde{h}^0 \\ \tilde{H}^0 \end{pmatrix}, \quad (3.13)$$

where N satisfies:

$$N^* \mathcal{M}_N N^{-1} = N_D. \quad (3.14)$$

3. THE MINIMAL SUPERSYMMETRIC STANDARD MODEL

Here N_D is the diagonal neutralino mass matrix. The result of the diagonalization of \mathcal{M} must have real positive entries on the diagonal:

$$N_D = \begin{pmatrix} m_{\tilde{\chi}_1^0} & 0 & 0 & 0 \\ 0 & m_{\tilde{\chi}_2^0} & 0 & 0 \\ 0 & 0 & m_{\tilde{\chi}_3^0} & 0 \\ 0 & 0 & 0 & m_{\tilde{\chi}_4^0} \end{pmatrix}, \quad (3.15)$$

The $m_{\tilde{\chi}_i^0}$, $i = 1, \dots, 4$, are the (non-negative) masses of the physical neutralino states with $m_{\tilde{\chi}_1^0} < \dots < m_{\tilde{\chi}_4^0}$. The lightest neutralino — the lowest-lying mass eigenstate of the two gauginos and the two higgsinos — is then decomposed as

$$\tilde{\chi}_1^0 = N_{11}\tilde{B} + N_{12}\tilde{W}^0 + N_{13}\tilde{h}^0 + N_{14}\tilde{H}^0. \quad (3.16)$$

The coefficients N_{ij} are the entries of the neutralino mixing matrix. They are normalized such that

$$\sum_{j=1}^4 |N_{ij}|^2 = 1, \quad i = 1, 2, 3, 4. \quad (3.17)$$

The lightest neutralino is the most likely LSP in the MSSM [21], which is why they are among the most widely studied dark matter candidates. We will from now on call the lightest neutralino for just the neutralino.

The minimal supersymmetric model has 63 free parameters with real mass matrices and couplings. To make the MSSM more easy to handle, we assume a common value for the masses of scalar fermions and the trilinear couplings ($M_{SUSY} = m_{\tilde{f}} = A_f$) [53].

The most relevant of the remaining free parameters are the $SU(2)$ gaugino mass (M_2), the Higgs mixing parameter (μ), the ratio of vacuum expectation values (VEVs) of Higgs fields ($\tan\beta \equiv v_2/v_1$) and the CP-odd Higgs-boson mass (m_A).

The dimensionality in parameter space can be further reduced. Since the gauge couplings in the MSSM apparently unifies at $Q = M_{GUT} = 2 \times 10^{16}$ GeV, it is assumed that the gaugino masses also unify near that scale. This value is called $m_{1/2}$. It then follows that

$$\frac{M_1}{g_1^2} = \frac{M_2}{g_2^2} = \frac{M_3}{g_3^2} = \frac{M_{1/2}}{g_{GUT}^2} \quad (3.18)$$

valid up to small two-loop effects and possible much larger threshold effects near M_{GUT} [50]. Here g_{GUT} is the unified gauge coupling at $Q = M_{GUT}$. This leads to the GUT-relation

$$M_1 \approx \frac{5}{3} \tan^2 \theta_W M_2 \approx 0.5 M_2 \quad (3.19)$$

3.4. THE PARTICLE CONTENT OF THE MSSM

at the electroweak scale. Taking this assumption into account, the neutralino masses and mixing angles depend on only three unknown parameters.

The values of the four parameters M_1, M_2, μ and $\tan\beta$ determine the masses and mixing angles of the neutralinos. If $|\mu| \gg M_2 \gg M_Z$, the two lightest neutralino states will be dominated by the gaugino components, with $\tilde{\chi}_1^0$ being mostly \tilde{B} and $\tilde{\chi}_2^0$ being mostly \tilde{W}^0 . Such neutralinos will annihilate mostly into heavy quarks [53]. For $|\mu| \ll |M_1|$, the two lightest neutralino is dominated by the higgsino components, $\tilde{\chi}_1^0, \tilde{\chi}_2^0 \sim (\tilde{H}_u^0 \pm \tilde{H}_d^0)/\sqrt{2}$ with masses close to $|\mu|$. Such neutralinos will annihilate mostly into gauge bosons. If $|\mu| \simeq |M_2|$, some of the states will be strongly mixed. The size of the mixing also depends to some extent on $\tan\beta$.

The bino (f_B) and wino (f_W) fraction is defined as

$$f_B = |N_{11}|^2, f_W = |N_{12}|^2, \quad (3.20)$$

or combined, as the gaugino fraction (f_g)

$$f_g = |N_{11}|^2 + |N_{12}|^2. \quad (3.21)$$

The higgsino (f_H) fraction is defined as

$$f_H = |N_{13}|^2 + |N_{14}|^2. \quad (3.22)$$

Despite the many free parameters present in SUSY theories, the state that seems to most naturally give $\Omega_\chi h^2 \sim 1$ is the nearly pure bino. The higgsino disfavored out because of the efficient annihilation to $WW, ZZ, \bar{t}t$ and coannihilation, which typically gives $\Omega_\chi h^2 \ll 1$.

“All men by nature desire to know. An indication of this is the delight we take in our senses; for even apart from their usefulness they are loved for themselves; and above all others the sense of sight. For not only with a view to action, but even when we are not going to do anything, we prefer sight to almost everything else. The reason is that this, most of all the senses, makes us know and brings to light many differences between things.”

Aristotle

4

Indirect detection

Indirect detection of dark matter is the technique of observing the products produced in dark matter particle-antiparticle annihilation or dark matter decays. There are several proposed methods of detecting these products. One of the most discussed method is looking for signals from neutralino annihilation at the galactic center or from the core of the Sun or the Earth. We will however, investigate the probability of detecting high energy neutrinos and neutralinos from decays of superheavy dark matter.

4.1 Decay of superheavy dark matter

It is possible that decays of superheavy X particles produce supersymmetric particles that ultimately decay to the lightest supersymmetric particle [54, 55]. The primary decay of a superheavy X particle is into two or more particles of the MSSM that are generally off-shell. Instead of being on-shell, they have large (time-like) virtualities Q of order M_X . Thus each particle produced in the primary decay will generate a parton shower. The shower development is driven by the splitting of a virtual particle into two other particles with smaller virtualities. All MSSM particles participate in this shower as long as the virtuality is larger than the typical sparticle mass scale M_{SUSY} . The energy and the virtuality Q of the cascade particles diminish progressively in the process of the cascade development.

The breaking of both supersymmetry and $SU(2) \times U(1)_Y$ gauge invariance becomes important at virtuality $M_{\text{SUSY}} \sim 1\text{TeV}$. All the massive superparticles that have been produced so far can now be considered on-shell. The superparticles will now decay into Standard Model particles and the only possible stable sparticle, the LSP [54, 55]. This also applies to the heavy SM particles, i.e. the top quarks and the massive bosons, while the lighter

quarks and gluons will continue a perturbative parton shower until they have reached either their on-shell mass scale or the typical scale of hadronization $Q_{\text{had}} \sim 1\text{GeV}$. At the hadronization scale, strong interactions become non-perturbative, forcing partons to hadronize into mesons or baryons. In the end, the unstable hadrons and leptons will also decay, leaving only the stable particles behind [54, 55]. A schematic representation of the whole process is depicted in figure 4.1.

4.1.1 Neutralino and neutrino fluxes

The fluxes of the particles produced in decay of supermassive X -particles are of course not known, but some predictions can be made. The fragmentation spectra of the neutrino and neutralino fluxes can be calculated from Monte Carlo simulations for jet fragmentation in SUSY QCD. The predicted fragmentation spectra used in this thesis are from ref. [56].

A fragmentation function is the average number of particles i released per decay, per unit interval of x at the value x ,

$$\frac{dN_i}{dx}. \quad (4.1)$$

Here we assume that a superheavy X -particle with mass M_X decays into two jets with energy fraction

$$x = \frac{E}{E_{\text{jet}}} = \frac{2E}{m_X}, \quad x \in [0, 1]. \quad (4.2)$$

Furthermore, it is assumed that the primary partons produced have the maximum virtuality $Q^2 = M_X^2/4$, and for simplicity that the X -particle has equal branching ratios to all partons. It is assumed that the SUSY mass scale is $M_{\text{SUSY}} = 200\text{ GeV}$. For $M_{\text{SUSY}} = 1\text{ TeV}$, the predicted neutralino spectra are about half of the spectra for $M_{\text{SUSY}} = 200\text{ GeV}$.

In general, the particle flux is

$$\frac{d\Phi_i}{dE} = A \frac{dN_i}{dE}, \quad (4.3)$$

where A is the flux normalization with dimension $\text{cm}^{-2}\text{sr}^{-1}\text{s}^{-1}$.

No non-atmospheric component of the neutrino spectrum has yet been observed because of the high atmospheric neutrino flux that dominates at lower energies $E_\nu < 50\text{ GeV}$. The atmospheric flux decreases roughly with $E_\nu^{-3.7}$ in contrast to the extraterrestrial contribution, which is expected to decrease with E_ν^{-2} [57]. Consequently, the extraterrestrial contribution should dominate at higher energies.

4.1. DECAY OF SUPERHEAVY DARK MATTER

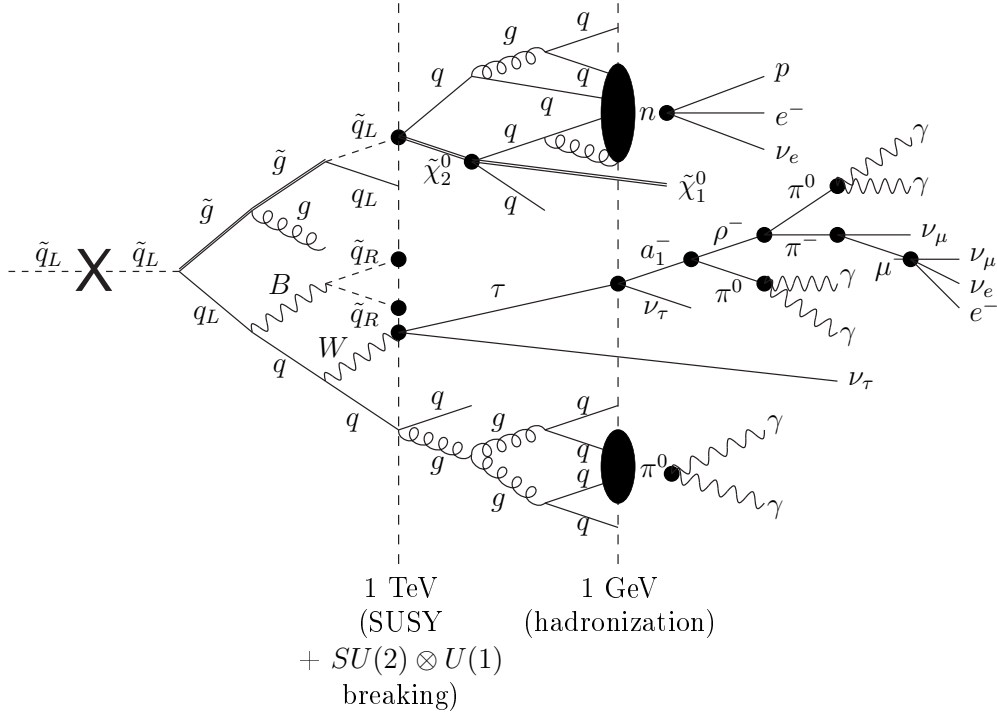


Figure 4.1: Schematic MSSM cascade for an initial squark with a virtuality $Q \simeq M_X$. The initial squark decays into partons, whose virtuality decrease in the fragmentation process. The full circles indicate decays of massive particles. The evolution of the cascade is separated into two epochs, which is shown with the two vertical dashed lines. At the first epoch with virtuality $Q > M_{\text{SUSY}}$, all MSSM particles can be produced in fragmentation processes. Particles with mass of order M_{SUSY} decay at the first vertical line. For $M_{\text{SUSY}} > Q > Q_{\text{had}}$ light QCD degrees of freedom still contribute to the perturbative evolution of the cascade. At the second vertical line, all partons hadronize, and unstable hadrons and leptons decay. [55]. The final shower consists mostly of photons, neutrinos and to a lesser extent protons and neutralinos.

The normalization of the neutrino flux is determined by the source properties. Since we do not know the properties of superheavy dark matter particles, we normalize the flux so that it is just below the deduced upper limit of the muon-neutrino flux from the neutrino telescope AMANDA-II. The sensitivity obtained for a diffuse neutrino flux is about [58]

$$E_\nu^2 \frac{dN_\nu}{dE_\nu} \leq 7.4 \times 10^{-8} \text{ GeV cm}^{-2} \text{ s}^{-1} \text{ sr}^{-1}, \quad (4.4)$$

valid in the energy range (16 – 2500) TeV. The predicted fluxes from decay of a supermassive particle with mass $M_X = 10^{12} \text{ GeV}$, weighted with E^2 and with normalization constant $A = 1.0 \times 10^{-20} \text{ cm}^{-2} \text{ s}^{-1} \text{ sr}^{-1}$, are shown in figure 4.2, together with the AMANDA-II limit.

Both neutrinos and neutralinos can interact with matter, resulting in secondaries that can be observed. The neutrino can be converted into its corresponding charged lepton through charged-current scattering, while neutralinos can scatter on matter and also produce charged leptons via flavor-changing weak decays of quarks.

Because of the similarities between neutrino and neutralino interactions, it should in principle be possible to observe neutralinos with high energy neutrino telescopes. The challenge will then be to distinguish them from neutrinos. If the cross section of neutralino-nucleon scattering is smaller than the neutrino-nucleon scattering, ultra-high energy cosmic neutralinos may travel a longer distance through the Earth than neutrinos before interacting, hence producing events at much higher energies than neutrinos.

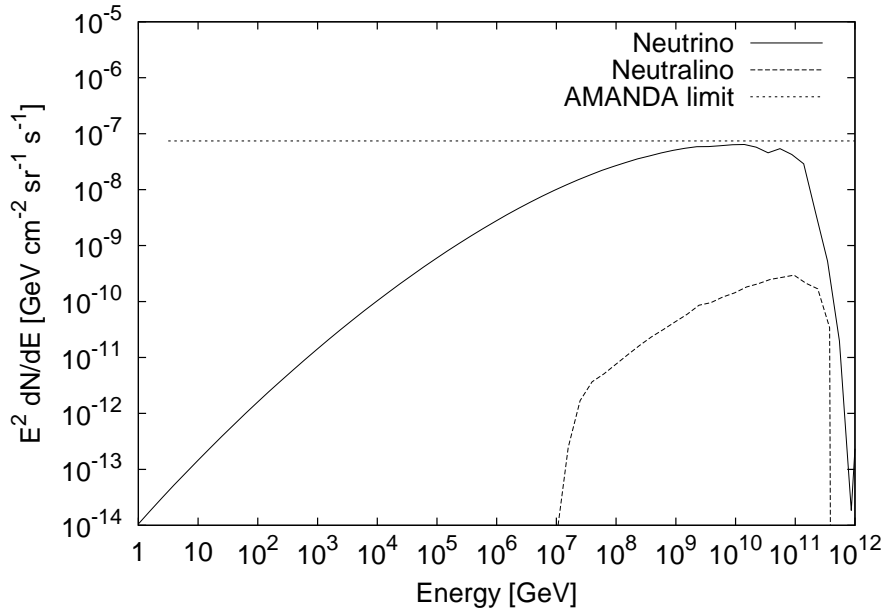


Figure 4.2: The predicted neutrino and neutralino fluxes for $M_{\text{SUSY}} = 200$ GeV, scaled to be just below the AMANDA-II upper limit (which is valid in the energy range $(16 - 2500)$ TeV). For $M_{\text{SUSY}} = 1$ TeV, the neutralino flux is approximately half of the value for the flux of for $M_{\text{SUSY}} = 250$ GeV.

4.2 Neutrino telescopes

Neutrinos are very elusive particles and scientists need to think big to capture them. Even though they are some of the most pervasive forms of matter in the Universe, they interact so feebly with matter that they are so to speak invisible to us. There is only a slight chance that occasionally one of the 337 relic neutrinos and antineutrinos per cm^3 that fills the Universe, will hit an atom and cause an observable effect. To increase the probability to observe such an effect, a neutrino detector has to contain enough matter for the neutrinos to interact with.

Neutrino telescopes operate by looking for neutrino-induced muons, which approximately conserves the direction of the incoming neutrino. A muon can be produced if an energetic muon-neutrino undergoes a charged-current interaction. Muons are also produced copiously in the atmosphere. Any downward flux of neutrinos would be completely overshadowed by atmospheric muons from pion decay in the atmosphere overhead. To distinguish between the muons created from cosmic ray showers in the atmosphere and the ones created from cosmic neutrinos, detectors look for upward-going muons with the Earth acting as a filter. Any upward-going muon can only have been created when neutrinos from sources on the opposite side of the Earth interacted in the medium beneath the detector.

Muons are penetrating particles, but they cannot traverse the Earth. They can travel a reasonable range in matter before decaying, in contrast to electrons and τ -leptons. Electrons have a very short range because of their much smaller mass, while the much heavier τ -leptons have a very short lifetime¹, making them difficult to detect.

When traveling through a medium, charged particles can cause Čerenkov radiation, which can be picked up by an array of phototubes. Čerenkov radiation is electromagnetic radiation emitted when a charged particle, e.g a muon, passes through an insulator at a speed greater than the speed of light in the medium. As the charged particle travels, it disrupts the local electromagnetic field in its medium, causing the electrons in the atoms of the insulator to be displaced and polarized. When the insulator's electrons restore themselves to equilibrium after the disruption has passed, photons are emitted. Most of the radiation is in the UV spectrum, but some of it can be observed as blue light.

¹The lifetime is $t_\tau \sim 3 \cdot 10^{-13}$ sec. Although, if PeV τ -neutrinos exist, a τ -lepton will travel around 100 m, thanks to time dilation [26].

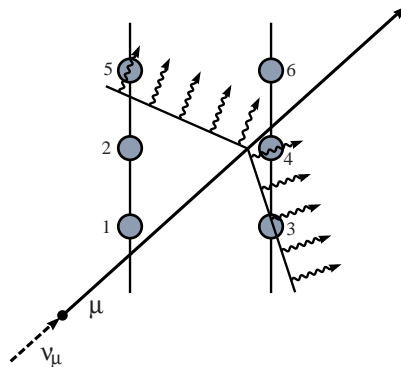


Figure 4.3: Six optical sensors, which record the arrival times of Čerenkov radiation, is needed to determine the direction of the muon track [59].

4.2.1 IceCube

IceCube is a 1 km^3 high energy optical neutrino detector under construction at the South Pole, which purpose is to detect high energy cosmic neutrinos, spanning from energies of 10^{11} eV to about 10^{21} eV . IceCube succeeds the first high energy neutrino telescope set in ice, AMANDA - the Antarctic Muon and Neutrino Detector Array².

The Antarctic ice that lies a kilometer below the surface condensed from snow that fell over ten thousand years ago, right after the last ice age. At this depth the pressure is so high that all the air bubbles is squeezed out, leaving the ice remarkably pure. The Antarctic polar ice is also free of radioactivity, which makes it an ideal medium for observing neutrinos.

Čerenkov radiation can travel undimmed for more than a hundred meters. Along its way in the ice, the light will pass sensitive photomultipliers which convert the faint light to an electrical signal which the surface equipment records. The direction of the neutrino can be deduced from the muon track, which can be reconstructed from the difference in arrival time of the Čerenkov wave front at the photomultipliers, shown schematically in figure 4.3.

By the time it is finished, IceCube will consist of 4200 spherical optical sensors (photomultiplier tubes) set in the Antarctic ice at depths between 1,450 and 2,450 meters, encompassing a cubic kilometer of ice in total. A surface air shower detector, IceTop, set to detect muons of atmospheric origin, will also be constructed. The design of IceCube is shown in figures 4.4 and 4.5. If everything proceed as planned, construction will finish in 2011 [62].

²The first high energy neutrino telescope was the Baikal Neutrino Telescope deployed in Lake Baikal in Siberia — the deepest fresh-water lake in the world.

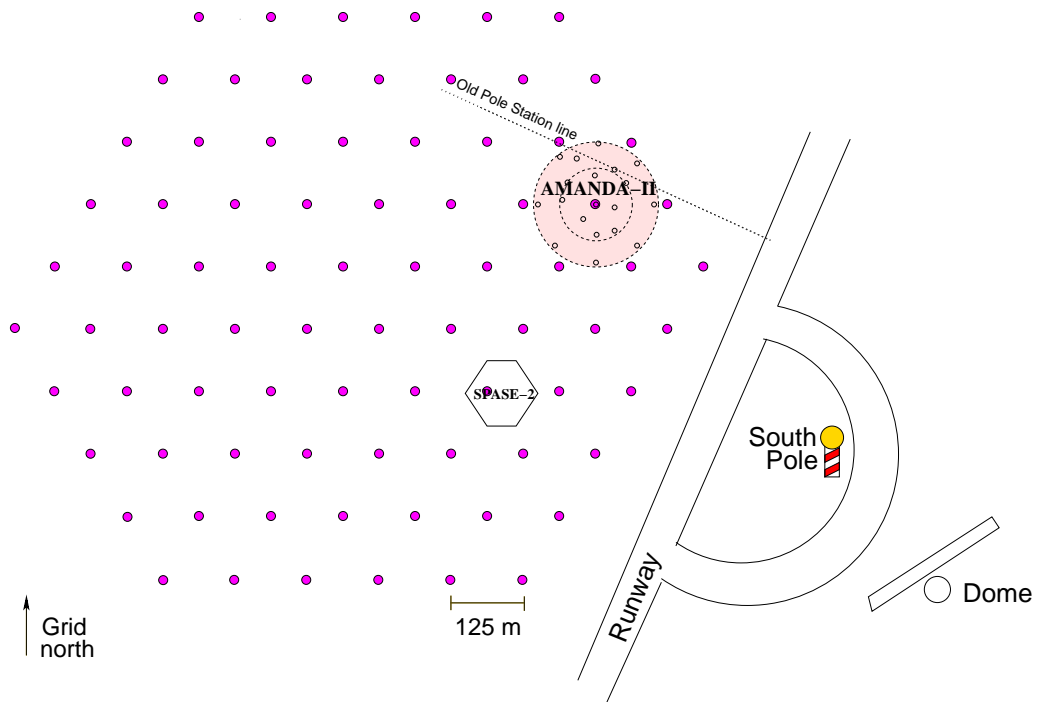


Figure 4.4: Overview of the arrangements of strings in the IceCube detector at the South Pole station. Also shown is the existing AMANDA detector and the SPASE air shower array [60].

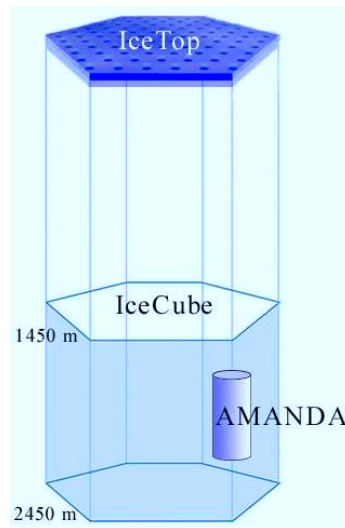


Figure 4.5: Conceptual design of the IceCube detector at the South Pole station. The existing AMANDA detector and an air shower array IceTop will be embedded in the new detector. Adapted from [61].

4.3 Deep inelastic scattering in the parton model

4.3.1 The naive parton model

Since we are dealing with high energy neutrinos and neutralinos, it is necessary to take quarks into account when considering the interaction of these particles with matter. Highly energetic leptons and neutralinos ($E \gg \text{GeV}$) have a very small wavelength, $\lambda \approx \frac{1}{E} < 0.2 \text{ fm}$. In contrast to nucleons, they do not possess a resolvable internal structure and behave as point particles. Thus, the cross sections of these reactions depend merely on the internal structure of the nucleon.

In the parton model, which was first introduced by Richard Feynman and James Bjorken in the late 60s [63, 64], we assume that hadrons are made up of point-like particles called partons. We now recognize the partons to be quarks and their mediators, the gluons.

Beside the three quarks (called valence quarks) from which the quantum numbers of the nucleon are constructed, it is possible for gluons to split into virtual quark-antiquark pairs (called sea quarks) or more gluons. The quark-antiquark pairs can emerge briefly from the vacuum by borrowing energy according to Heisenberg's uncertainty principle. This notion is supported by experiments, which show that only about half of the proton's momentum is carried by the valence quarks [65]. If the valence quarks were the only constituents of the proton, the sum of their momenta should be equal to the momentum of the proton. This implies that there must be something else besides the valence quarks contributing to the momentum of the proton.

The quantum numbers of the nucleon are still determined by the valence quarks. The sea quarks will have no net effect since they emerge in quark-antiquark pairs [66].

Following this, the scattering off the nucleon is due to the scattering off its individual constituents. At high energies, the incoming particle will scatter inelastically off a nucleon, colliding with one of the partons within the nucleon. We need to know how the partons are distributed inside the nucleon through the so called parton distribution functions [67]

$$f_i(x, Q^2). \tag{4.5}$$

The parton distribution functions are, at lowest order in perturbation theory, identical to the probability density for finding a particle with a certain fraction x of the hadron momentum when probed by the momentum transfer Q^2 . Experimental values of the distributions are obtained from global quantum chromodynamics (QCD) analysis of hard scattering processes [68].

The total momentum p^μ of the hadron is shared between the partons. Any relevant parton entering the hard scattering from an initial state hadron has momentum xp^μ , with $0 \leq x \leq 1$. (Within the hard scattering we make the approximation $p^2 = 0$ [67].) The total momentum of the hadron is constant

$$\int dx \sum_i x f_i(Q^2) = 1. \quad (4.6)$$

4.3.2 Deep inelastic scattering

The deep inelastic regime is the regime where $Q^2 \gtrsim 1 \text{ GeV}^2$, where $Q^2 \equiv -q^2$ is the four-momentum transfer to the target. At such high Q^2 , the strong coupling constant $\alpha_s(Q^2)$ becomes small enough to allow calculations in a perturbative approximation. These very large momentum transfers allows us to resolve smaller structures that might exist only for shorter times.

A deep inelastic probe scatters incoherently off the free, individual partons from which the hadron is made of. The struck parton has enough energy to escape the hadron, but is required by confinement to produce additional partons, such that they bind together into colorless hadrons.

A deeply inelastic scattering (DIS) process is generically of the form

$$l(k) + h(p) \rightarrow l'(k') + X, \quad (4.7)$$

where $l(k)$ represents a lepton with momentum k^μ , $h(p)$ a hadron of momentum p^μ , and X an arbitrary hadronic state. The process is mediated by the exchange of a vector boson. In the case of charged-current neutrino-nucleon scattering, the vector boson is a W -boson. The DIS process is totally inclusive in the hadronic final state, i.e. we are not interested in the hadronic “left-overs”. Because of this it is only relevant to observe the outgoing lepton of momentum k'^μ . The term inelastic refers to the fact that the final hadronic state X has an invariant mass much larger than that of the nucleon.

In DIS, the momentum transfer between lepton and hadron, q , is space-like,

$$\begin{aligned} q^\mu &= k^\mu - k'^\mu, \\ -q^2 &= Q^2. \end{aligned} \quad (4.8)$$

The kinematics in a deeply inelastic scattering process, can be completely described by the negative of the four-momentum transfer squared, Q^2 , and a scaling factor x ,

$$x = \frac{Q^2}{2M_N \nu} \quad (4.9)$$

4.3. DEEP INELASTIC SCATTERING IN THE PARTON MODEL

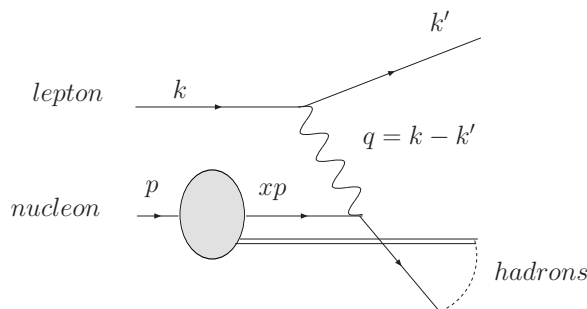


Figure 4.6: Kinematics in a deep inelastic scattering.

called Bjorken x . In the naive parton model, the dependence of the inelastic scattering functions on Q^2 fades away, and they become functions of the dimensionless scaling variable x alone. The phenomenon of scaling was first predicted by James Bjorken [64], hence the name Bjorken x .

The physical interpretation of x is as follows. Imagine a lepton colliding with a single massless quark, and that the quark scatters elastically. Then x is the fraction of the hadron's momentum the struck quark was carrying, evaluated in the *infinite momentum frame* (or *Breit frame*). In the infinite momentum frame, the hadron's momentum is assumed to be infinitely large, $|\vec{p}| \rightarrow \infty$. It is the frame where the hadron is initially approaching the lepton at very high energy. Because of time dilation in the infinite momentum frame, the proper motion of the parton constituents of the hadron is slowed down. This effectively freezes the partons during the scattering process so that the partons do not interact with each other. The lepton interacts only with one of the partons.

Let p and p' be the four-momenta of the partons before and after the interactions. Since x is the momentum fraction of the partons in the hadron, e.g. a nucleon, $p = xp_N$, the conservation of four-momentum gives

$$\begin{aligned}
 p' - p &= q & (4.10) \\
 q + p &= p' \\
 q + xp_N &= p' \\
 \Rightarrow (q + xp_N)^2 &= (p')^2 = m_p^2 \approx 0 \\
 \Rightarrow q^2 + \underbrace{(xp_N)^2}_{m_p^2 \approx 0} + 2qxp_N &\approx 0
 \end{aligned}$$

In the end we get

$$2qxp_N = -q^2 = Q^2, \quad (4.11)$$

so that

$$x = \frac{Q^2}{2qp_N} \quad (4.12)$$

describes the momentum fraction of the partons on the nucleon.

As we will see in the next section, however, Bjorken scaling is not exact. QCD effects break the scale invariance by inducing a dependence of the structure functions of order $\sim \ln(Q^2)$.

4.3.3 The QCD improved parton model

QCD processes become more important for increasing momentum transfers, and it is therefore necessary to calculate QCD corrections to the parton model of deep inelastic scattering. Such corrections extend the naive quark parton model by allowing interactions between the partons via gluons. On average, more quarks, antiquarks, and gluons occur with increasing Q^2 , between which the total momentum of the nucleon is distributed. Because more quark-antiquark pairs can be excited, the number of partons in a nucleon increases with higher Q^2 . Hence, the total momentum of the nucleon is distributed over more partons, so that the distribution function $f_i(x, Q^2)$ has to decrease. For small values of x , vacuum excitations in form of quark-antiquark pairs will dominate. The bigger Q^2 , the more partons with decreasing x is resolved [69].

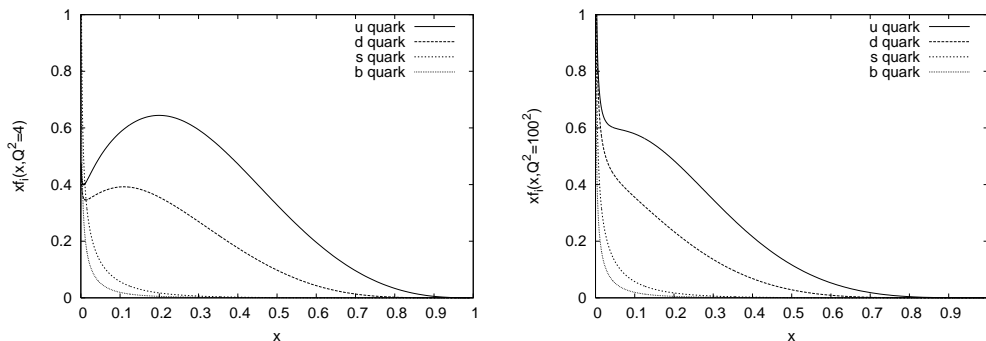


Figure 4.7: The CTEQ6-DIS parton distribution functions $x f_i(x, Q^2)$ in a proton for $i = u, d, s, b$ as function of x for $Q^2 = 4 \text{ GeV}^2$ (left) and $Q^2 = 100^2 \text{ GeV}^2$ (right). The divergence of the functions for $x \rightarrow 0$ indicates that the interaction is large for small momentum transfers.

The Q^2 -dependence of the distribution functions that enter the parton model of deep inelastic scattering processes, is successfully described in perturbative QCD by the Dokshitzer-Gribov-Lipatov-Altarelli-Parisi (DGLAP)

4.3. DEEP INELASTIC SCATTERING IN THE PARTON MODEL

equations [69]

$$\frac{dq_i(x, Q^2)}{d(\ln Q^2)} = \frac{\alpha_s(Q^2)}{2\pi} \int_x^1 \frac{dy}{y} \left[q_i(y, Q^2) P_{qq}\left(\frac{x}{y}\right) + g(y, Q^2) P_{qg}\left(\frac{x}{y}\right) \right], \quad (4.13)$$

$$\begin{aligned} \frac{dg_i(x, Q^2)}{d(\ln Q^2)} = \frac{\alpha_s(Q^2)}{2\pi} \int_x^1 \frac{dy}{y} \left[\sum_{j=1}^{N_f} [q_j(y, Q^2) + \bar{q}_j(y, Q^2)] P_{gq}\left(\frac{x}{y}\right) + \right. \\ \left. g(y, Q^2) P_{gg}\left(\frac{x}{y}\right) \right], \end{aligned} \quad (4.14)$$

where $q_i(y, Q^2)$ and $g(y, Q^2)$ refers to the parton distribution functions for quarks and gluons, respectively. The splitting functions $P_{ij}\left(\frac{x}{y}\right)$, with $i, j = q, g$ give the probability that parton j with momentum y radiates a quark or gluon and becomes a parton of type i with fraction $\left(\frac{x}{y}\right)$ of the momentum of parton j . The first equation describes the change of the quark densities with Q^2 because of gluon radiation and gluon splitting, while the second equation describes the change of the gluon density with Q^2 because of gluon radiation off quarks and gluons. The distribution in x at an initial value Q_0^2 , however, depends on non-perturbative QCD dynamics of the bound state hadron and must therefore be obtained by fitting parameterizations to data.

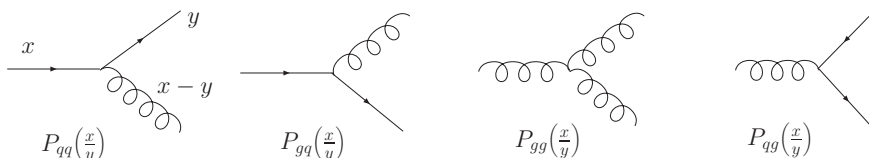


Figure 4.8: The lowest order QCD splitting functions $P_{ij}\left(\frac{x}{y}\right)$, with $i, j = q, g$. Each splitting functions gives the probability that a parton of type p converts into a parton of type p' , carrying a fraction $\frac{y}{x}$ of the momentum of parton p .

The CTEQ³ parton distribution functions that we have used, has been obtained by fitting DGLAP-evolved ansätze with experimental data from structure measurements in deep inelastic lepton-nucleon scattering [68]. The parton distribution functions are universal, that is, they can be extracted from some dedicated experiments and then used to predict cross sections for other processes involving initial state hadrons.

³CTEQ is an abbreviation for the Coordinated Theoretical/Experimental Project on QCD Phenomenology and Tests of the Standard Model.

The DGLAP equations are an approximation valid for large Q^2 and sufficiently large x . In CTEQ6, the values of Q and x are

$$10^{-6} < x < 1, \quad 1.3 \text{ GeV} < Q < 10^4 \text{ GeV}. \quad (4.15)$$

4.4 Neutrino interactions with matter

A neutrino can produce a muon in the inelastic charged-current scattering process $\nu_\mu + N \rightarrow \mu^- + \text{hadrons}(X)$, which is called an inclusive process since it is independently of the final hadron configuration.

The kinematics in the process can be described by the four-momenta $k, k', q = k - k', p_N, p_X$ of the incoming neutrino, outgoing muon, the exchanged W -boson, the incoming nucleon N and the outgoing final hadron state X given in the laboratory frame as

$$k = (E_\nu, k_\nu) \quad k' = (E_\mu, k_\mu) \quad q = (\nu, q) \quad (4.16)$$

$$p_N = (M_N, 0) \quad p_X = (E_X, p_X), \quad (4.17)$$

with E_ν is the neutrino energy, E_X is the energy of the final hadron state and M_N is the nucleon mass.

The energy difference ν in the nucleon rest frame is

$$\nu = \frac{p_N \cdot q}{M_N} = E_\nu - E_\mu. \quad (4.18)$$

while the negative four-momentum transfer is

$$\begin{aligned} Q^2 = -q^2 &= -(k - k')^2 = -(E_\nu - E_\mu)^2 + (k - k')^2 \\ &= 4E_\nu E_\mu \sin^2 \frac{\theta}{2}, \end{aligned} \quad (4.19)$$

where θ is the scattering angle of the outgoing muon.

It is useful to express the cross section in terms of the Bjorken scaling variable x and the inelasticity parameter y . The scaling variable x is given by

$$x = \frac{-q^2}{2qp_N} = \frac{Q^2}{2M_N\nu} \quad \text{with } 0 < x \leq 1. \quad (4.20)$$

The fraction of the lepton energy transferred to the proton in its rest frame is

$$y = \frac{p_N \cdot q}{p_N \cdot k} = \frac{\nu}{E_\nu} = 1 - \frac{E_\mu}{E_\nu} = \frac{Q^2}{sx}, \quad \text{with } 0 \leq y < 1, \quad (4.21)$$

where s is the square of the total center-of-mass (c.m.) energy of the lepton-nucleon collision

$$s = (k + p_N)^2 = 2M_N E + M_N^2 \sim 2M_N E. \quad (4.22)$$

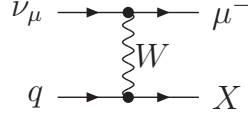


Figure 4.9: Feynman diagram for deep inelastic inclusive charged-current neutrino-nucleon scattering.

4.4.1 Quark distribution functions

The parton model predicts deep inelastic scattering as an incoherent sum of lq or $l\bar{q}$ scattering on partons. The double differential cross section can be written as [70]

$$\frac{d\sigma}{dx dy}(lp \rightarrow l'X) = \sum_{q,q'} q(x, Q^2) \frac{d\sigma}{dy}(lq \rightarrow l'q') + \sum_{\bar{q},\bar{q}'} \bar{q}(x, Q^2) \frac{d\sigma}{dy}(l\bar{q} \rightarrow l'\bar{q}'), \quad (4.23)$$

where $q(x, Q^2)$ and $\bar{q}(x, Q^2)$ is the quark and anti-quark distribution functions. The quark-parton distribution functions can be split into a valence- and a sea-quark contribution

$$u(x, Q^2) = u_v(x, Q^2) + u_s(x, Q^2) \quad d(x, Q^2) = d_v(x, Q^2) + d_s(x, Q^2). \quad (4.24)$$

Because of the symmetry of the $q\bar{q}$ sea, it is required that

$$u_s(x, Q^2) = \bar{u}(x, Q^2) \quad s(x, Q^2) = \bar{s}(x, Q^2) \quad (4.25)$$

$$d_s(x, Q^2) = \bar{d}(x, Q^2) \quad c(x, Q^2) = \bar{c}(x, Q^2). \quad (4.26)$$

The valence quark distributions of the proton satisfy the quark number sum rules

$$N_u = \int_0^1 dx(u(x) - \bar{u}(x)) = 2, \quad N_d = \int_0^1 dx(d(x) - \bar{d}(x)) = 1. \quad (4.27)$$

In terms of the quark distribution functions $q(x, Q^2)$ the differential cross sections of neutrinos on quarks and antiquarks with mass m_q are [70]

$$\begin{aligned} \frac{d\sigma}{dy dx}(\nu q) &= \frac{G_F^2 2m_q E_\nu}{\pi} q(x, Q^2) \\ \frac{d\sigma}{dy dx}(\nu \bar{q}) &= \frac{G_F^2 2m_q E_\nu}{\pi} \bar{q}(x, Q^2)(1-y)^2. \end{aligned} \quad (4.28)$$

The factor $(1 - y)^2$ describes the suppression of the scattering cross section in the weak interaction between two states of opposite helicity.

In charged-current interactions, neutrinos scatter only off quarks with negative charge (d, \bar{u}, s).

$$\begin{aligned}\nu_\mu + d\left(-\frac{1}{3}e\right) &\rightarrow \mu^- + u\left(\frac{2}{3}e\right) \\ \nu_\mu + \bar{u}\left(-\frac{2}{3}e\right) &\rightarrow \mu^- + \bar{d}\left(\frac{1}{3}e\right)\end{aligned}\quad (4.29)$$

The corresponding neutrino-proton cross section can be written as

$$\frac{d\sigma}{dx dy}(\nu p) = \frac{G_F^2 M_p E}{\pi} \times 2x \left[[d(x, Q^2) + s(x, Q^2)] + [\bar{u}(x, Q^2) + \bar{c}(x, Q^2)](1-y)^2 \right]. \quad (4.30)$$

Since the proton and neutron are in an isospin doublet we have that

$$\begin{aligned}u_p(x) &\rightarrow d_n(x) \\ d_p(x) &\rightarrow u_n(x).\end{aligned}\quad (4.31)$$

This leads to the neutrino-neutron cross section

$$\frac{d\sigma}{dx dy}(\nu n) = \frac{G_F^2 M_n E}{\pi} \times 2x \left[[u(x, Q^2) + s(x, Q^2)] + [\bar{d}(x, Q^2) + \bar{c}(x, Q^2)](1-y)^2 \right]. \quad (4.32)$$

In the previous calculations we have neglected the W -propagator term. This we can not do for very high energies, and in equations (4.30) and (4.32) the replacement

$$G_F^2 \rightarrow G_F^2 / \left(1 + \frac{Q^2}{M_W^2}\right)^2 \quad (4.33)$$

has to be made.

The cross section for neutrino scattering on an isoscalar target $N \equiv \frac{n+p}{2}$ is obtained by averaging the neutrino-proton and neutrino-neutron cross sections

$$\begin{aligned}\frac{d\sigma}{dx dy}(\nu N) &= \frac{1}{2} \left(\frac{d\sigma}{dx dy}(\nu p) + \frac{d\sigma}{dx dy}(\nu n) \right) \\ &= \frac{2G_F^2 M E_\nu}{\pi} \left(\frac{M_W^2}{Q^2 + M_W^2} \right)^2 \left[xq(x, Q^2) + x\bar{q}(x, Q^2)(1-y)^2 \right],\end{aligned}\quad (4.34)$$

4.4. NEUTRINO INTERACTIONS WITH MATTER

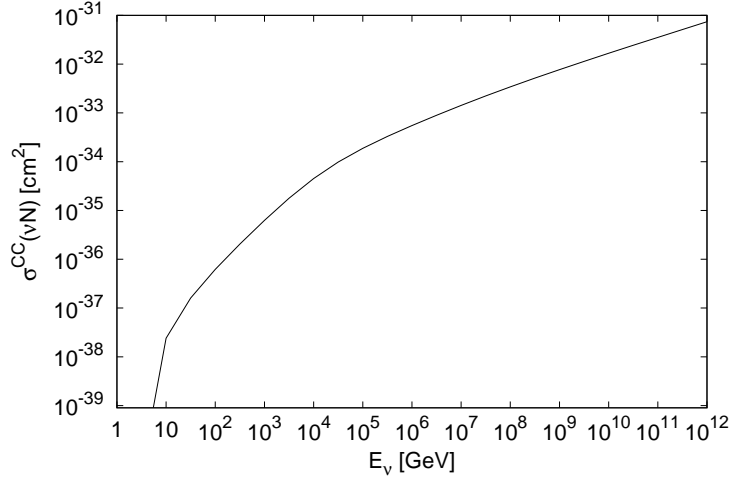


Figure 4.10: The charged-current cross section of neutrino scattering off nucleons as a function of the neutrino energy.

with the quark and anti-quark distribution functions

$$q(x, Q^2) = \frac{u_v(x, Q^2) + d_v(x, Q^2)}{2} + \frac{u_s(x, Q^2) + d_s(x, Q^2)}{2} + \frac{s_s(x, Q^2) + b_s(x, Q^2)}{2} \quad (4.35)$$

$$\bar{q}(x, Q^2) = \frac{u_s(x, Q^2) + d_s(x, Q^2)}{2} + c_s(x, Q^2) + t_s(x, Q^2). \quad (4.36)$$

Thus, in perturbative QCD (pQCD), the neutrino-nucleon cross section can be written as

$$\sigma^{\nu N} = \int_0^1 dx \int_0^1 dy \frac{d^2\sigma^{\nu N}}{dx dy}. \quad (4.37)$$

Because of the great mass of the charm (c), bottom (b) and top (t) quarks, we have neglected contributions from $c\bar{c}$, $s\bar{s}$, $t\bar{t}$ pairs in our calculations. Lighter quarks — the up (u), down (d) and strange (s) quarks — are the main components of the nucleon over the Q^2 -range relevant to neutrino-nucleon scattering. The resulting cross section for neutrinos off nucleons is shown in figure 4.10.

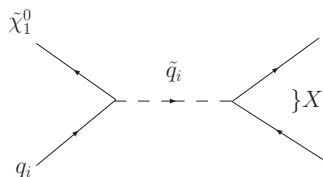


Figure 4.11: The Feynman diagram for s -channel $\tilde{\chi}_1^0 q_i$ scattering into all allowed final states X , where \tilde{q}_i is a virtual squark.

4.5 Neutralino interactions with matter

Ultra-relativistic neutralinos can interact with quarks by exchange of squarks in the s -channel⁴. Such an interaction can either directly yield a lightest supersymmetric particle — a neutralino, or a heavier superparticle that quickly decays to the lightest neutralino by virtue of R -parity. Hence, neutralinos will generate less energetic neutralinos in each interactions, and the number of neutralinos will not be depleted.

4.5.1 Kinematics and cross section

The cross section of s -channel neutralino-quark scattering through a resonance particle, $\tilde{\chi}_1^0 q_i \rightarrow \tilde{q}_i \rightarrow X$, is

$$\sigma(s) = \sum_q \int dx q(x, Q^2) \hat{\sigma}(\hat{s}), \quad (4.38)$$

where x is the fraction of the proton's momentum carried by the quark, $q(x)$ is the quark structure function and $\hat{\sigma}$ is the partonic cross section for $\tilde{\chi}_1^0 q_i \rightarrow \tilde{q}_i$. Figure 4.11 shows the Feynman diagram for the process.

To calculate the partonic cross section, $\hat{\sigma}$, we need the (relativistic) Breit-Wigner formula [71]

$$\sigma_{\text{tot}}(i \rightarrow X) = 4\pi \frac{m^2}{p^2} \frac{2J+1}{(2s_1+1)(2s_2+1)} \frac{\Gamma_i \Gamma_X}{(s-m^2)^2 + m^2 \Gamma_{\text{tot}}^2} \quad (s \approx m^2) \quad (4.39)$$

for the contribution of an unstable particle (or resonance) of spin J , mass m and total decay width Γ_{tot} to the total center-of-mass (c.m.) cross section of a reaction $i \rightarrow X$ near the resonance energy $\sqrt{s} = m$. Γ_i and Γ_X are the

⁴The term s -channel represents Feynman diagrams where the interaction involves the exchange of an intermediate particle whose squared momentum equals the Mandelstam variable s .

4.5. NEUTRALINO INTERACTIONS WITH MATTER

partial widths of this resonance for decay to the incident channel (i) and the exit channel (X) respectively. The spins for the colliding particles are s_1 and s_2 .

For the case of the total partonic cross-section of neutralino-quark scattering we get

$$\hat{\sigma}(\hat{s}) = \pi \frac{1}{|\vec{P}_1^*|^2} \frac{\hat{s}}{(\hat{s} - m_{\tilde{q}_i}^2)^2 + m_{\tilde{q}_i}^2 \Gamma_{\tilde{q}_i}^2} \Gamma(\tilde{q}_i \rightarrow q_i + \tilde{\chi}_1^0) \Gamma_{\tilde{q}_i}, \quad (4.40)$$

where \hat{s} is the square of the partonic c.m. energy, $|\vec{P}_1^*| = (\hat{s} - m_{\tilde{\chi}_1^0}^2)/2\sqrt{\hat{s}}$ is the c.m. 3-momentum of the incoming particles, $\Gamma_{\tilde{q}_i}$ is the total decay width of the squark and $\Gamma(\tilde{q}_i \rightarrow q_i + \tilde{\chi}_1^0)$ is the partial $\tilde{q}_i \rightarrow q_i + \tilde{\chi}_1^0$ decay width. We have put $s_1 = s_2 = \frac{1}{2}$ for the spins of the incoming particles and the spin of our unstable particle, the squark \tilde{q}_i , is $J = 0$.

Since $\Gamma \ll m$ we can use the narrow width approximation

$$\frac{1}{(\hat{s} - m^2)^2 + m^2 \Gamma^2} \xrightarrow{\Gamma \rightarrow 0} \frac{\pi}{m \Gamma} \delta(\hat{s} - m^2) \quad (4.41)$$

to simplify the expression for the partonic cross-section to

$$\hat{\sigma}(\hat{s}) = \pi^2 \frac{1}{|\vec{P}_1^*|^2} \frac{\hat{s}}{m_{\tilde{q}_i}} \delta(\hat{s} - m^2) \Gamma(\tilde{q}_i \rightarrow q_i + \tilde{\chi}_1^0). \quad (4.42)$$

The partial $\tilde{q}_i \rightarrow q_i + \tilde{\chi}_1^0$ differential rate for the decay is

$$d\Gamma(\tilde{q}_i \rightarrow q_i + \tilde{\chi}_1^0) = \frac{1}{32\pi^2} \overline{|\mathcal{M}|^2} \frac{|\vec{p}_1|}{m_{\tilde{q}_i}^2} d\Omega, \quad (4.43)$$

where $\overline{|\mathcal{M}|^2}$ is the amplitude squared of the decay process summed and averaged over various degrees of freedoms not observed, like spin and color. Here $m_{\tilde{q}_i}$ is the mass of the decaying squark and $d\Omega = d\phi_1 d(\cos \theta_1)$ is the solid angle of particle 1. The 3-momentum of either of the decaying particles $|\vec{p}_1|$ is

$$|\vec{p}_1| = |\vec{p}_2| = \frac{[(m_{\tilde{q}_i}^2 - (m_1 + m_2)^2)(m_{\tilde{q}_i}^2 - (m_1 - m_2)^2)]^{1/2}}{2m_{\tilde{q}_i}}. \quad (4.44)$$

In all simplicity, we assume equal masses $m_{\tilde{q}}$ for the L and R squarks of a given flavor, so that the left- and right-handed couplings contribute symmetrically. In general, the left- and right-handed couplings contribute only to L and R squark exchange, respectively. This approximation can be justified by the fact that most SUSY models predict small mass splittings between squarks (at least for the first two generations) [72]. Furthermore,

any squark produced in this interaction is too short-lived to lose energy prior to its decay [73]. If we also ignore the small Higgsino components N_{13} and N_{14} of the neutralino mass matrix, and apply the Feynman rules in the MSSM given in Appendix B, we get the matrix element

$$\mathcal{M} = \bar{u}(1)i \left[a_{qR} \left(\frac{1 - \gamma^5}{2} \right) + a_{qL} \left(\frac{1 + \gamma^5}{2} \right) \right] u(2), \quad (4.45)$$

where a_{qL} and a_{qR} are

$$\begin{aligned} a_{qL} &= \sqrt{2}g_2 \left(T_{3,q}N_{12} + \frac{\tan\theta_W}{6}N_{11} \right) & \text{for } q = u, d, s, c; \\ a_{qR} &= \sqrt{2}g_2 \tan\theta_W Q_q N_{11} & \text{for } q = u, d, s, c; \end{aligned} \quad (4.46)$$

Here $g_2 = 0.65$ is the weak $SU(2)$ coupling constant, $\sin\theta_W = 0.23120$ is the weak-mixing parameter, $T_{3,u} = -T_{3,d} = 1/2$ is the weak isospin, Q_q is the electric charge of quark q in units of the proton charge and N_{ij} are the entries of the neutralino mixing matrix in the notation of Ref. [52].

The square of the amplitude is

$$\begin{aligned} |\mathcal{M}|^2 &= \mathcal{M}\mathcal{M}^* = \bar{u}(1)i \left\{ a_{qR} \left(\frac{1 - \gamma^5}{2} \right) + a_{qL} \left(\frac{1 + \gamma^5}{2} \right) \right\} u(2) \times \\ &\quad \left[\bar{u}(1)i \left\{ \left[a_{qR} \left(\frac{1 - \gamma^5}{2} \right) + a_{qL} \left(\frac{1 + \gamma^5}{2} \right) \right] u(2) \right\} \right]^* \\ &= \bar{u}(1)i \left\{ a_{qR} \left(\frac{1 - \gamma^5}{2} \right) + a_{qL} \left(\frac{1 + \gamma^5}{2} \right) \right\} u(2) \times \\ &\quad - iu(2)^\dagger \left\{ a_{qL}^* \left(\frac{1 + \gamma^5}{2} \right) + a_{qR}^* \left(\frac{1 - \gamma^5}{2} \right) \right\} \gamma^0 u(1) \\ &= \bar{u}(1) \left\{ a_{qR} \left(\frac{1 - \gamma^5}{2} \right) + a_{qL} \left(\frac{1 + \gamma^5}{2} \right) \right\} u(2) \times \\ &\quad \bar{u}(2) \left\{ a_{qL}^* \left(\frac{1 - \gamma^5}{2} \right) + a_{qR}^* \left(\frac{1 + \gamma^5}{2} \right) \right\} u(1). \end{aligned} \quad (4.47)$$

Here we have used the fact that the complex conjugate is the same as the Hermitian conjugate for the quantity in the bracket, that $\bar{u}(1) = u(1)^\dagger \gamma^0$ and that γ^5 is Hermitian ($\gamma^{5\dagger} = \gamma^5$) and anticommutes with γ^μ ($\gamma^\mu \gamma^5 = -\gamma^5 \gamma^\mu$).

Since there is only one particle with only one allowed spin orientation in the initial state we get 1 when we average over the initial spins. If we then

sum over the final spins we get

$$\begin{aligned}
 \overline{|\mathcal{M}|^2} &= \sum_{\text{spins}} |\mathcal{M}|^2 = \text{Tr} \left\{ \left[a_{qR} \left(\frac{1 - \gamma^5}{2} \right) + a_{qL} \left(\frac{1 + \gamma^5}{2} \right) \right] \not{p}_{\tilde{q}_i} \times \right. \\
 &\quad \left. \left[a_{qL}^* \left(\frac{1 - \gamma^5}{2} \right) + a_{qR}^* \left(\frac{1 + \gamma^5}{2} \right) \right] (\not{p}_{\tilde{\chi}^0} + m_\chi) \right\} \\
 &= \text{Tr} \left\{ \left[|a_{qR}|^2 \left(\frac{1 - \gamma^5}{2} \right) + |a_{qL}|^2 \left(\frac{1 + \gamma^5}{2} \right) \right] \times \right. \\
 &\quad \left. \not{p}_{\tilde{q}_i} (\not{p}_{\tilde{\chi}^0} + m_\chi) \right\}. \tag{4.48}
 \end{aligned}$$

Here we have used that

$$(1 - \gamma^5)(1 + \gamma^5) = 1 - (\gamma^5)^2 = 0 \tag{4.49}$$

so that the cross terms cancel and that

$$\left(\frac{1 \pm \gamma^5}{2} \right)^2 = \left(\frac{1 \pm \gamma^5}{2} \right). \tag{4.50}$$

Applying the trace theorems given in Appendix A, this simplifies greatly to

$$\overline{|\mathcal{M}|^2} = \left[\frac{1}{2} (|a_{qR}|^2 + |a_{qL}|^2) \text{Tr} \{ \not{p}_{\tilde{q}_i} \not{p}_{\tilde{\chi}^0} \} \right] = 2(|a_{qR}|^2 + |a_{qL}|^2) p_{\tilde{q}_i} p_{\tilde{\chi}^0}. \tag{4.51}$$

The product of the four-momentum of incoming particles is pure kinematics:

$$\begin{aligned}
 p_{q_i} &= p_{\tilde{q}_i} + p_{\tilde{\chi}^0} \\
 p_{\tilde{q}_i} p_{\tilde{\chi}^0} &= \frac{1}{2} (m_{\tilde{q}_i}^2 - m_{\tilde{\chi}^0}^2). \tag{4.52}
 \end{aligned}$$

Since in our case $\overline{|\mathcal{M}|^2}$ does not depend on any angle we can integrate over the solid angle to get

$$\Gamma = \frac{1}{8\pi} \overline{|\mathcal{M}|^2} \frac{|\vec{p}_{\tilde{\chi}^0}|}{m_{\tilde{q}_i}}, \tag{4.53}$$

with

$$|\vec{p}_{\tilde{\chi}^0}| = \frac{1}{2m_{\tilde{q}_i}^2} (m_{\tilde{q}_i}^2 - m_{\tilde{\chi}^0}^2).$$

Here we have uses the standard formula for two-body decays, equation (4.43), with $|\vec{p}_1| = |\vec{p}_{\tilde{\chi}^0}|$ and $m_1 = m_{\tilde{\chi}^0} \gg m_2 = m_{q_i}$. If we neglect the mass of

the quark compared to the neutralino, the incoming particles have the c.m. energy

$$E_{1\text{CM}} = \frac{\hat{s} + m_{\tilde{\chi}^0}^2}{2\sqrt{\hat{s}}}, \quad (4.54)$$

and the c.m. 3-momentum

$$\begin{aligned} \vec{P}_1^* &= \sqrt{E_{1\text{CM}}^2 - m_{\tilde{\chi}^0}^2} = \sqrt{\frac{(\hat{s} + m_{\tilde{\chi}^0}^2)^2}{4\hat{s}} - m_{\tilde{\chi}^0}^2} \\ &= \frac{\hat{s} - m_{\tilde{\chi}^0}^2}{2\sqrt{\hat{s}}}. \end{aligned} \quad (4.55)$$

\hat{s} is the partonic center of mass energy for the interaction

$$\begin{aligned} \hat{s} &= m_{\tilde{q}_i}^2 = (p_{\tilde{\chi}^0} + p_{\tilde{q}_i})^2 = p_{\tilde{\chi}^0}^2 + p_{\tilde{q}_i}^2 + 2p_{\tilde{\chi}^0}p_{\tilde{q}_i} \\ &= m_{\tilde{\chi}^0}^2 + 2p_{\tilde{\chi}^0}p_{\tilde{q}_i}. \end{aligned} \quad (4.56)$$

Since $2p_{\tilde{\chi}^0}p_{\tilde{q}_i} = 2xP_Np_{\tilde{\chi}^0} = 2xM_N E_{\tilde{\chi}^0}$ we have

$$\hat{s} = m_{\tilde{\chi}^0}^2 + 2xM_N E_{\tilde{\chi}^0}. \quad (4.57)$$

If we then put the results of equations (4.51) and (4.52) into equation (4.53) we get

$$\Gamma = \frac{1}{8\pi} \overline{|\mathcal{M}|^2} \frac{|\vec{p}_{\tilde{\chi}^0}|}{m_{\tilde{q}_i}} = \frac{1}{16\pi} \frac{1}{m_{\tilde{q}_i}^3} (m_{\tilde{q}_i}^2 - m_{\tilde{\chi}^0}^2)^2 (|a_{qR}|^2 + |a_{qL}|^2). \quad (4.58)$$

The Breit-Wigner peak is not visible in cross sections for resonant squark production. Because the quark momentum distribution inside a nucleon N is continuous, any value of the incident neutralino energy larger than the threshold ($E_{\tilde{\chi}^0} > \frac{m_{\tilde{q}_i}^2 - m_{\tilde{\chi}^0}^2}{2M_N}$) can produce a squark at resonance. In this case, the cross section involves a convolution of the partonic cross section in equation (4.42) with a parton distribution function $q(x, Q^2)$. The cross section can then be obtained by inserting equation (4.58) into equation (4.42)

and convoluting with the parton distribution functions:

$$\begin{aligned}
 \sigma(s) &= \sum_q \int dx q(x, Q^2) \pi^2 \frac{1}{|\vec{P}_1^*|^2 m_{\tilde{q}_i}} \hat{s} \delta(\hat{s} - m^2) \Gamma(\tilde{q}_i \rightarrow q_i + \tilde{\chi}_1^0) \\
 &= \frac{\pi}{16} \sum_q \frac{1}{m_{\tilde{q}_i}^4} (m_{\tilde{q}_i}^2 - m_{\tilde{\chi}_0}^2)^2 (|a_{qR}|^2 + |a_{qL}|^2) \times \\
 &\quad \int dx \frac{4\hat{s}^2}{\hat{s} - m_{\tilde{\chi}_0}^2} q(x, Q^2) \delta(\hat{s} - m^2) \\
 &= \frac{\pi}{4} \sum_q \frac{1}{m_{\tilde{q}_i}^4} (m_{\tilde{q}_i}^2 - m_{\tilde{\chi}_0}^2)^2 (|a_{qR}|^2 + |a_{qL}|^2) \times \\
 &\quad \int dx \frac{(sx)^2}{sx - m_{\tilde{\chi}_0}^2} q(x, Q^2) \delta(m_{\tilde{\chi}_0}^2 + 2xM_N E_{\tilde{\chi}_0} - m_{\tilde{q}_i}^2) \\
 &= \frac{\pi}{4} \sum_q \frac{1}{m_{\tilde{q}_i}^4} (m_{\tilde{q}_i}^2 - m_{\tilde{\chi}_0}^2)^2 (|a_{qR}|^2 + |a_{qL}|^2) \times \\
 &\quad \int dx \frac{(sx)^2}{sx - m_{\tilde{\chi}_0}^2} q(x, Q^2) \frac{1}{2M_N E_{\tilde{\chi}_0}} \delta\left(x - \left(\frac{m_{\tilde{q}_i}^2 - m_{\tilde{\chi}_0}^2}{2M_N E_{\tilde{\chi}_0}}\right)\right) \\
 &= \frac{\pi}{4} \sum_q (|a_{qR}|^2 + |a_{qL}|^2) \frac{1}{m_{\tilde{q}_i}^2} x q(x, Q^2), \tag{4.59}
 \end{aligned}$$

with

$$x = \frac{m_{\tilde{q}_i}^2 - m_{\tilde{\chi}_0}^2}{2M_N E_{\tilde{\chi}_0}}. \tag{4.60}$$

The numerical calculations of the cross sections have been carried out with the use of the CTEQ6-DIS parton distributions sets. In one of the calculations, we have been optimistic and have set the mass of the squark to the lower experimental limit $m_{\tilde{q}_i} = 250$ GeV and used the lowest experimental limit for the lightest neutralino mass $m_{\tilde{\chi}_0} = 46$ GeV. We have also investigated the cross section for the highest value of the squark mass compatible with fine tuning, $m_{\tilde{q}} = 1$ TeV. The momentum scale in the quark distribution functions is set as $Q^2 = m_{\tilde{q}}^2$. The resulting cross sections for bino- and wino-like neutralinos as function of the neutralino energy are given in figure 4.12 for $m_{\tilde{q}} = 250$ GeV and in figure 4.13 for $m_{\tilde{q}} = 1$ TeV.

Squark decays are isotropic in the squark rest frame, implying

$$\frac{d\sigma_s}{d(\cos \theta^*)} = \frac{\sigma^{\text{tot}_s}}{2}, \tag{4.61}$$

where θ^* is the angle between the ingoing and outgoing $\tilde{\chi}_1^0$ in this frame. In boosting from the c.m. system into the nucleon rest frame, we obtain the

expression for the y distribution. The cross section differential in the scaling variable $y \equiv E_{\text{out}}/E_{\text{in}}$, where E_{in} and E_{out} is the incoming and outgoing $\tilde{\chi}_1^0$ energy in the nucleon rest frame, can then be written as

$$\frac{d\sigma_s}{dy} = \frac{\sigma^{\text{tot}_s}}{y_{\text{max}}}, \quad (4.62)$$

where

$$y_{\text{max}} = 1 - \frac{m_{\tilde{\chi}_1^0}^2}{m_{\tilde{q}}^2};$$

$$y_{\text{min}} = 0. \quad (4.63)$$

In order to obtain the maximum value of y , we have used $\hat{s} = m_{\tilde{q}}^2$ for on-shell squark production. The lower limit of y is always zero, because forward scattering in the squark rest frame leads to $E_{\text{out}} = E_{\text{in}}$. The value $y = 1$ is only reached for $m_{\tilde{\chi}_1^0}^2 \rightarrow 0$, i.e. for $E_{\text{out}} = 0$. The maximal value is quite close to unity for our values of $m_{\tilde{\chi}_1^0}$ and $m_{\tilde{q}}$. Assuming that the squarks are lighter than gluinos, a bino-like neutralino undergoing s -channel scattering on a nucleon, will lose on average about half its energy [72].

4.5. NEUTRALINO INTERACTIONS WITH MATTER

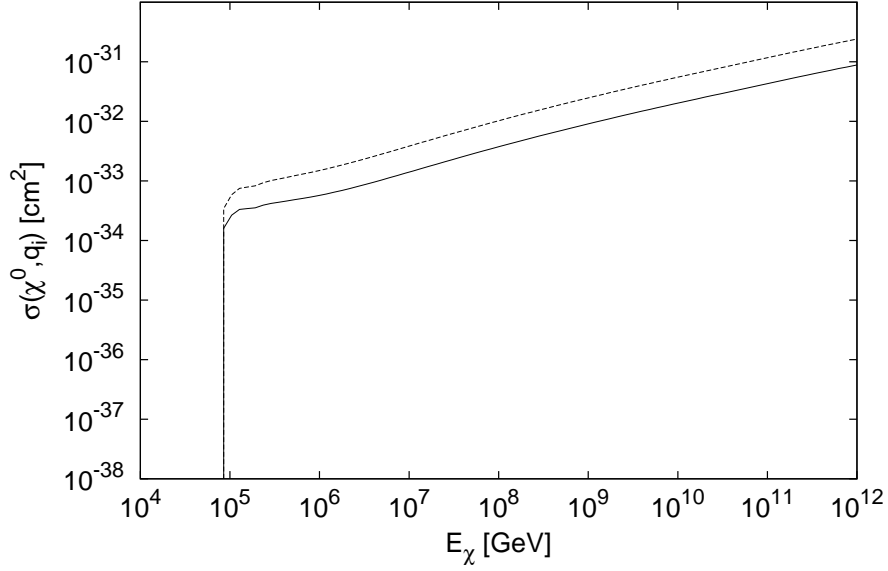


Figure 4.12: The cross section for s -channel neutralino-nucleon scattering as function of the energy for $m_{\tilde{q}} = 250$ GeV. The solid line is for pure binos, while the dashed is for pure winos.

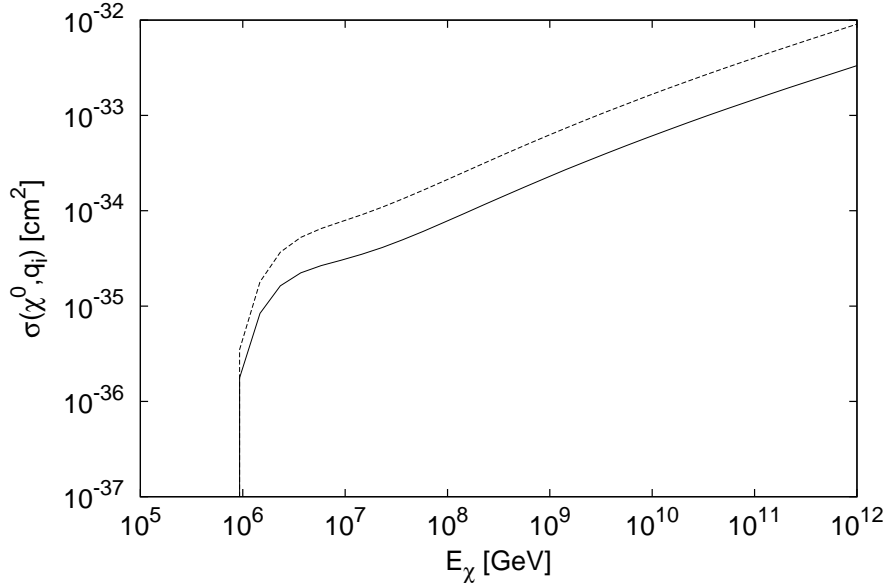


Figure 4.13: The cross section for s -channel neutralino-nucleon scattering as function of the energy for $m_{\tilde{q}} = 1$ TeV. The solid line is for pure binos, while the dashed line is for pure winos.

4.6 Influence of the Earth

4.6.1 The Preliminary Earth Model

On their journey through the Earth, the particles traverse different densities, depending on their arrival directions. For simplicity, the Earth can be regarded as a spherically symmetric ball with a simple internal structure, which is divided into layers. The inner structure of the Earth consists of a dense inner (solid) and outer (liquid) core and a lower mantle (highly viscous) of medium density, covered by a transition zone, lid, crust and oceans. A representation of the density profile of the Earth is given by the Preliminary Earth Model [74]

$$\rho(r) = \begin{cases} 13.0885 - 8.8381x^2, & r < 1221.5 \\ 12.5815 - 1.2638x - 3.6426x^2 - 5.5281x^3, & 1221.5 < r < 3480 \\ 7.9565 - 6.4761x + 5.5283x^2 - 3.0807x^3, & 3480 < r < 5701 \\ 5.3197 - 1.4836x, & 5701 < r < 5771 \\ 11.2494 - 8.0298x, & 5771 < r < 5971 \\ 7.1089 - 3.8045x, & 5971 < r < 6151 \\ 2.691 + 0.6924x, & 6151 < r < 6346.6 \\ 2.9, & 6346.6 < r < 6356 \\ 2.6, & 6356 < r < 6368 \\ 1.02, & r \leq R_{\oplus}, \end{cases}$$

where the density is measured in g/cm^3 , the distance r from the center of the Earth is measured in kilometers and $x \equiv r/R_{\oplus}$ is the scaled radial variable with the Earth's radius $R_{\oplus} = 6371$ km. A graphic representation of the density profile is given in figure 4.14.

We consider only upward-going muons, that is, neutrinos or neutralinos with arrival directions θ such that $0 < \theta < \pi/2$, where $\theta = 0$ denotes arrivals from the nadir. The amount of matter the particle passes on its way can be expressed as a column depth. In order to calculate the column depth, $z(\theta)$, one needs the angle

$$\rho = \tan^{-1} \left(\frac{R_{\oplus} - x}{(R_{\oplus} + x) \tan \frac{\theta}{2}} \right) + \frac{\pi}{2} - \frac{\theta}{2} \quad (4.64)$$

which we obtain from geometrical considerations. Using the sine law, we can then find an expression for the distance r from the center of the Earth,

$$r = R_{\oplus} \frac{\sin \theta}{\sin \rho}, \quad (4.65)$$

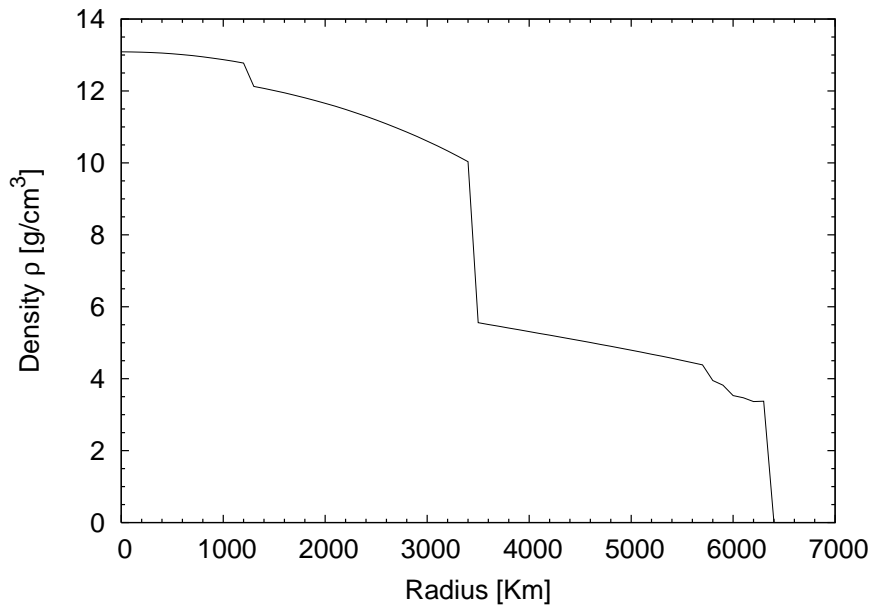


Figure 4.14: Density profile of the Earth according to the Preliminary Earth Model.

measured in kilometers and the scaled variable $x \equiv r/R_{\oplus}$. The amount of matter the upward-going particle encounters when traversing the Earth, is shown in figure 4.15 as a function of the particle direction. The core obviously has a big influence at angles below about 0.2π . A neutrino arriving from the nadir will in its passage through the Earth traverse a column whose depth is 11 kilotonnes/cm², or 1.1×10^{10} cmwe (centimeter water equivalent).

4.6.2 Interaction length

During its journey the particle can interact with the matter along its path. The length it can travel before interacting, is given by a (water-equivalent) interaction length [74]

$$\lambda_{\text{int}} = \frac{1}{\sigma(E)N_A}, \quad (4.66)$$

where $N_A = 6.022 \times 10^{23} \text{ mol}^{-1} = 6.022 \times 10^{23} \text{ cm}^3$ (water equivalent) is Avogadro's number, and σ is the particle's cross section with matter. The charged-current interaction lengths of neutrinos with energies greater than 40 TeV is less than the Earth's diameter. Thus, neutrinos arriving from the north-pole, with energies above this value, are effectively extinguished. The interaction length as a function of energy is shown in figure 4.16 for neutrinos.

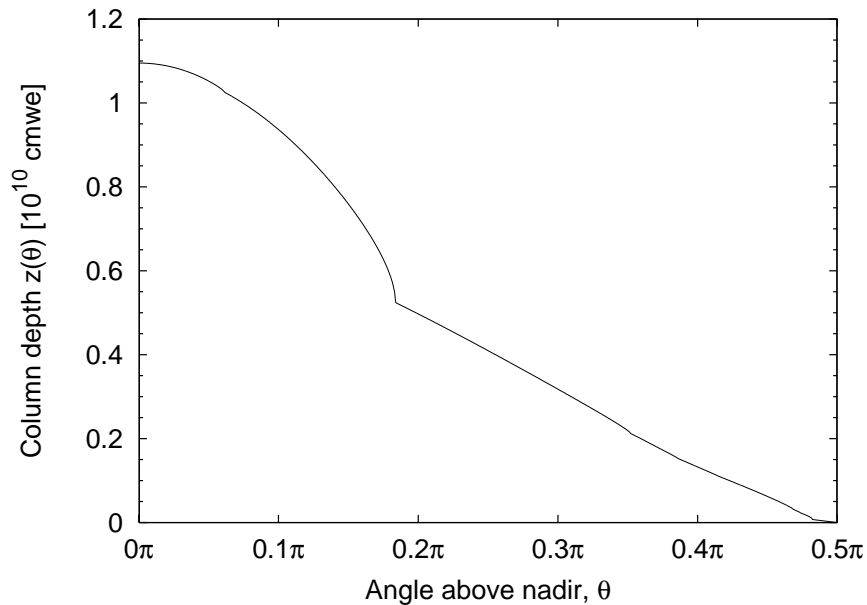


Figure 4.15: Column depth; thickness of the Earth as a function of the angle of incidence of the incoming particles.

For neutralinos, we consider the interaction lengths for the two squark masses $m_{\tilde{q}} = 250$ GeV and $m_{\tilde{q}} = 1$ TeV for pure bins in figure 4.17 and for pure winos in figure 4.18.

4.6.3 Shadow factor

As the particles travel through the Earth, the flux will be weakened. The attenuation is strongly dependent on the interaction length of the particles (or equivalently the cross section) and the column depth. If we neglect any regeneration effects and assume that the flux is isotropic, this attenuation can be represented by a shadow factor. The shadow factor is equivalent to the effective solid angle for upward-going muons divided by 2π [74]

$$S(E) = \frac{1}{2\pi} \int_{-1}^0 d \cos \theta \int d\phi \exp[-z(\theta)/\mathcal{L}_{\text{int}}(E)]. \quad (4.67)$$

The shadowing factor for the neutrino flux is given in figure 4.19, while the shadowing factors for neutralino fluxes in case of $m_{\tilde{q}} = 250$ GeV and $m_{\tilde{q}} = 1$ TeV are shown in figures 4.20 and 4.21, respectively.

If the neutralino-nucleon cross section is significantly smaller than the neutrino-nucleon cross section, it should be possible to distinguish between

4.6. INFLUENCE OF THE EARTH

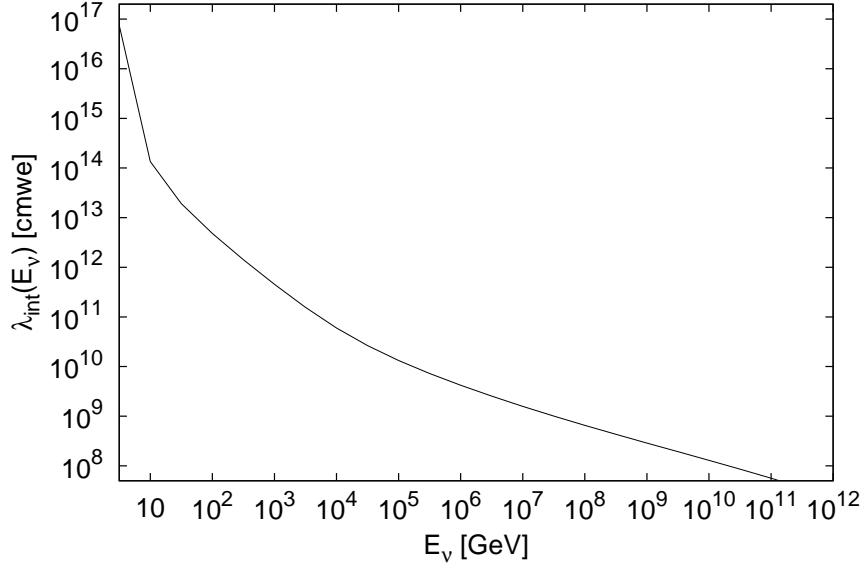


Figure 4.16: The interaction length for charged-current neutrino interactions on nucleons using the CTEQ6-DIS data set.

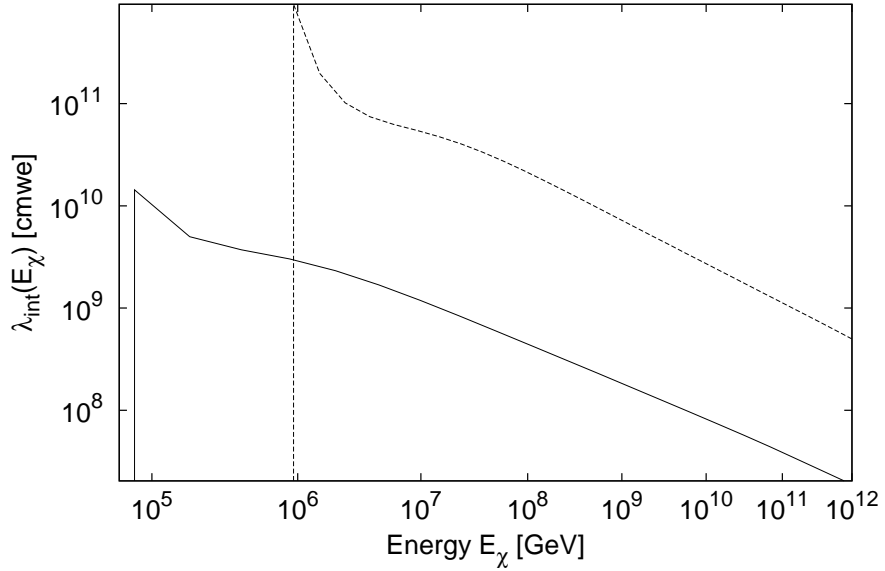


Figure 4.17: The interaction length for s -channel neutralino interactions on nucleons in case of a pure bino using the CTEQ6-DIS data set for $m_{\bar{q}} = 250$ GeV (solid line) and $m_{\bar{q}} = 1$ TeV (dashed line).

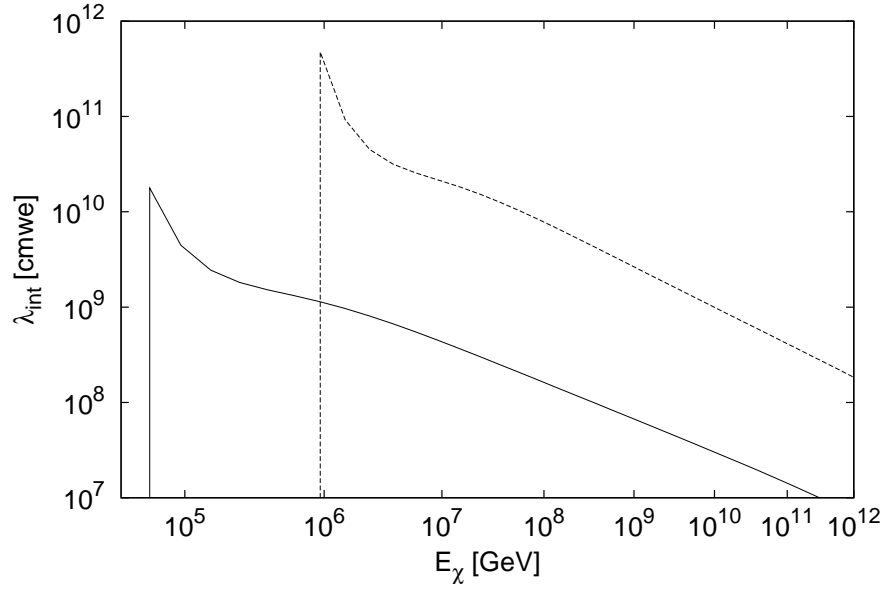


Figure 4.18: The interaction length for s -channel neutralino interactions on nucleons in the case of a pure wino using the CTEQ6-DIS data set for $m_{\tilde{q}} = 250$ GeV (solid line) and $m_{\tilde{q}} = 1$ TeV (dashed line).

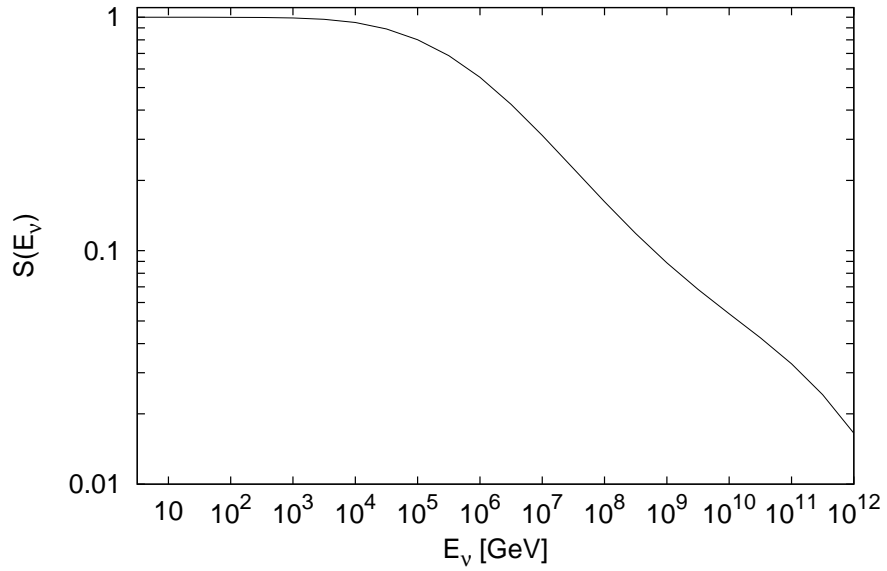


Figure 4.19: Shadow factor of neutrinos traversing the Earth as a function of the neutrino energy.

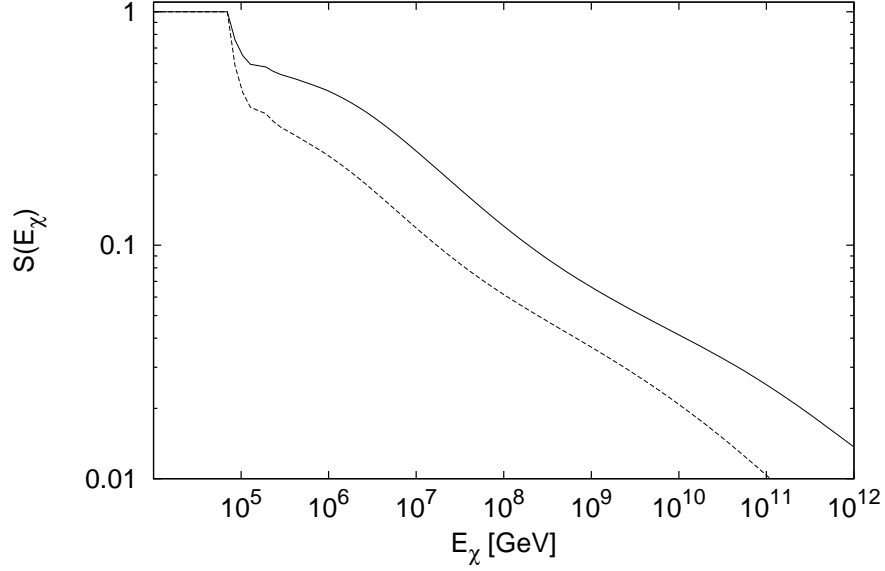


Figure 4.20: Shadow factor of pure binos (solid line) and pure winos (dashed line) traversing the Earth in the case of $m_{\tilde{q}} = 250$ GeV.

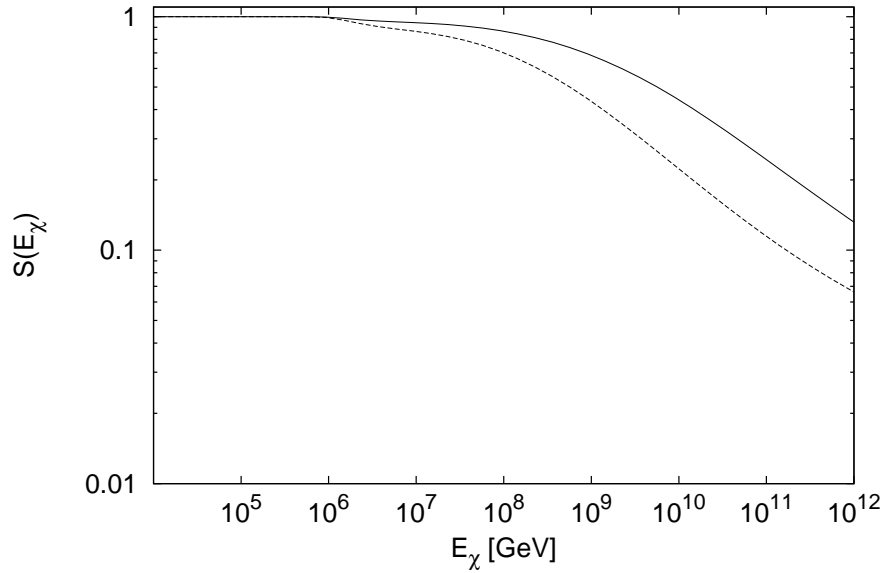


Figure 4.21: Shadow factor of pure binos (solid line) and pure winos (dashed line) traversing the Earth in the case of $m_{\tilde{q}} = 1$ TeV.

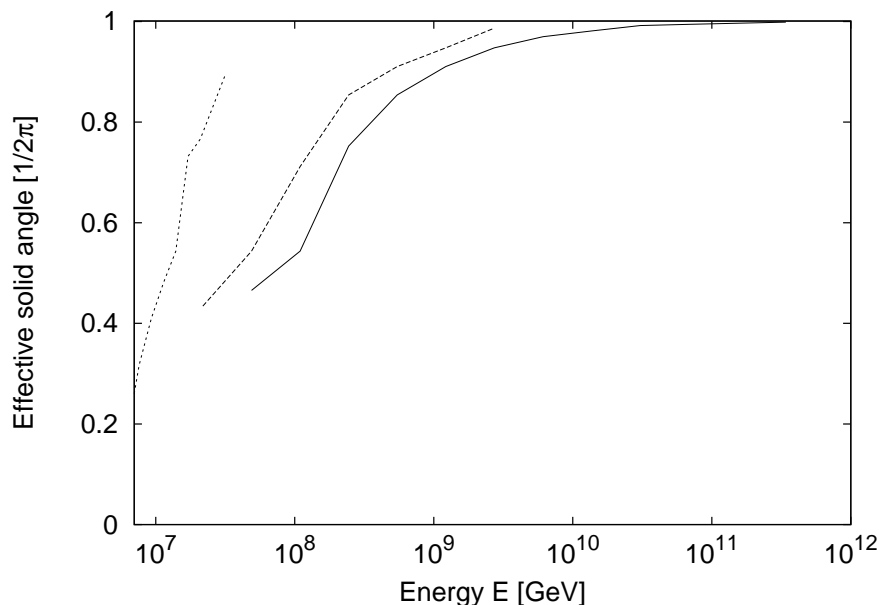


Figure 4.22: The effective solid angle divided by 2π as a function of energy for bino-like neutralinos produced in decays of superheavy dark matter particles of mass $M_X = 12$ GeV (solid line), $M_X = 10$ GeV (dashed line) and $M_X = 8$ GeV (dotted line). The mass of the squark is $m_{\tilde{q}} \sim 1$ TeV. The dotted line should be extended up to the value of 1 and the other two lines should decrease to zero.

the signals of neutrinos and neutralinos, since their shadowing factors and fluxes differ from each other. We can divide the Earth into two regions; one where it is likely that the signal is from neutralinos, and one where one cannot distinguish between neutrinos and neutralinos. The division between the two regions is set by an effective angle that varies with energy. It is then possible to determine an effective solid angle. Our calculations show that for squark masses of about $m_{\tilde{q}} \sim 250$ GeV it is not possible to differentiate neutralinos from neutrinos. In the case of $m_{\tilde{q}} \sim 1$ TeV, the bino-like neutralino-matter cross section is of order 10^{-2} , making it possible to distinguish the signals.

4.6.4 Average range of muons

In addition to the dependence on the attenuation of the particle flux, the upward muon event rate also depends on the probability that the particle creates a muon that is energetic enough to arrive at the detector with an energy E_μ larger than the detector's threshold energy E_μ^{\min} — the minimum muon energy triggering the detector. On average, a muon produced with

4.6. INFLUENCE OF THE EARTH

$E_\mu = 10$ TeV will travel a few kilometers until its energy is degraded to 1 TeV. The probability that a muon can be recorded in a detector depends on the average range $\langle R \rangle$ of a muon in rock [74],

$$\langle R(E_\nu; E_\mu^{\min}) \rangle = \frac{1}{\sigma_{CC}(E_\nu)} \int_0^{1-E_\mu^{\min}/E_\nu} dy R(E_\mu, E_\mu^{\min}) \frac{d\sigma_{CC}(E_\nu, y)}{dy}, \quad (4.68)$$

where the muon energy is

$$E_\mu = E_\nu(1 - y), \quad (4.69)$$

for muons produced in a charged-current interaction of neutrinos with matter. After a high energy muon is produced, it undergoes continuous energy loss as it propagates. The range R of an energetic muon follows from the energy-loss relation [1]

$$-dE_\mu/dX = \alpha(E_\mu) + \beta(E_\mu)E_\mu, \quad (4.70)$$

where X is the thickness of matter traversed by the muon in g/cm^2 . The first term represents ionization losses, while the second term represents catastrophic processes of bremsstrahlung, e^+e^- pair production and nuclear interactions. If the coefficients α and β are independent of energy, we can approximate their values to be $\alpha = 2.0 \times 10^{-3} \text{ GeV cmwe}^{-1}$ ($\text{cmwe} = \text{g}/\text{cm}^3$) and $\beta = 3.9 \times 10^{-6} \text{ cmwe}^{-1}$. Integrating equation (4.70), the muon range is

$$R(E_\mu, E_\mu^{\min}) \equiv X(E_\mu^{\min}) - X(E_\mu) = \frac{1}{b} \ln \frac{a + bE_\mu}{a + bE_\mu^{\min}}. \quad (4.71)$$

The average range of muons from charged-current neutrino interactions is shown in figure 4.23 for threshold energies 1 TeV and 10 TeV.

The average range is somewhat different in the case of muons produced in s -channel neutralino interactions with matter. The quarks produced in the decay of squarks can undergo flavor-changing weak decays, like $d \rightarrow u + W^-$, as well as cross-generational decays like $s \rightarrow u + W^-$. The W -boson can then decay into a muon-neutrino and a muon, $W^- \rightarrow \mu^- + \nu_\mu$. The muon energy will then be approximately 1/3 of the squark energy [75]

$$E_\mu = \frac{1}{3} E_\chi(1 - y). \quad (4.72)$$

The average range of a muon originating from neutralino interactions is then given by

$$\langle R(E_{\chi^0}; E_\mu^{\min}) \rangle = \frac{1}{\sigma_s(E_\nu)} \int_0^{1-m_{\chi^0}/m_{\tilde{q}}} dy R\left(\frac{1}{3} E_{\chi^0}(1 - y), E_\mu^{\min}\right) \frac{d\sigma_s(E_{\chi^0}, y)}{dy}, \quad (4.73)$$

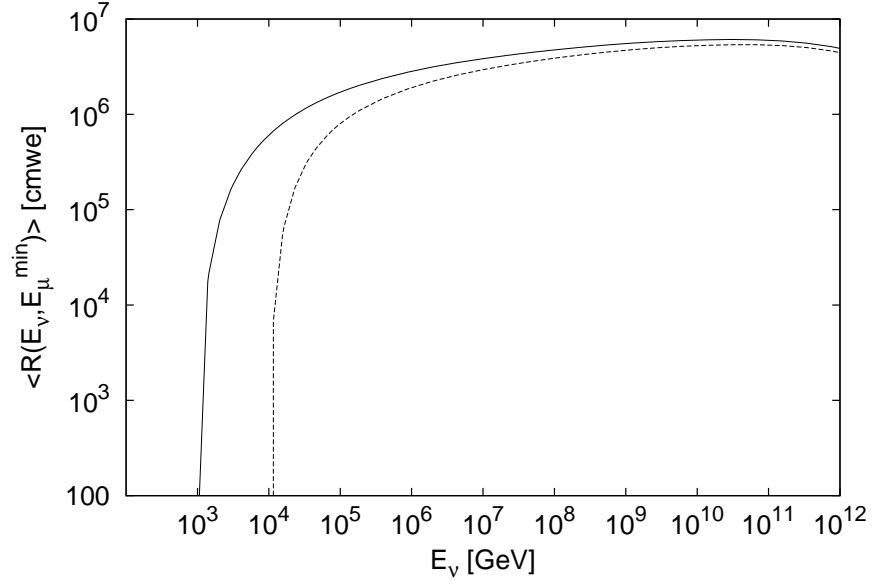


Figure 4.23: Average ranges for muons produced in charged-current interactions of neutrinos with energy E_ν , at threshold energies $E_\mu^{\min} = 1$ and 10 TeV.

where the differential cross section in the variable y is given in equation 4.62. The average ranges of such muons are shown in figure 4.24 (for $m_{\bar{q}} = 250$ GeV) and figure 4.25 (for $m_{\bar{q}} = 1$ TeV), with energy threshold of 1 TeV and 10 TeV.

4.6. INFLUENCE OF THE EARTH

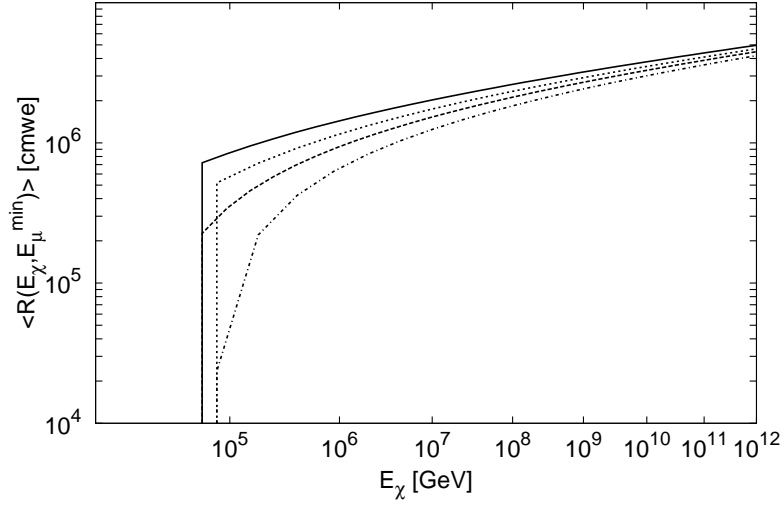


Figure 4.24: Average ranges for muons produced in s -channel interactions of neutralinos with energy E_χ on nucleons for wino-like neutralinos at threshold energies $E_\mu^{\min} = 1$ TeV (solid) and 10 TeV (dashed), and for bino-like neutralinos at $E_\mu^{\min} = 1$ TeV (dot dashed) and 10 TeV (dotted). The mass of the squark is $m_{\tilde{q}} = 250$ GeV.

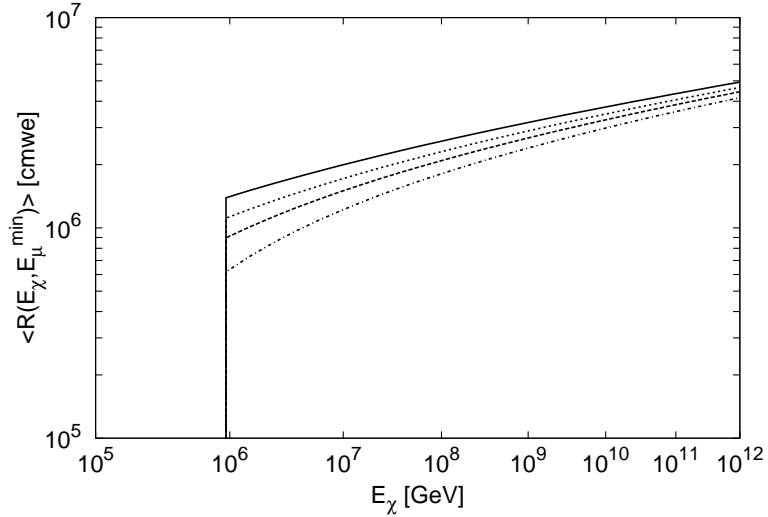


Figure 4.25: Average ranges for muons produced in s -channel interactions of neutralinos with energy E_χ for wino-like neutralinos at threshold energies $E_\mu^{\min} = 1$ TeV (solid) and 10 TeV (long dashed), and for bino-like neutralinos at $E_\mu^{\min} = 1$ TeV (short dashed) and 10 TeV (dotted). The mass of the squark is $m_{\tilde{q}} = 1$ TeV.

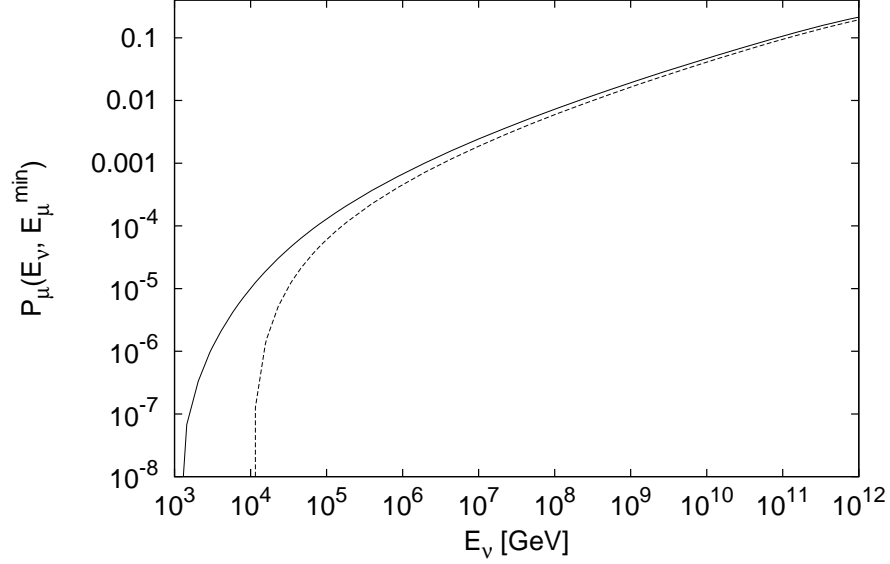


Figure 4.26: Probability that a neutrino of energy E_ν produces an observable muon with energy exceeding $E_\mu^{\min} = 1 \text{ TeV}$ and 10 TeV .

4.6.5 Probability for creating muons

The probability that a particle of energy E produces an observable muon is then [74]

$$P_\mu(E, E_\mu^{\min}) = N_A \sigma(E) \langle R(E; E_\mu^{\min}) \rangle. \quad (4.74)$$

The probability for creating observable muons from neutrino interactions is shown in figure 4.26. Probabilities for creating observable muons from neutralino interactions are shown in figure 4.27 and figure 4.28 for $m_{\tilde{q}} = 250 \text{ GeV}$ and $m_{\tilde{q}} = 1 \text{ TeV}$, respectively.

4.6. INFLUENCE OF THE EARTH

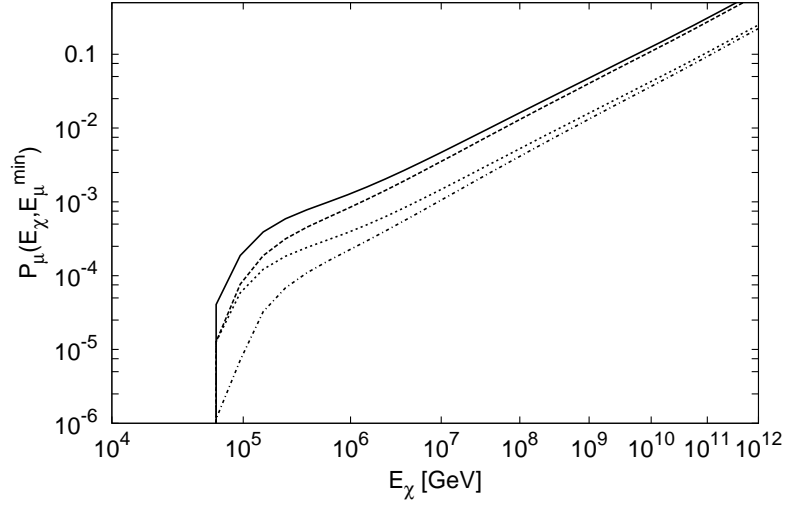


Figure 4.27: Probability that a neutralino of energy E_χ produces an observable muon with energy exceeding E_μ^{\min} for wino-like neutralinos with $E_\mu^{\min} = 1$ TeV (solid) and 10 TeV (dashed), and for bino-like neutralinos with $E_\mu^{\min} = 1$ TeV (dotted) and 10 TeV (dot-dashed). The mass of the squark is $m_{\tilde{q}} = 250$ GeV.

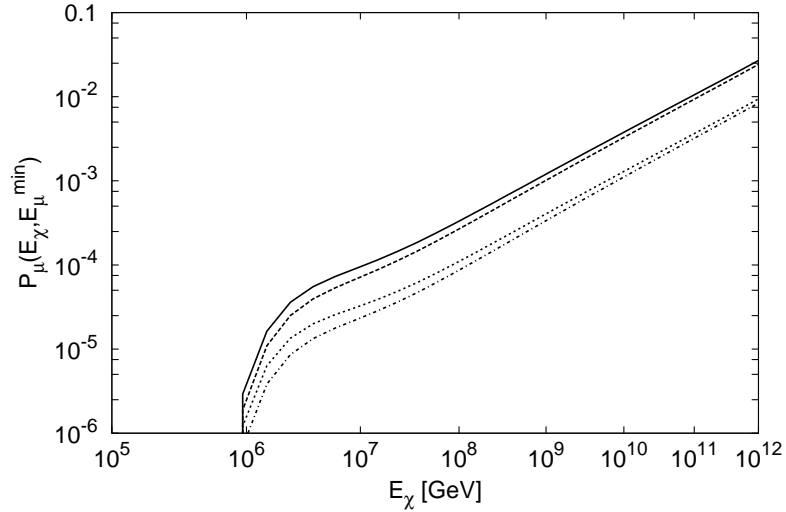


Figure 4.28: Probability that a neutralino of energy E_χ produces an observable muon with energy exceeding E_μ^{\min} for wino-like neutralinos with $E_\mu^{\min} = 1$ TeV (solid) and 10 TeV (dashed), and for bino-like neutralinos with $E_\mu^{\min} = 1$ TeV (dotted) and 10 TeV (dot-dashed). The mass of the squark is $m_{\tilde{q}} = 1$ TeV.

4.6.6 Event rates

The event rate of upward-going muons is proportional to the area of the detector. If we record interactions that occur in the rock or ice surrounding the detector, the effective volume can be enhanced over the instrumented volume. The event rate for a particle with energy E in a detector with effective area A is [74]

$$\text{Rate} = A \int dE P_\mu(E; E_\mu^{\min}) S(E) \frac{dN}{dE}. \quad (4.75)$$

The total event rate for detecting neutralinos in the energy range $10^7 - 10^{12}$ GeV in a detector with area $A = 1 \text{ km}^2$, like IceCube, is shown in table 4.1 for bins. The corresponding total event rate for neutrinos is shown in table 4.2.

E_{\min}^μ	Bino event rate, $m_{\tilde{q}} = 250 \text{ GeV}$	Bino event rate, $m_{\tilde{q}} = 1 \text{ TeV}$
1 TeV	$1.2713 \times 10^{-4} \text{ year}^{-1} \text{ sr}^{-1}$	$2.8623 \times 10^{-5} \text{ year}^{-1} \text{ sr}^{-1}$
10 TeV	$1.0393 \times 10^{-4} \text{ year}^{-1} \text{ sr}^{-1}$	$2.3703 \times 10^{-5} \text{ year}^{-1} \text{ sr}^{-1}$

Table 4.1: The total bino-produced μ^- event rates per steradian per year corresponding to the neutralino fluxes given in figure 4.2 for two different muon energy thresholds. The effective area is $A = 1 \text{ km}^2$.

E_{\min}^μ	Rate of ν
1 TeV	$0.77415 \text{ year}^{-1} \text{ sr}^{-1}$
10 TeV	$0.62058 \text{ year}^{-1} \text{ sr}^{-1}$

Table 4.2: The total μ^- event rates per steradian per year corresponding to the neutrino flux given in figure 4.2 for two different muon energy thresholds. The effective area is $A = 1 \text{ km}^2$.

The expected total event rates for wino-like neutralinos have been omitted on the grounds that they were suspiciously large (of the order of 10^7 events per year per steradian).

“That is all as it should be, for in a question like this truth is only to be had by laying together many varieties of error.”

Virginia Woolf — *A Room of Ones Own*

5

Discussions

There are several assumptions behind the estimates that have been presented in the previous chapter. Whether these assumptions are valid or not is difficult to say for sure. Many are very model dependent, and since we are to a large extent ignorant of the true nature of interactions at ultra-high energies, several uncertainties arise.

5.1 Theoretical and experimental uncertainty

Estimates of the uncertainties on the parton distributions can have an impact on the predicted cross sections. Since measurements of deep-inelastic scattering by photon exchange is most sensitive to the u -quark, the u -quark distribution is the most accurately known. The d -quark distribution is affected by the various data sets that are sensitive to u - d differences. The most uncertain distribution is the gluon distribution, for which the uncertainty is of order $\sim 15\%$ for x values up to ~ 0.3 . This uncertainty increases rapidly for larger values of x [68].

The cascade decay to cosmic ray particles relies on the ratio of the volume density of the X -particle, $n_X = \rho_c \Omega_X / m_X$, to its decay time, τ_X [76]. Neither the cosmic average mass density Ω_X , nor τ_X is of course known, so the values of these are very model dependent. To further complicate matters, the mechanisms of the decay rely on the exact nature of the particles. Alas, no firm prediction on the expected flux of neutralinos can be made.

For light squarks, the cross section for bino-like neutralinos is comparable to the neutrino-nucleon cross section at high energies, as shown in figure 5.1. For wino-like neutralinos it is even considerably larger than the neutrino-nucleon cross section. The assumptions we have made about the neutralino-nucleon cross section in chapter 4.5 could be responsible for the large expected

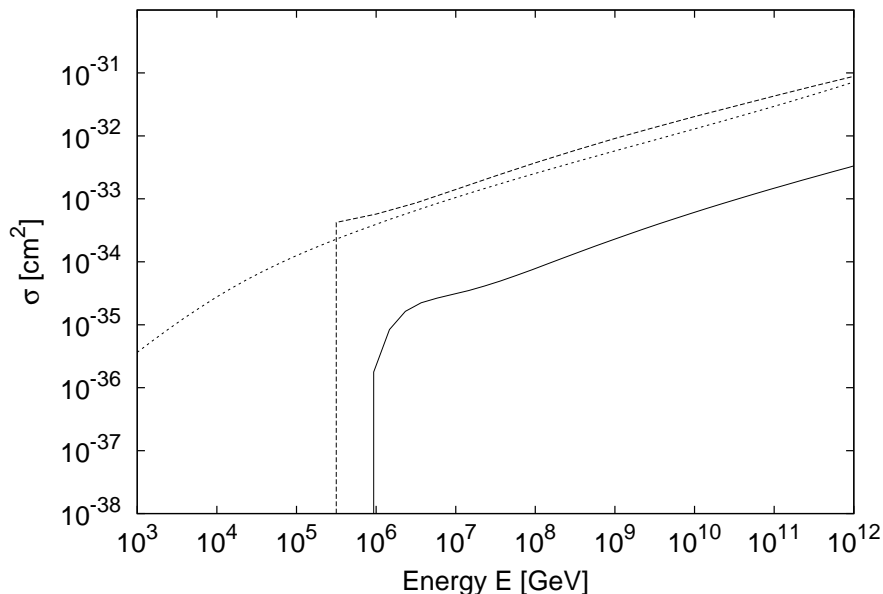


Figure 5.1: The cross sections for charged-current neutrino-nucleon scattering (dotted line) and for s -channel bino-like neutralino-nucleon scattering as function of the energy for $m_{\tilde{q}} = 250$ GeV (dashed line), $m_{\tilde{q}} = 1$ TeV (continuous line).

event rates for winos, or it could simply be a consequence of miscalculations.

The s -channel neutralino-nucleon cross section depends heavily on the squark mass. If the masses of the squarks are not much larger than the experimental lower value of $m_{\tilde{q}} \sim 250$ GeV, there is no chance of distinguishing between events from bino-like neutralinos from events from neutrinos in neutrino telescopes like IceCube. For $m_{\tilde{q}} = 1$ TeV, the cross section is of order $\sim 10^{-2}$ smaller than the neutrino-nucleon cross section, and hence the event rate for a given flux is reduced. This is compensated by a smaller attenuation of the flux. Consequently, it is possible to discern neutralinos from neutrinos. However, the event rate is too small for optical neutrino telescopes covering 1 km^3 , even if they are expanded tremendously, to give a firm signal of neutralinos.

The numbers presented include only neutralino interactions with matter in the s -channel. Neutralinos could also interact in the t -channel, which should be taken into account when calculating these interactions.

According to ref. [77], it is not even enough with a Teraton target to detect a reliable event rate for bino-like LSPs. This seems to hold even for the lightest squark we have used in our prediction of the cross section.

5.2 Numerical limitations

In our numerical evaluation of the the cross sections, we have chosen certain values for the energies and used polynomial interpolation routines to evaluate the cross sections at intermediate energy values. Similar inter- and extrapolation routines have been used in the computation of the particle spectra. The argument values in these routines must be in either strictly increasing or strictly decreasing order. The loss in accuracy is naturally greatest with extrapolation.

The integrals in the neutrino cross section have been performed with the subroutine “trapzd” together with the function “qtrap” from *Numerical Recipes in Fortran 90* [78]. The charged-current neutrino cross section with matter is slightly larger than the one given in ref. [74], which was evaluated with the CTEQ3-DIS parton distribution. This discrepancy could at least partially be explained by improved values for the parton distributions.

In the evaluation of the effective solid angle it was difficult to pinpoint the exact energy values needed for the surviving differential fluxes ($dS(E, \theta)$) to be equal, i.e. distinguishing the effective angle. Because of this, the lines are not complete and the values are only approximately equal to the “correct” values.

“It is the mark of an instructed mind to rest satisfied with the degree of precision which the nature of the subject admits and not to seek exactness when only an approximation of the truth is possible.”

Aristotle

6

Closing remarks

To summarize, the possibility of detecting high energy neutralinos in neutrino telescopes depends strongly on the parameters of SUSY that the cross section relies on, the effective detector volume and the unknown neutralino and neutrino fluxes from decay of superheavy dark matter particles. The prospect of detecting bino-like neutralinos in IceCube is therefore not promising. New methods must be investigated if such neutralinos are to be detected in the future. Already alternative methods have been proposed — like detecting radio Čerenkov radiation instead of optical Čerenkov radiation. One could also detect light from fluorescence emitted by very energetic particle showers in the atmosphere. Some of the planned cosmic ray experiments are the space-based Extreme Universe Space Observatory (EUSO) [79], which can monitor the entire Earth, and the Overwhelmingly Large Telescope (OWL) [80], a detector with even bigger target volume than IceCube.

The suggestion that the dark matter distributed in the Universe consists to some extent on superheavy X -particles will remain open for still some time.

Appendices

A

Pauli and Dirac matrices

Pauli matrices

The Pauli matrices are three Hermitian, unitary, traceless 2×2 matrices:

$$\sigma_1 \equiv \begin{pmatrix} 0 & 1 \\ 1 & 0 \end{pmatrix}, \quad \sigma_2 \equiv \begin{pmatrix} 0 & -i \\ i & 0 \end{pmatrix}, \quad \sigma_3 \equiv \begin{pmatrix} 1 & 0 \\ 0 & -1 \end{pmatrix}. \quad (\text{A.1})$$

The product rule is as follows:

$$\sigma_i \sigma_j = \delta_{ij} + i\epsilon_{ijk} \sigma_k \quad (\text{A.2})$$

In particular, we have:

$$\sigma_1^2 = \sigma_2^2 = \sigma_3^2 = 1 \quad (\text{A.3})$$

$$\sigma_1 \sigma_2 = i\sigma_3, \quad \sigma_2 \sigma_3 = i\sigma_1, \quad \sigma_3 \sigma_1 = i\sigma_2 \quad (\text{A.4})$$

Dirac matrices

The Dirac matrices are four unitary traceless 4×4 matrices:

$$\gamma^0 \equiv \begin{pmatrix} 1 & 0 \\ 0 & 1 \end{pmatrix}, \quad \gamma^i \equiv \begin{pmatrix} 0 & \sigma^i \\ -\sigma^i & 0 \end{pmatrix}, \quad (\text{A.5})$$

where 1 is the 2×2 unit matrix, 0 is the 2×2 matrix of zeros and σ^i are the Pauli matrices. If we lower the index, the sign changes for the “spatial” components: $\gamma_0 = \gamma^0$, $\gamma_i = -\gamma^i$.

The γ^5 matrix is defined by

$$\gamma^5 = i\gamma^0\gamma^1\gamma^2\gamma^3 = \begin{pmatrix} 0 & 1 \\ 1 & 0 \end{pmatrix}, \quad (\text{A.6})$$

and has the properties

$$(\gamma^5)^2 = 1, \quad \gamma^{5\dagger} = \gamma^5, \quad \gamma^5 = \gamma_5. \quad (\text{A.7})$$

For any 4-vector a^μ , we define the 4×4 matrix \not{a} as follows:

$$\not{a} \equiv a_\mu \gamma^\mu. \quad (\text{A.8})$$

In terms of the metric

$$g^{\mu\nu} \equiv \begin{pmatrix} 1 & 0 & 0 & 0 \\ 0 & -1 & 0 & 0 \\ 0 & 0 & -1 & 0 \\ 0 & 0 & 0 & -1 \end{pmatrix}, \quad (\text{A.9})$$

the product rules are as follows:

$$\gamma^\mu \gamma^\nu + \gamma^\nu \gamma^\mu = 2g^{\mu\nu}, \quad \not{a}\not{b} + \not{b}\not{a} = 2a \cdot b \quad (\text{A.10})$$

$$\gamma_\mu \gamma^\mu = 4 \quad (\text{A.11})$$

$$\gamma_\mu \gamma^\nu \gamma^\mu = -2\gamma^\nu, \quad \gamma_\mu \not{a} \gamma^\mu = -2\not{a} \quad (\text{A.12})$$

$$\gamma_\mu \gamma^\nu \gamma^\lambda \gamma^\mu = 4g^{\nu\lambda}, \quad \gamma_\mu \not{a}\not{b}\not{a} \gamma^\mu = 4a \cdot b \quad (\text{A.13})$$

The trace theorems are as follows:

$$\text{Tr}(1) = 4 \quad (\text{A.14})$$

$$\text{Tr}(\gamma^\mu \gamma^\nu) = 4g^{\mu\nu}, \quad \text{Tr}(\not{a}\not{b}) = 4a \cdot b \quad (\text{A.15})$$

$$\text{Tr}(\gamma^\mu \gamma^\nu \gamma^\lambda \gamma^\sigma) = 4(g^{\mu\nu} g^{\lambda\sigma} - g^{\mu\lambda} g^{\nu\sigma} + g^{\mu\sigma} g^{\nu\lambda}) \quad (\text{A.16})$$

In addition, the trace of a product of an odd number of γ -matrices is zero.

Since γ^5 is the product of an even number of γ -matrices, it follows that $\text{Tr}(\gamma^5 \gamma^\mu) = 0$ and $\text{Tr}(\gamma^5 \gamma^\mu \gamma^\nu \gamma^\lambda) = 0$. If γ^5 is multiplied by an even number of γ 's, we find

$$\text{Tr}(\gamma^5) = 0 \quad (\text{A.17})$$

$$\text{Tr}(\gamma^5 \gamma^\mu \gamma^\nu) = 0 \quad (\text{A.18})$$

$$\text{Tr}(\gamma^5 \gamma^\mu \gamma^\nu \gamma^\lambda \gamma^\sigma) = 4i\epsilon^{\mu\nu\lambda\sigma}, \quad (\text{A.19})$$

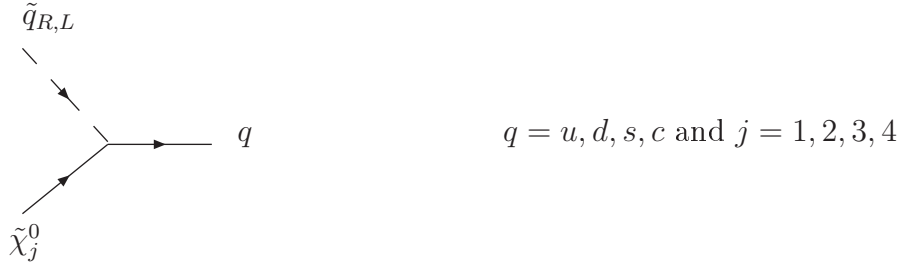
where

$$\epsilon^{\mu\nu\lambda\sigma} = \begin{cases} -1 & \text{if } \mu\nu\lambda\sigma \text{ is an even permutation of } 0123 \\ 1 & \text{if } \mu\nu\lambda\sigma \text{ is an odd permutation of } 0123 \\ 0 & \text{if any two indices are the same} \end{cases} .$$

B

Selected Feynman rules in the MSSM

Vertex factors



The following vertex factors are in the notation of Ref. [52]. For vertices with $\tilde{q}_L = \tilde{u}_L$ and $q = u$ we have

$$\frac{-i}{\sqrt{2}} \left\{ \frac{gm_u}{2m_W \sin \beta} N_{j4}^* (1 - \gamma_5) + \left[e e_u N'_{j1} + \frac{g}{\cos \theta_W} (1/2 - e_u \sin^2 \theta_W) N'_{j2} \right] (1 + \gamma_5) \right\}. \quad (\text{B.1})$$

For vertices with $\tilde{q}_R = \tilde{u}_R$ and $q = u$ we have

$$\frac{-i}{\sqrt{2}} \left\{ \frac{gm_u}{2m_W \sin \beta} N_{j4} (1 + \gamma_5) - \left[e e_u N_{j1}^* + -\frac{g e_u \sin^2 \theta_W}{\cos \theta_W} N_{j2}^* \right] (1 - \gamma_5) \right\}. \quad (\text{B.2})$$

For vertices with $\tilde{q}_L = \tilde{d}_L$ and $q = d$ we have

$$\frac{-i}{\sqrt{2}} \left\{ \frac{gm_d}{2m_W \cos \beta} N_{j3}^* (1 - \gamma_5) + \left[e e_d N'_{j1} - \frac{g}{\cos \theta_W} (1/2 + e_d \sin^2 \theta_W) N'_{j2} \right] (1 + \gamma_5) \right\}. \quad (\text{B.3})$$

For vertices with $\tilde{q}_R = \tilde{d}_R$ and $q = d$ we have

$$\frac{-i}{\sqrt{2}} \left\{ \frac{gm_d}{2m_W \cos \beta} N_{j3} (1 + \gamma_5) - \left[e e_d N_{j1}^* - \frac{g e_d \sin^2 \theta_W}{\cos \theta_W} N_{j2}^* \right] (1 - \gamma_5) \right\}. \quad (\text{B.4})$$

Similar factors hold for the charm and strange squarks.

Here g is the weak $SU(2)$ gauge coupling constant, θ_W is the weak mixing angle, $e = g \sin \theta_W$ is the $U(1)_{EM}$ charge. The quark charges are given by $e_u = \frac{2}{3}$ and $e_d = -\frac{1}{3}$. The matrix elements N'_{ij} appearing in the vertex factors are

$$\begin{aligned}
 N_{j1'} &= N_{j1} \cos \theta_W + N_{j2} \sin \theta_W, \\
 N_{j2'} &= -N_{j1} \sin \theta_W + N_{j2} \cos \theta_W, \\
 N_{j3'} &= N_{j3}, \\
 N_{j4'} &= N_{j4},
 \end{aligned} \tag{B.5}$$

where N_{ji} ($i = 1, 2, 3, 4$) are the entries in the neutralino mixing matrix.

External lines

$$\begin{array}{ll}
 \text{Spin 0:} & \text{(nothing)} \\
 \text{Spin } \frac{1}{2}: & \left\{ \begin{array}{l} \text{Incoming particle: } u \\ \text{Incoming antiparticle: } \bar{v} \\ \text{Outgoing particle: } \bar{u} \\ \text{Outgoing antiparticle: } v \end{array} \right. \\
 \text{Spin 1:} & \left\{ \begin{array}{l} \text{Incoming: } \epsilon^\mu \\ \text{Outgoing: } \epsilon^{\mu*} \end{array} \right.
 \end{array}$$

Bibliography

- [1] W.-M. Yao et al. Review of Particle Physics. *J. Phys. G: Nucl. Part. Phys.*, 33:1, 2006.
- [2] G. S. Watson. An Exposition on Inflationary Cosmology. *arXiv:astro-ph/005003v2*, 2000.
- [3] A. H. Guth. The Inflationary Universe: A Possible Solution to the Horizon and Flatness Problems. *Phys. Rev. D*, 23:347, 1981.
- [4] A. Linde. A New Inflationary Universe Scenario: A Possible Solution to the Horizon, Flatness, Homogeneity, Isotropy And Primordial Monopole Problems. *Phys. Lett. B*, 108:389, 1982.
- [5] A. Albrecht and P. J. Steinhardt. Cosmology For Grand Unified Theories With Radiatively Induced Symmetry Breaking. *Phys. Rev. Lett.*, 48:1220, 1982.
- [6] A. H. Guth. Was cosmic Inflation the 'Bang' of the Big Bang? *The Beamline*, 27:14, 1997.
- [7] E. W. Kolb and M. S. Turner. *The Early Universe*. Addison-Wesley Publishing Company, 1990.
- [8] F. Zwicky. Die Rotverschiebung von extragalaktischen Nebeln. *Helv. Phys. Acta*, 6:110–127, 1933.
- [9] F. Zwicky. On the masses of nebulae and of clusters of nebulae. *Astrophys. J.*, 86, 1937.
- [10] V. C. Rubin and W. K. Ford. Rotation of the Andromeda Nebula from a Spectroscopic Survey of Emission Regions. *Astrophys. J.*, 159:379, 1970.
- [11] G. Bertone, D. Hooper, and J. Silk. Particle Dark Matter: Evidence, Candidates and Constraints. *Phys. Rept.*, 405:279–390, 2005.
- [12] K. G. Begeman, A. H. Broeils, and R. H. Sanders. Extended rotation curves of spiral galaxies - Dark haloes and modified dynamics. *MNRAS*, 249:523, 1991.

- [13] D. Clowe et.al. A direct empirical proof of the existence of dark matter. *arXiv: astro-ph/0608407*, 2006.
- [14] D. Clowe, S. W. Randall, and M. Markevitch. Catching a bullet: direct evidence for the existence of dark matter. *arXiv: astro-ph/0611496*, 2006.
- [15] M. Milgrom. A Modification of the Newtonian dynamics as a possible alternative to the hidden mass hypothesis. *Astrophys. J.*, 270:365, 1983.
- [16] M. Milgrom. A Modification of the Newtonian dynamics - Implications for galaxies. *Astrophys. J.*, 270:371, 1983.
- [17] J. D. Bekenstein. Relativistic gravitation theory for the MOND paradigm. *Phys. Rev. D*, 70:083509, 2004.
- [18] C. Skordis, D. F. Mota, P.G. Ferreira, and C. Boehm. Large scale structure in Bekenstein's theory of relativistic Modified Newtonian Dynamics. *Phys. Rev. Lett.*, 96:011301, 2006.
- [19] G. W. Angus, H. Shan, H. Zhao, and B. Famaey. On the Proof of Dark Matter, the Law of Gravity and the Mass of Neutrinos. *Astrophys. J.*, 654:L13–L16, 2007.
- [20] A. Slosar, A. Melchiorri, and J. I. Silk. Did Boomerang hit MOND? *Phys. Rev. D*, 72:101301, 2005.
- [21] G. Jungman, M. Kamionkowski, and K. Griest. Supersymmetric dark matter. *Phys. Rept.*, 267:195, 1996.
- [22] H. V. Klapdor-Kleingrothaus and K. Zuber. *Particle Astrophysics*. Institute of Physics Publishing, 1997.
- [23] M. S. Turner. Dark Matter and Energy in the Universe. *Phys. Scripta*, T85:210–220, 2000.
- [24] S. Burles and D. Tytler. The Deuterium abundance toward QSO 1009+2956. *Astrophys. J.*, 507:732, 1998.
- [25] L. Roszkowski. Particle Dark Matter: A Theorist's Perspective. *Pramana*, 62:389–401, 2004.
- [26] L. Bergström and A. Goobar. *Cosmology and Particle Astrophysics*. Springer-Verlag, second edition, 2004.

BIBLIOGRAPHY

- [27] S. Dodelson. *Modern Cosmology*. Academic Press, 2003.
- [28] M. Kamionkowski. Particle Dark Matter. *arXiv: hep-ph/9609531v2*, 1996.
- [29] S. Weinberg. A New Light Boson? *Phys. Rev. Lett.*, 40:223, 1978.
- [30] F. Wilczek. Problem of Strong P and T Invariance in the Presence of Instantons. *Phys. Rev. Lett.*, 40:279, 1978.
- [31] R.D. Peccei and Helen Quinn. CP Conservation in the Presence of Pseudoparticles. *Phys. Rev. Lett.*, 38:1440, 1977.
- [32] G. G. Raffelt. Astrophysical methods to constrain axions and other novel particle phenomena. *Phys. Rept.*, 198:1–113, 1990.
- [33] J. Preskill, M. Wise, and F. Wilczek. Cosmology of the Invisible Axion. *Phys. Lett. B*, 120:127–132, 1983.
- [34] L. F. Abbott and P. Sikivie. A cosmological bound on the invisible Axion. *Phys. Lett. B*, 120:133–136, 1983.
- [35] M. Dine and W. Fischler. The not so harmless Axion. *Phys. Lett. B*, 120:137–141, 1983.
- [36] R. L. Davis. Cosmic axions from cosmic strings. *Phys. Lett. B*, 180:225–230, 1986.
- [37] R. L. Davis and E. P. S. Shellard. Do axions need inflation? *Nucl. Phys. B*, 324:167–186, 1989.
- [38] R. Aloisio, V. Berezhinsky, and M. Kachelriess. On the status of super-heavy dark matter. *Phys. Rev. D*, 74:023516, 2006.
- [39] E. W. Kolb, D. J. H. Chung, and A. Riotto. Wimpzillas! *arXiv: hep-ph/9810361v1*, 1998.
- [40] D. J. H. Chung, E. W. Kolb, and A. Riotto. Superheavy dark matter. *Phys. Rev. D*, 59:023501, 1999.
- [41] V. Kuzmin and I. Tkachev. Ultra-High Energy Cosmic Rays, Super-heavy Long-Living Particles and Matter Creation after Inflation. *JETP Lett.*, 68:271–275, 1998.

- [42] V. Berezhinsky, M. Kachelriess, and A. Vilenkin. Ultrahigh Energy Cosmic Rays without Greisen-Zatsepin-Kuzmin Cutoff. *Phys. Rev. Lett.*, 79:4302, 1997.
- [43] V. A. Kuzmin and V. A. Rubakov. Ultra-High Energy Cosmic Rays: a Window to Post-Inflationary Reheating Epoch of the Universe? *Phys. Atom. Nucl.*, 61:1028–1039, 1998.
- [44] K. Greisen. End to the Cosmic Ray Spectrum? *Phys. Rev. Lett.*, 16:748, 1966.
- [45] G. T. Zatsepin and V. A. Kuzmin. Upper limit of the spectrum of cosmic rays. *JETP Lett.*, 4:78, 1966.
- [46] D. Bird et al. [Fly’s Eye Collaboration]. Detection of a Cosmic Ray with Measured Energy Well Beyond the Expected Spectral cutoff due to Cosmic Microwave Radiation. *arXiv:astro-ph/9410067v1*, 1994.
- [47] M. Takeda et al. [AGASA collaboration]. Extension of the Cosmic-Ray Energy Spectrum Beyond the Predicted Greisen-Zatsepin-Kuzmin Cutoff. *Phys. Rev. Lett.*, 81:1163–1166, 1998.
- [48] H. Murayama. Supersymmetry Phenomenology. *arXiv: hep-ph/0002232v2*, 2000.
- [49] G. R. Farrar and P. Fayet. Phenomenology of the production, decay, and the detection of new hadronic states associated with supersymmetry. *Phys. Lett. B*, 76:575–579, 1978.
- [50] S. P. Martin. A Supersymmetric Primer. *arXiv:hep-ph/9709356*, 1997.
- [51] J. Edsjo. *Aspects of Neutrino Detection of Neutralino Dark Matter*. PhD thesis, Uppsala University, 1997.
- [52] J. F. Gunion and H. E. Haber. Higgs Bosons in Supersymmetric Models. *Nucl. Phys. B*, 272:1–76, 1988.
- [53] V. Barger et al. Indirect Search for Neutralino Dark Matter with High Energy Neutrinos. *Phys. Rev. D*, 65:075022, 2001.
- [54] V. Berezhinsky and M. Kachelriess. Ultra-high energy LSP. *Phys. Lett. B*, 422:163–170, 1998.
- [55] C. Barbot and M. Drees. Detailed analysis of the decay spectrum of a super-heavy X particle. *Astropart. Phys.*, 20:5–44, 2002.

BIBLIOGRAPHY

- [56] V. Berezhinsky and M. Kachelriess. Monte Carlo simulation for jet fragmentation in SUSY QCD. *Phys. Rev. D*, 63:034007, 2001.
- [57] K. Munich [The IceCube Collaboration]. Search for a diffuse flux of non-terrestrial muon neutrinos with the AMANDA detector. *arXiv:astro-ph/0509330*, 2005.
- [58] A. Achterberg [The IceCube Collaboration]. Multi-year search for a diffuse flux of muon neutrinos with AMANDA-II. *arXiv:0705.1315v1 [astro-ph]*, 2007.
- [59] F. Halzen and D. Hooper. High-energy Neutrino Astronomy: The Cosmic Ray Connection. *Rept. Prog. Phys.*, 65:1025–1078, 2002.
- [60] J. Ahrens et al. [The IceCube Collaboration]. Sensitivity of the IceCube Detector to Astrophysical sources of High Energy Muon Neutrinos. *Astropart. Phys.*, 20:507–532, 2004.
- [61] IceCube Neutrino Observatory. url: <http://icecube.wisc.edu/>.
- [62] A. Karle et al. [The IceCube Collaboration]. IceCube - the next generation neutrino telescope at the South Pole. *arXiv:astro-ph/0209556v1*, 2002.
- [63] R. P. Feynman. Very high-energy collisions of hadrons. *Phys. Rev. Lett.*, 23:1415, 1969.
- [64] J. D. Bjorken. Asymptotic Sum Rules at Infinite Momentum. *Phys. Rev.*, 179:1547, 1969.
- [65] D. Griffiths. *Introduction to Elementary Particles*. Wiley-VCH, 2004.
- [66] G. D. Coughlan and J. E. Dodd. *The ideas of particle physics. An introduction for scientists*. Cambridge University Press, 2nd edition, 1991.
- [67] G. Sterman et al. [The CTEQ Collaboration]. Handbook of perturbative QCD. *Reviews of Modern Physics*, 67(1):157–248, 1995.
- [68] J. Pumplin et. al. [The CTEQ Collaboration]. New Generation of Parton Distributions with Uncertainties from Global QCD Analysis. *JHEP*, 0207:012, 2002.
- [69] W. Greiner, S. Schramm, and E. Stein. *Quantum Chromodynamics*. Springer-Verlag, 2nd edition, 2002.

- [70] K. Zuber. *Neutrino physics*. Institute of Physics Publishing, 2004.
- [71] G. Kane. *Modern Elementary Particle Physics*. Addison-Wesley, 1987.
- [72] S. Bornhauser and M. Drees. The Passage of Ultrarelativistic Neutralinos through Matter. *Astropart. Phys.*, 27:30–45, 2007.
- [73] C. Barbot et al. SUSY In The Sky: Observing Ultra-High Energy Cosmic Neutralinos. *Phys. Lett. B*, 563:132–139, 2003.
- [74] R. Gandhi et al. Ultrahigh-Energy Neutrino Interactions. *Astropart. Phys.*, 5:81–110, 1996.
- [75] M. Kachelrieß. Private communications.
- [76] L. Anchordoqui, H. Goldberg, and P. Nath. Probing mSUGRA via the Extreme Universe Space Observatory. *Phys. Rev. D*, 70:025014, 2004.
- [77] S. Bornhauser and M. Drees. Signals of Very High Energy Neutralinos in Future Cosmic Ray Detectors. *arXiv:0704.3934v1*, 2007.
- [78] W. H. Press et al. *Numerical Recipes in Fortran 90*. Cambridge University Press, second edition edition, 1996.
- [79] P. Gorodetzky et al. [EUSO Collaboration]. EUSO In September 2004. *Nucl. Phys. Pro. Suppl.*, 151:401, 2006.
- [80] F. W. Stecker et al. Observing the Ultrahigh Energy Universe with OWL Eyes. *Nucl. Phys. B*, 136C:433–438, 2004.